UNIVERSITA' DEGLI STUDI DI NAPOLI
FEDERICO II

Dipartimento di Ingegneria Industriale

Ph.D. Thesis in

INGEGNERIA DEI SISTEMI MECCANICI – XXV CICLO

Essentiality of Temperature Management while Modeling and Analyzing Tires Contact Forces

Tutors:

Prof. Eng.
Michele Russo
Dipartimento Ingegneria Industriale

Ph.D. Eng.
Vincenzo Ciaravola
Bridgestone Technical Center Europe

Candidate

Alfredo Corollaro

2014

Contents

Chapter I – The target of the work and the background

I.1 – Introduction

The influence of temperature on tire performance is subject of matter in Research for many years. It is well known that the temperature affects the grip level of the tire and the cornering stiffness at the same time. Anyway, while the influence of temperature on grip level has been deeply investigated in different activities, the influence on cornering stiffness seems to be not sufficiently discussed yet.

As will be shown in the next chapters, the reason could be that the cornering stiffness is not influenced by the surface temperature – i.e. the temperature that can be measured on the tread surface – but instead by the bulk temperature – i.e. the core of the tire that means everything is between tread surface and inner liner.

Again, different mathematical models, more or less complex, have been developed to simulate the tire performance during the last 20 years. Some of them are quite simple in their formulation (Pacejka Magic Formula) while others using FEM approach appear very detailed and able to simulate many kind of exercise conditions.

Anyway, one limit of all these models is that they usually do not consider the influence of temperature probably because of the tradeoff between computational effort and benefits.

In the next paragraphs a short excursus on the most used commercial tire models will be showed.

The purpose of the entire activity is deeply investigating the influence of the bulk temperature on tire cornering stiffness also implementing a thermal model able to estimate this temperature correcting the cornering stiffness in consequence.

The discussion will be divided into two main parts.

The first part will be focused on the experimental activity: an intensive indoor test campaign has been conducted in the laboratories of the Technical Center of Bridgestone Europe using particular sensors (developed by the TÜV) able to measure the bulk temperature of a tire during its normal exercise. The activity has been focused only on the linear range of the tire characteristic (i.e. no more than 1 degree of Slip Angle has been applied). How the bulk temperature and surface temperature follow very different dynamics reaching very different values will be showed. At the same time, it will be clear that is the bulk temperature influencing the cornering stiffness and not the surface temperature that remains very similar to the ambient temperature instead.

Again, outdoor tests have been performed in the European Proving Ground of Bridgestone Europe to analyze the bulk temperature levels reached by a tire when it works fitted on a generic vehicle.

It will be showed that the bulk reaches very high temperatures (80-90°C) during its normal exercise (i.e. cruising at constant speed on highway); furthermore the strong influence of the camber angle will be highlighted: a significant difference between outside shoulder and inside shoulder appeared during the test.

Outdoor tests confirmed that in the linear range (that means up to 0.3-0.4 g of lateral acceleration) the bulk temperature is not influenced by the lateral force generated by the tire. The temperature is influenced only by the vertical load on the tire and by the vehicle speed.

The second part of the discussion will be focused on the implementation of a model able to predict the bulk temperature and its influence on the cornering stiffness of the tire.

The model is almost completely physical and has been projected to be as much user-friendly as possible.

As will be showed, to build up a generic tire model it is sufficient to perform some typical indoor tests that are usually performed by tire manufacturers (Flat Trac tests, static footprint test, loaded radius and rolling radius evaluation, etc.). No tuning phase has been required until now to tune the model.

To be reliable and *light* to be used in vehicle dynamics simulations, the model interacts with Pacejka Magic Formula to evaluate the lateral force in real-time, but taking into account the influence of the bulk temperature on the cornering stiffness value. As will be showed, the evaluation of the tire force in linear range is significantly better than the standard Magic Formula alone.

I.2 – Tire Models Overview

Several types of mathematical models have been developed in the last years to model the tire behavior. Of course different levels of accuracy may be introduced taking into account the purpose of the specific model. The Figure I.1 lets to have a look on the different approach – and the consequences in terms of complexity – to model the tire.

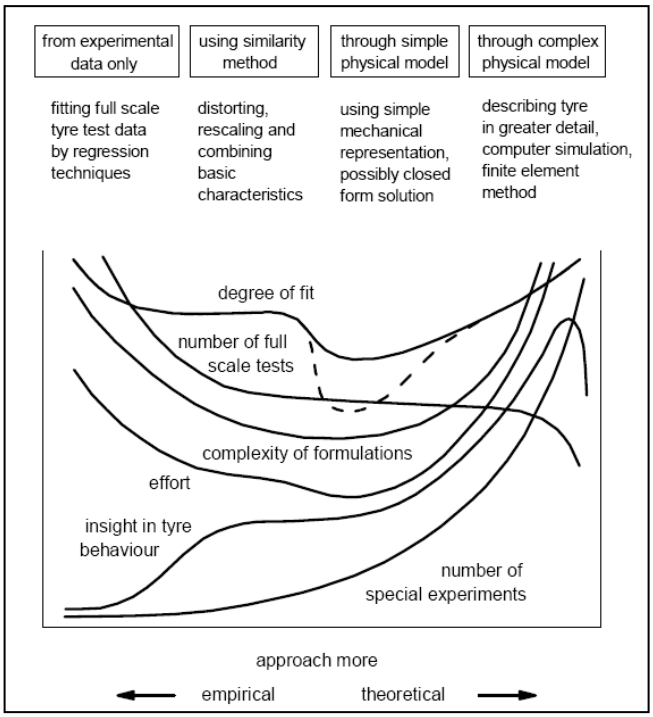

Figure I.1 – Tire Models Description

From left to right the model is based less on full scale tire experiments and more on the theory of the behavior of the physical structure of the tire. In the middle, the model will be simpler but possibly less accurate while at the far right the descriptions becomes complex and less suitable for application in vehicle simulations and may be more appropriate for the analysis of detailed tire performance in relation to its construction.

At the left-hand category there are mathematical tire models which describe measured tire characteristics through tables or mathematical formulae and interpolation schemes.

In the next paragraphs the most known models based on the third category in the figure will be analyzed.

In this kind of models – simple physical models – four fundamental factors play a role: frictional properties in tire-road interaction, distribution of the normal contact pressure, compliance of the tread rubber and compliance of the belt/carcass.

For what concern the belt/carcass behavior, in literature usually are three kind of modeling: the belt is considered rigid; the belt is considered a stretched string and the belt is considered a beam; this last model is more complex than the stretched string because the equation of the lateral deflection becomes of the fourth order instead of the second.

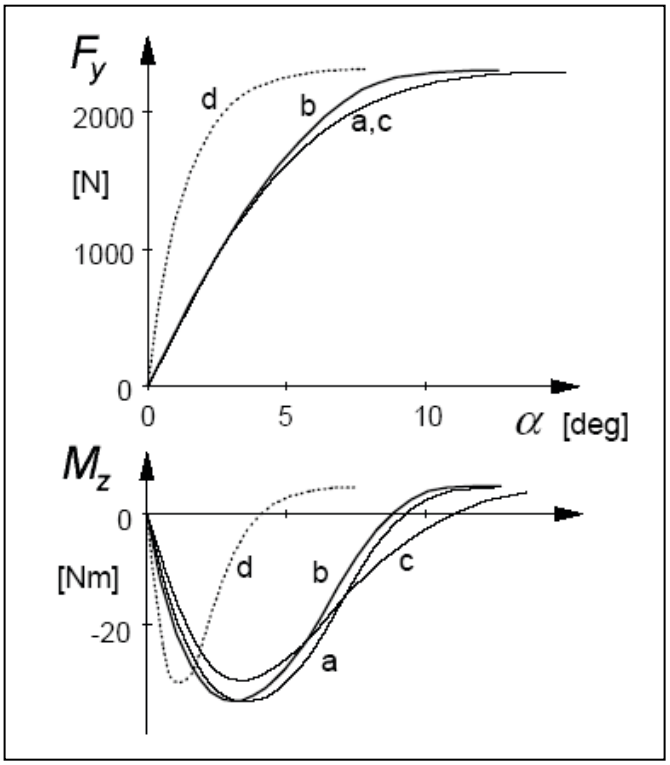

Figure I.2 – Different results with different tire structure models

Anyway, referring at the Figure I.2, the following belts are considered: *a* refers to the stretched string model, *b* is the beam model, *c* is a model proposed by Fiala [1] that considers a symmetric parabolic carcass deflection, and *d* is a rigid belt.

The tread elements stiffness is the same for all the models.

All the models show equal peak value of the lateral force.

This means that choosing the model parameters properly, so that the cornering stiffness of all the model would be the same, all the resulting curves would be identical.

So, the choice of the carcass model has only a limited influence.

These considerations are fundamental to introduce the *brush model* that is based on the concept of a rigid carcass. This model appears very simple in its

hypothesis, and at the same time it gives back very good results in terms of qualitative correspondence with experimental tire behavior.

I.2.1 – The Brush Model

This model consists in a row of elastic bristles (the brushes) that touch the road surface and can deflect in a direction parallel to the road surface itself. Their compliance is a combination of the compliances of carcass, belt and tread blocks.

When the tire is in free rolling conditions, the brushes enter in the contact patch and remain vertical – without any horizontal deformation – from the leading edge to the trailing edge, so without generating any force. The rolling resistance is not considered here.

If the speed vector shows an angle with the longitudinal axis of the tire, a side slip occurs.

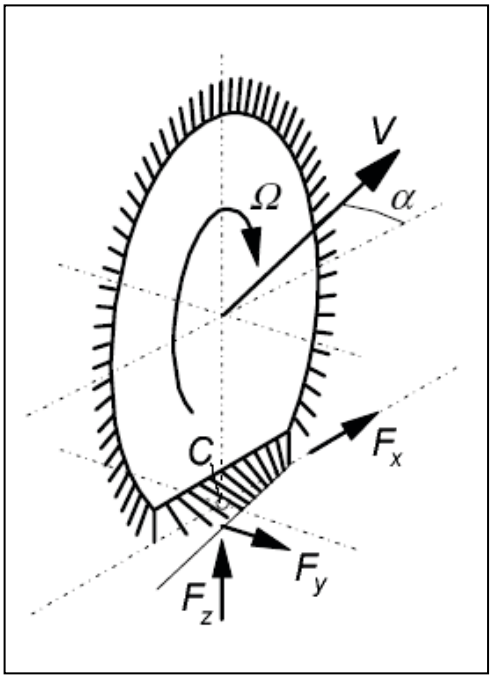

Figure I.3 – The classical Brush model

As showed in the Figure I.3, in these conditions the brushes in the contact patch are deformed along lateral direction reacting with a tangential stress that opposes to this.

In the Figure I.4 the stress field along the contact patch is showed in pure side slip conditions.

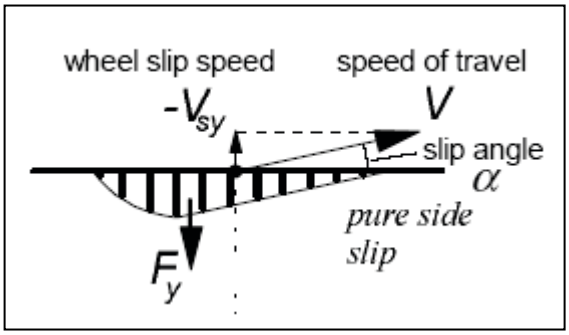

Figure I.4 – Stress field in the contact patch

Moving from the leading edge to the trailing edge the entity of the deformation increases and so the stress too. Anyway the stress in the brushes cannot increase indefinitely of course: when the limit of adhesion is reached, so that is:

$$\tau = \mu \cdot p \qquad (1)$$

where μ is the friction coefficient and p is the local contact pressure, the brush starts to slide against the road surface.

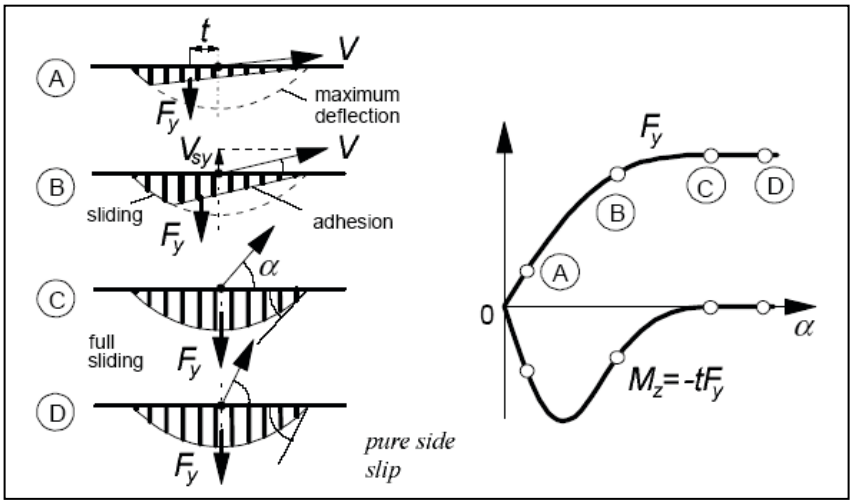

Figure I.5 – Different contact patch conditions for different tire exercise conditions

In the Figure I.5 is highlighted what happens increasing the slip angle: at low values of slip angle (condition A), the most part of the contact patch is in adhesion; being the resulting force not centered, a *pneumatic trail* results causing a self-alignment torque Mz.

When the slip angle increases (condition B), as said before, the part of the contact patch in sliding conditions increases; anyway the lateral force resulting from the lateral stresses increases while the pneumatic trail decreases. So, the

self-alignment torque increases, it reaches a maximum and then decreases again.

With an additional increasing of the slip angle, the entire contact patch slides (condition C) and the lateral force cannot increase further (condition D). Due to the hypothesis that the contact pressure is symmetrical (parabolic), in full sliding conditions the lateral force resulting from the lateral stresses is centered. In consequence the pneumatic trail is null and so the self-aligning torque too.

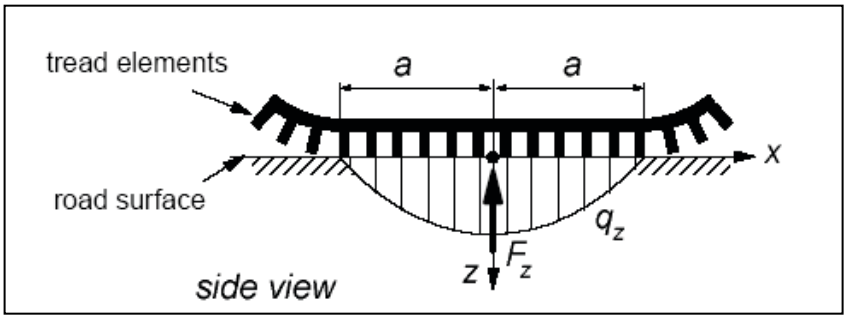

Figure I.6 – Contact pressure distribution at limit

Considering the origin of the reference system in the center of the contact patch (as showed in the Figure I.6), the following equations can be written:

$$F_y = c_{py} \int_{-a}^{a} v\,dx = 2\,c_{py} a^2 \alpha$$

$$M_z = c_{py} \int_{-a}^{a} v\,x\,dx = -\frac{2}{3} c_{py} a^3 \alpha \qquad (2)$$

where *a* is the half contact length.

Consequently, the cornering stiffness and the self-aligning torque stiffness are:

$$C_{F\alpha} = (\partial F_y/\partial\alpha)_{\alpha=0} = 2 c_{py} a^2 \qquad (3)$$

$$C_{M\alpha} = -(\partial M_z/\partial\alpha)_{\alpha=0} = \frac{2}{3} c_{py} a^3$$

The considerations done in lateral conditions can be done in longitudinal of course.

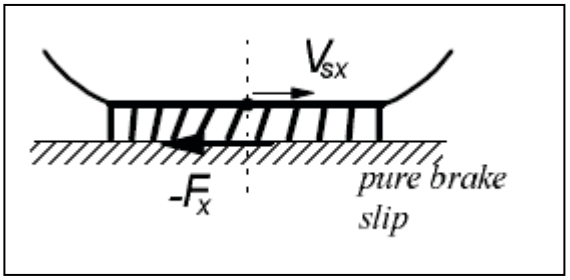

Figure I.7 – Brush model in pure slip conditions

In this case, if a torque is applied on the tire, the brushes are deformed in longitudinal direction reacting with a horizontal stress that results in a longitudinal force. Increasing the slip ratio, the longitudinal stress in the brushes increases until the limit of adhesion is reached; in consequence part of the contact patch starts sliding. If the slip ratio exceeds a critical value, the entire contact patch slides and the longitudinal force saturates.

I.2.2 – The SWIFT Model

The S.W.I.F.T. Model (Short Wavelength Intermediate Frequency Tire Model) has been developed by Zegalaar [30] and Maurice [31] at the University of Delft and it is a relatively simple model that belongs to the third category again.

Respect to the brush model, this model can simulate the behavior of the tire on uneven surfaces with wavelength relatively short (ca. 20 cm and even shorter to modeling road obstacle enveloping).

Furthermore, the presence of traverse road irregularities (cleats) can be modeled.

The peculiarity of the model is to separate the contribution of the carcass and the contact patch.

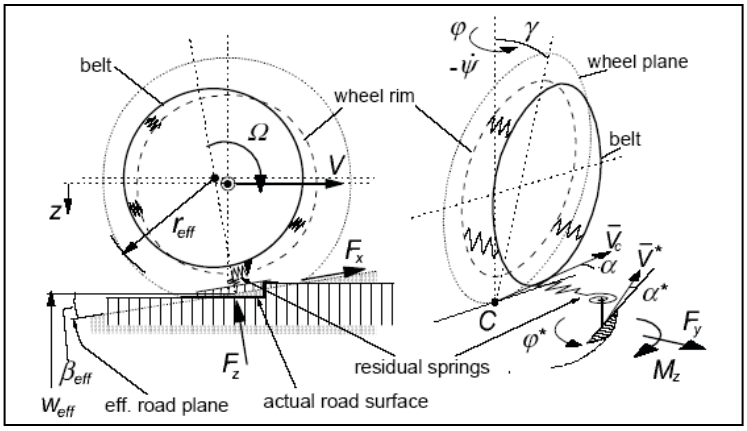

Figure I.9 – The SWIFT Model

The base of the model is the presence of five distinguished elements: the inertia of the belt, so to properly describe the dynamics of the tire; the belt can be considered a rigid circular ring when the excitation frequencies are lower than 60 Hz[1]. The so called residual stiffness has been introduced between the contact patch and the ring to correct the total tire static stiffness; in this way the total compliance of the tire is due to the carcass compliance, the residual compliance and the tread compliance. The brush model is used to model the contact patch behavior in terms of horizontal compliance of the tread elements and the partial sliding phenomenon. This part of the model is the most complex and it allows reducing the wavelength to 20 cm. Three inputs are used to simulate the tire moving on uneven surfaces: the height and slope of the road profile and the effective variations of the rolling radius due to the enveloping of the obstacle by the tire. In the end the Magic Formula is used to describe the non-linear slip force and moments properties.

[1] Below 50-60 Hz all the natural vibrations of a tire are rigid modes.

I.2.3 – The FTire Model

The FTire Model (Flexible ring Tire Model) has been developed by Professor Gisper of Esslingen University of Applied Sciences [32], [33], [34]. Even if this model belongs to the fourth category (complex physical description of the tire parameters) is one of the most popular and used in the automotive industry.
It is a non-linear vibration model; the belt is represented by an extensible and flexible ring elastically founded on the rim and that can be bent in arbitrary directions respect to it.

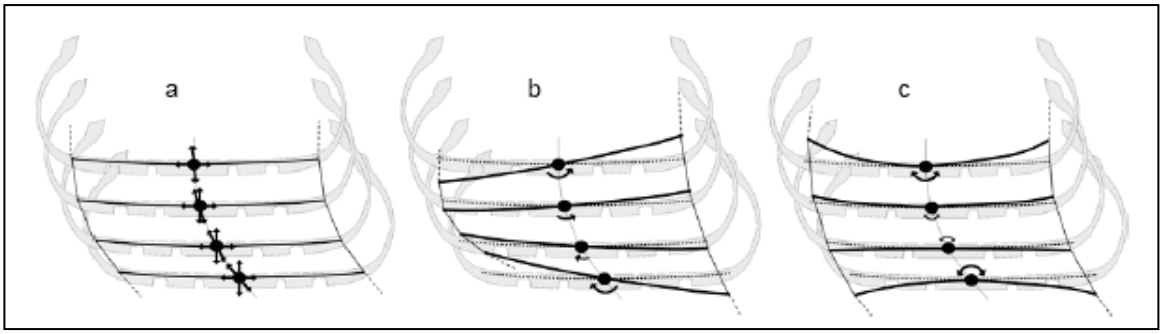

Figure I.10 – The belt DOF in F-Tire model

The ring itself is numerically approximated by a finite number (from 50 to 100) of point masses. These belt elements are coupled with their direct neighbors by stiff springs and by bending stiffness' both in-plane and out-of-plane.
As showed in the Figure I.11, the belt is connected by different stiffness to the rim.

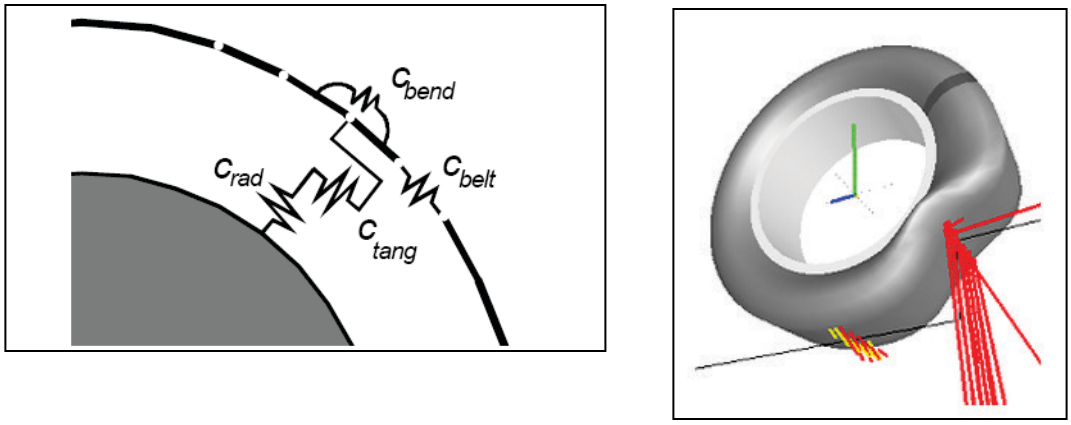

Figure I.11 – Belt and rim connection and the road contact modeling in F-Tire

Between two neighbored belt segments, there are placed a certain number (from 5 to 50) of mass-less contact and friction elements, to model the road contact (Figure I.11).

These elements carry nonlinear stiffness and damping properties in radial, tangential, and lateral direction. Their radial deflections depend on road profile, location and orientation of the associated belt elements.

Combined with a respective suspension or a full vehicle model, FTire can be used for many kinds of investigations such as road-contact induced vibrations along all three directions, up to about 150 Hz; dynamic force reaction to obstacle wave lengths, both in longitudinal and lateral direction, and for sharp-edged obstacles like high cleats; vibration excitation by different kinds of tire imperfections; moving ground and all kinds of test-bench simulations; generation of accurate spatial load histories for durability simulations on measured 3D road surfaces; traction and handling properties on even roads as well as on uneven roads; steering torque amount during parking; tread wear prediction and more.

At the same time, the high number of parameters constituting the model – stiffness, masses, damping coefficients, Eigen frequencies, etc. – requires an

high number of experimental test on the tire followed by a hard identification job.

I.2.4 – RModK Model – Flexible Belt

RModK has been developed by Professor C. Oertel of Brandenburg University of Applied Sciences and A. Fandre of the T-Systems ES GmbH [35], [36]. This model belongs to the fourth category and it is the most complex between the ones analyzed in this dissertation.

Like FTire, RmodK contains two main parts, the structure part and the contact part. The model adopts FE method for the tire belt that is modeled by a nodes network connected each other by rebar elements (Figure I.12).

There are two different rebar elements used in the belt and in the sidewall area.

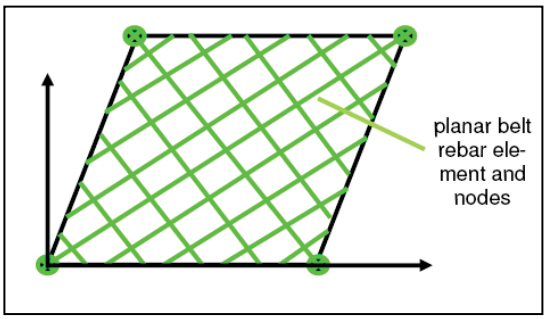

Figure I.12 – The rebar element in RModK

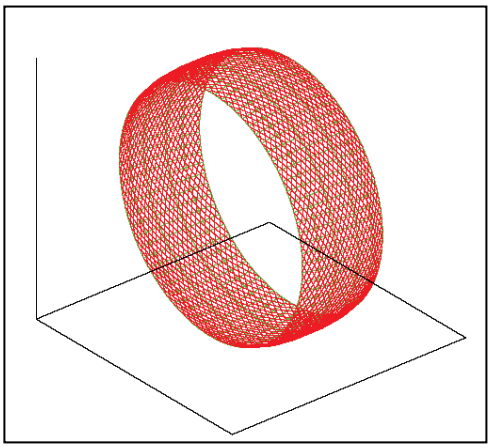

Figure I.13 – The belt modeled in RmodK

Each belt node is characterized by a mass, two bending stiffness (EI_x and EI_y) and longitudinal stiffness EA that differs depending on node position in the network (belt, carcass, torsion and circumferential in the Figure I.14).

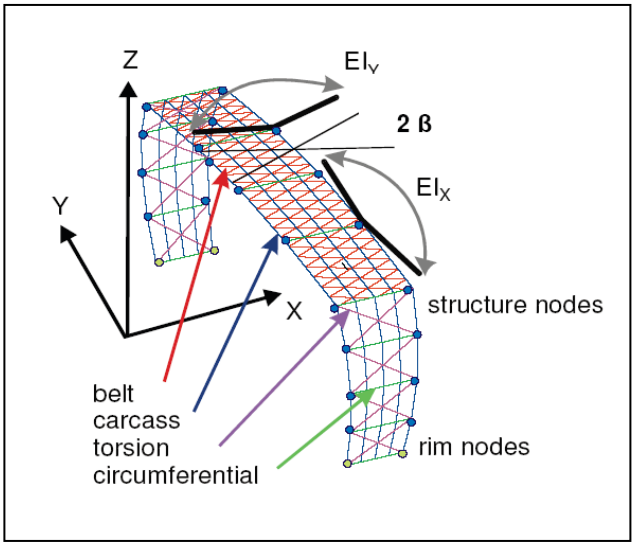

Figure I.14 – The structure of RmodK model

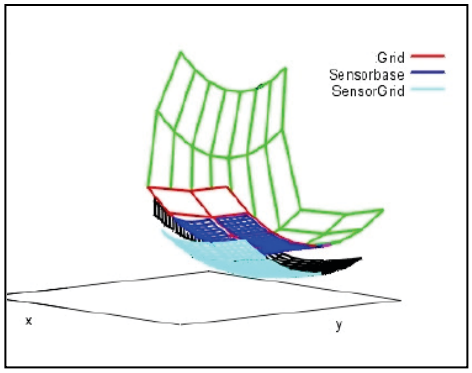

Figure I.15 – the contact sensors grid

Between the belt and the road surface, is placed the so called *contact module* that contains a grid of contact sensors. The numbers of gap sensors can be chosen independently from the structure's nodes grid, while the actual position and velocity of the sensors are calculated using the belt nodes positions and velocities as boundary conditions.

In the tangential direction, contact forces may result from sticking or sliding which is determined from the friction value, the normal contact force, the sliding velocity and the stick/slip state monitor. The normal force distribution is calculated using the gap sensor information and the tread stiffness.

Also RmodK needs a huge phase of parameters identification to be tuned and this passes through an important experimental activity.

I.2.5 – Pacejka Magic Formula

A well-known semi-empirical model is the Magic Formula developed by professor Pacejka from Delft University in 1987 [1]. This model is based on transcend equation – i.e. *sin(arctan(x))* – which provides good fit for F_y, F_x and M_z.

This approach is called semi-empirical because these models are based on measured data but may contain structures that find origin in physical characteristics. The description of the model will be limited to the steady state behavior but a transient version exists.

The Pacejka Magic Formula is based on the Similarity Method that is, in turn, based on the observation that the pure slip curves remain approximately similar in shape when the tire runs at conditions that are different from the reference ones – in terms of vertical load, zero camber angle and zero slip angle. Similar shape means that the characteristics belonging to reference conditions may be regained by vertical and horizontal multiplications and shifting the curve itself.

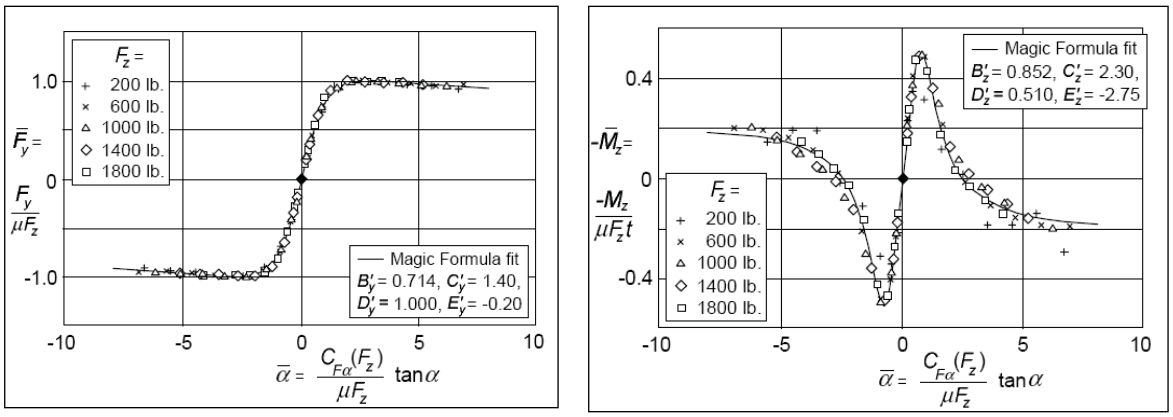

Figure I.16 – The similarity concept

In the Figure I.16 an example of the similarity concept is showed: for the same tire, the raw data obtained at different conditions – in particular in terms of vertical load – have been plotted all together, after they have been normalized in non-dimensional quantities on the axes.

The general form of the formula – for a given values of vertical load and camber angle – is:

$$y = D\sin[C\arctan\{Bx - E(Bx - \arctan Bx)\}] \qquad (4)$$

with:

$$\begin{aligned} Y(X) &= y(x) + S_V \\ x &= X + S_H \end{aligned} \qquad (5)$$

and:

Y is the output that could be F_x, F_y or M_z;
X is the input variable that means of side slip angle or slip ratio;
B is called *stiffness factor*;
C is called *shape factor*;
D is the *peak value*;
E is called *curvature factor*;
S_H is the horizontal shift;
S_V is the vertical shift;

The formula produces a curve that passes through the origin, reaches a maximum and then tends to a horizontal asymptote; an eventually offset respect to the origin is managed by the shifts S_H and S_V.

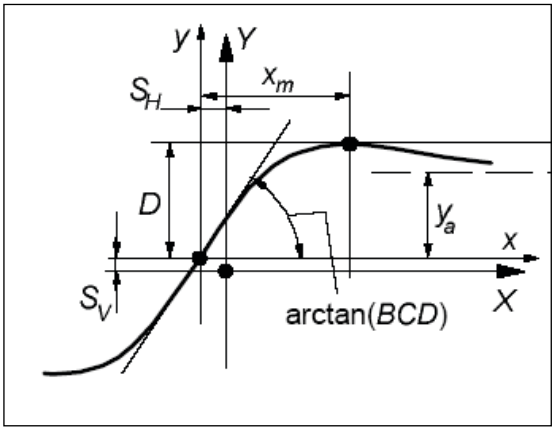

Figure I.17 – Pacejka model

The coefficient *D* represents the peak value of the force (as showed in the Figure I.17); the coefficient *C* manages the limits of the sine function determining the shape of the curve; the coefficient *B* controls the slope in the origin – in fact the slope in the origin is given by the product *BCD*.
Starting from the peak value *D* and the horizontal asymptote it is possible to compute the *C* factor:

$$C = 1 \pm \left(1 - \frac{2}{\pi} \arcsin \frac{y_a}{D} \right) \qquad (6)$$

while from *B*, *C* and the location of the peak value (x_m) the coefficient *E* can be computed:

$$E = \frac{Bx_m - \tan\{\pi/(2C)\}}{Bx_m - \arctan(Bx_m)} \quad (\text{if } C>1) \qquad (7)$$

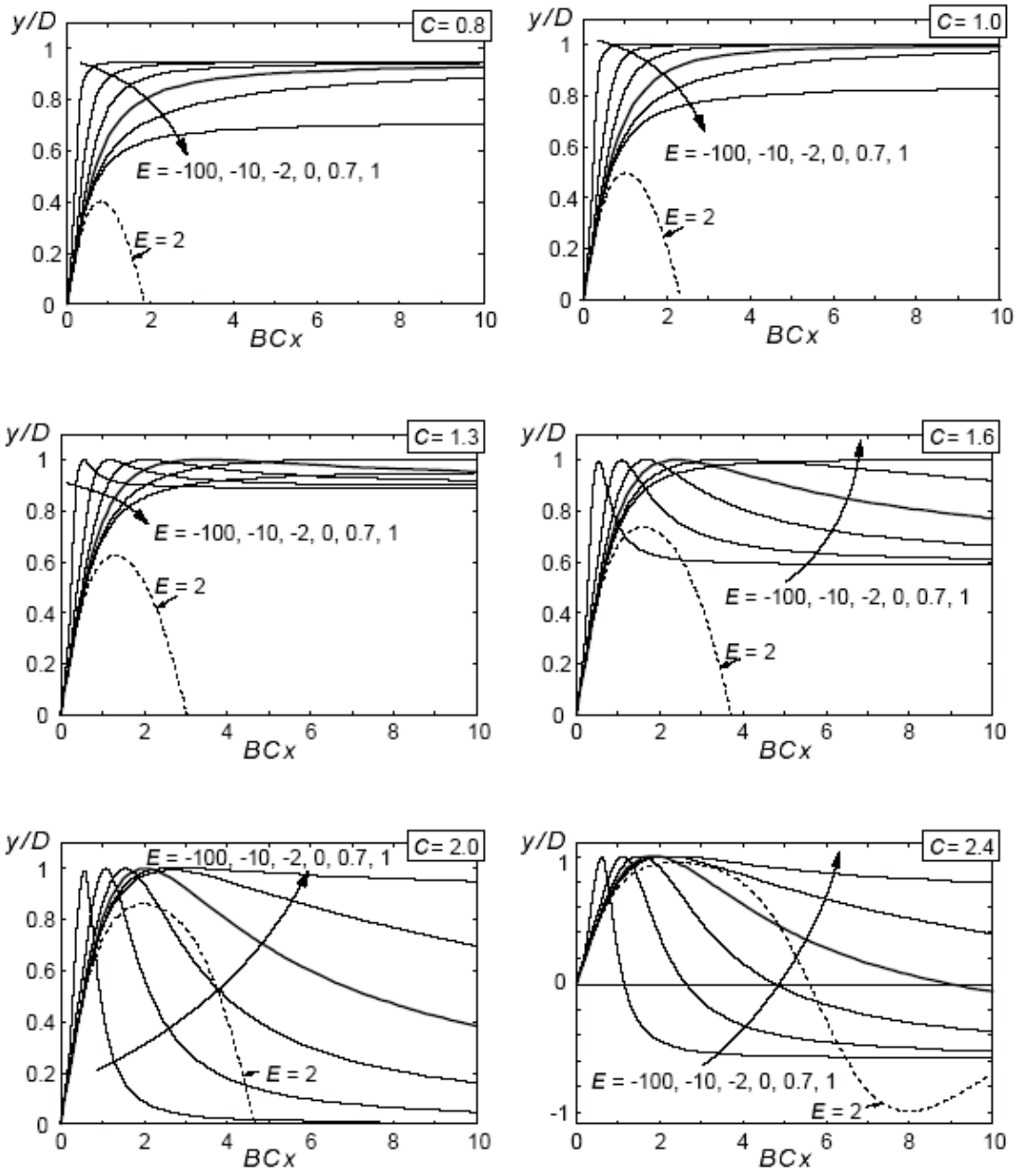

Figure I.18 – Pacejka results changing the parameters

In the Figure I.18 different curves are obtained changing all the coefficients.

As said, the formula seen in the previous pages is obtained at a given value of vertical load and camber angle; the coefficients *B*, *C*, *D* and *E* are called *macro-parameters*.

The similarity method is based on the concept that moving from the reference conditions the resulting curve can be obtained multiplying the coefficients by a gain.

All the macro-parameters can be so related to *micro-parameters* that take into account the influence of vertical load and camber angle. So, the full set of equations of the Magic Formula is – in case of pure longitudinal slip:

$$F_{xo} = D_x \sin[C_x \arctan\{B_x\kappa_x - E_x(B_x\kappa_x - \arctan(B_x\kappa_x))\}] + S_{Vx} \qquad (8)$$

$$\kappa_x = \kappa + S_{Hx}$$

$$C_x = p_{Cx1} \cdot \lambda_{Cx} \qquad (>0)$$

$$D_x = \mu_x \cdot F_z \cdot \zeta_1 \qquad (>0)$$

$$\mu_x = (p_{Dx1} + p_{Dx2} df_z) \cdot \lambda_{\mu x} / (1 + \lambda_{\mu V} V_s / V_o) \qquad (>0)$$

$$E_x = (p_{Ex1} + p_{Ex2} df_z + p_{Ex3} df_z^2) \cdot \{1 - p_{Ex4} \operatorname{sgn}(\kappa_x)\} \cdot \lambda_{Ex} \qquad (\leq 1)$$

$$K_{x\kappa} = F_z \cdot (p_{Kx1} + p_{Kx2} df_z) \cdot \exp(p_{Kx3} df_z) \cdot \lambda_{Kx\kappa}$$
$$(= B_x C_x D_x = \partial F_{xo} / \partial \kappa_x \quad \text{at } \kappa_x = 0) \quad (= C_{F\kappa})$$

$$B_x = K_{x\kappa} / (C_x D_x + \varepsilon_x)$$

$$S_{Hx} = (p_{Hx1} + p_{Hx2} df_z) \cdot \lambda_{Hx}$$

$$S_{Vx} = F_z \cdot (p_{Vx1} + p_{Vx2} df_z) \cdot \{|V_{cx}| / (\varepsilon_{Vx} + |V_{cx}|)\} \cdot \lambda_{Vx} \cdot \lambda'_{\mu x} \cdot \zeta_1$$

where is:

$$df_z = \frac{F_z - F'_{zo}}{F'_{zo}} \qquad (9)$$

with F_z the considered vertical load and F'_{zo} the reference vertical load.

All the λ in the formulas are scaling factors.

Instead the equations in case of pure side slip are:

$$F_{yo} = D_y \sin[C_y \arctan\{B_y\alpha_y - E_y(B_y\alpha_y - \arctan(B_y\alpha_y))\}] + S_{Vy} \qquad (10)$$

$$\alpha_y = \alpha^* + S_{Hy}$$

$$C_y = p_{Cy1}\cdot\lambda_{Cy} \qquad (>0)$$

$$D_y = \mu_y \cdot F_z \cdot \zeta_2$$

$$\mu_y = (p_{Dy1} + p_{Dy2}df_z)\cdot(1 - p_{Dy3}\gamma^{*2})\cdot\lambda_{\mu y}/(1+\lambda_{\mu V}V_s/V_o) \qquad (>0)$$

$$E_y = (p_{Ey1} + p_{Ey2}df_z)\cdot\{1 - (p_{Ey3} + p_{Ey4}\gamma^*)\,\mathrm{sgn}(\alpha_y)\}\cdot\lambda_{Ey} \qquad (\le 1)$$

$$K_{y\alpha o} = p_{Ky1}F'_{zo}\sin[2\arctan\{F_z/(p_{Ky2}F'_{zo})\}]\cdot\lambda_{Ky\alpha}$$
$$(= B_yC_yD_y = \partial F_{yo}/\partial\alpha_y \text{ at } \alpha_y = \gamma = 0) \quad (= C_{F\alpha})$$

$$K_{y\alpha} = K_{y\alpha o}\cdot(1 - p_{Ky3}\gamma^{*2})\cdot\zeta_3$$

$$B_y = K_{y\alpha}/(C_yD_y + \varepsilon_y)$$

$$S_{Hy} = (p_{Hy1} + p_{Hy2}df_z)\cdot\lambda_{Hy} + p_{Hy3}\gamma^*\cdot\lambda_{Ky\gamma}\cdot\zeta_0 + \zeta_4 - 1$$

$$S_{Vy} = F_z\cdot\{(p_{Vy1} + p_{Vy2}df_z)\cdot\lambda_{Vy} + (p_{Vy3} + p_{Vy4}df_z)\gamma^*\cdot\lambda_{Ky\gamma}\}\cdot\lambda'_{\mu y}\cdot\zeta_2$$

$$K_{y\gamma o} = \{p_{Hy3}K_{y\alpha o} + F_z(p_{Vy3} + p_{Vy4}df_z)\}\lambda_{Ky\gamma}$$
$$(= \sim\partial F_{yo}/\partial\gamma \text{ at } \alpha = \gamma = 0) \quad (= C_{F\gamma})$$

The reader is invited to focus the attention to the Cornering Stiffness equation,

$$K_{y\alpha o} = p_{Ky1} F'_{zo} \sin[2 \arctan\{F_z/(p_{Ky2} F'_{zo})\}] \cdot \lambda_{Ky\alpha}$$
$$(= B_y C_y D_y = \partial F_{yo}/\partial \alpha_y \text{ at } \alpha_y = \gamma = 0) \quad (= C_{F\alpha}) \tag{11}$$

because it will come back in the next chapters: the proposed model – in fact – exactly acts on this equation.

Chapter II – The Temperature Influence on Tire

Because the tire is composed mainly by rubber, in this chapter a short dissertation on the behavior of viscoelastic materials will be done. In particular, how the temperature – and frequency – influences their mechanical properties will be discussed.
Furthermore, the heat generation modes in a tire (the *friction power* and *strain energy loss*) will be presented.
In the end, basing on literature, how the temperature influences the grip and the cornering stiffness will be showed.

II.1 – The concept of the Viscoelasticity

As known, the classical theory of elasticity that asserts – in accordance with the Hooke's law – in small deformations, that the stress is directly proportional to the strain and independent on the strain rate, and the classical theory of the hydrodynamics that asserts – in accordance with the Newton's law – that the stress is directly proportional to the strain rate and independent on the strain itself, are idealizations. Moreover, in nature some materials are that exhibit both solid like and liquid like characteristics; these materials are so called viscoelastic.

II.1.1 – Behavior with frequency

The elastic materials such as the most part of the metals follow the Hooke's law:

$$\sigma(t) = E \cdot \varepsilon(t) \qquad (12)$$

This means that there is an instantaneous relationship between the stress and the strain in an elastic material.
In other words, as soon as the force put on to the material is released, it immediately goes back to its original shape. Viscoelastic materials on the other hand exhibit viscous effects. The viscous effect acts as a form of damping, which means that when the stress is released, the material will come back to its original shape *slowly*.

For a viscoelastic material we have dependence on time between the stress and the strain.

This means that when it is forced by a sinusoidal displacement:

$$\varepsilon_1 = \varepsilon_1^0 \cdot \sin(\omega t) \qquad (13)$$

this reacts with a sinusoidal stress characterized by the same frequency but *delayed* respect to the strain:

$$\sigma_1 = \sigma_1^0 \cdot \sin(\omega t + \delta) \qquad (14)$$

The stress can be described by the sum of two contributions: one in phase with the strain and the second one phased by 90°:

$$\sigma_1 = \varepsilon_1^0 \cdot (E' \cdot \sin(\omega t) + E'' \cdot \cos(\omega t)) \qquad (15)$$

The E' is so called *Storage Modulus* while E'' is so called *Loss Modulus* and is:

$$E' = \left(\frac{\sigma_1^0}{\varepsilon_1^0}\right) \cdot \cos\delta$$

$$E'' = \left(\frac{\sigma_1^0}{\varepsilon_1^0}\right) \cdot \sin\delta \qquad (16)$$

That involves in:

$$\frac{E''}{E'} = \tan\delta \qquad (17)$$

The same considerations can be done for the shear moduli G' (=1/E') and G'' (=1/E''). In the Figure II.1 the dependence on oscillation frequency is showed for G' and G''.

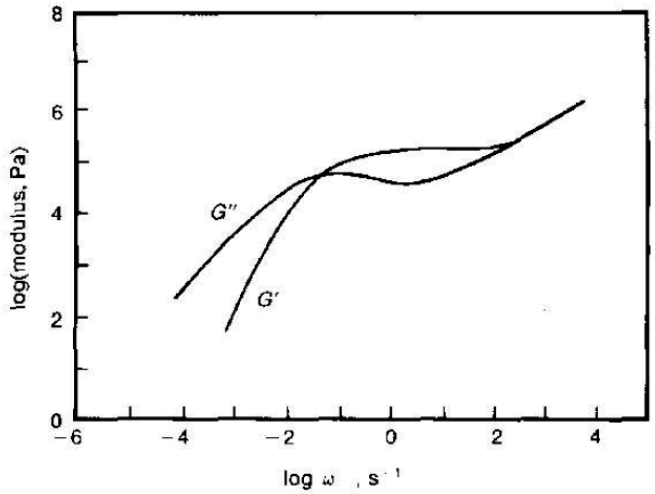

Figure II.1 – The Modulus in dependence on frequency

Omitting the behavior at the highest frequencies (that means 10 Hz and beyond), the figure shows that G' increases with the frequency squared until it reaches a plateau at high frequencies. G'' instead increases proportionally with the frequency, it reaches a maximum and then decreases.
This behavior can be well described with the Maxwell model [24]:

$$G' = G \cdot \frac{(\tau\omega)^2}{1 + (\tau\omega)^2}$$

$$G' = G \cdot \frac{\tau\omega}{1 + (\tau\omega)^2} \qquad (18)$$

where:

G is the elastic modulus measured in static conditions;
τ is a time constant;
ω is the oscillation frequency;

II.1.2 – Behavior with temperature

The Modulus of a viscoelastic material is proportional with the temperature.

$$G = avkT \qquad (19)$$

where:

ν is the density of polymeric chains;
k is the Boltzmann constant;
T is the absolute temperature;
a is a coefficient

Considering the expressions (18) of Maxwell model the reader will notice that the frequency response of a viscoelastic material is not dependent on frequency and relaxation time separately but both G' and G'' depend on their product. This means that Moduli measured at the same product $\tau\omega$ are equal. This concept is known as the Time Temperature Superposition (TTS).

To better understand this concept, a material characterized by a relaxation time τ_0 measured at the temperature T_0 will be considered.
In these conditions the G' will be:

$$G'(T_0, \omega) = G \cdot \frac{(\tau_0\omega)^2}{1+(\tau_0\omega)^2} \qquad (20)$$

If the material will be characterized at a different temperature T, so that the relaxation time will be τ, the material will show the same G' at a certain frequency $\bar{\omega}$ so that:

$$\tau_0 \omega = \tau \bar{\omega} \qquad (21)$$

That means:

$$\bar{\omega} = \frac{\tau_0}{\tau} \omega = \frac{1}{a_T} \omega \qquad (22)$$

where a_T is so-called *shift parameter* and it depends only on the new temperature T once the reference temperature T_0 has been fixed.

So, the following relationship exists between the G' moduli measured at the two different temperatures:

$$G'(T_0, \omega) = G'\left(T, \frac{\omega}{a_T}\right) \qquad (23)$$

All these considerations are valid for all the rheological properties of the viscoelastic materials.
Analyzing the Figure II.2, the concept of the shift factor will be clarified.

In this figure the G' modulus is measured at two different temperatures. As showed, the curves present very different shapes and values.

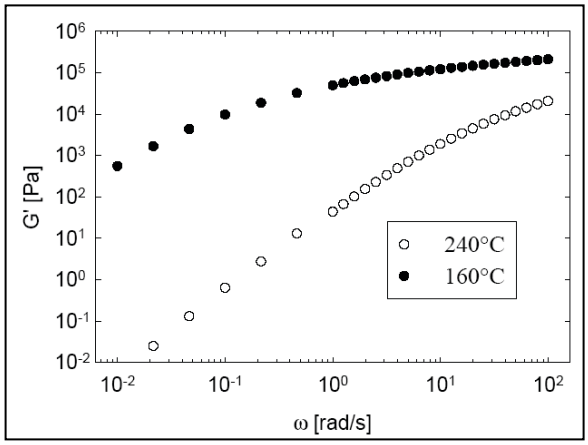

Figure II.2 – Modulus vs. frequency measured at two different temperatures

Anyway, due to the TTS principle, it is possible to multiply the G' measured at 160° C by a shift factor so to superimpose the curve at 160 on the curve measured at 240°C. In particular, using a shift factor a_t=395, the plots of Figure II.3 are obtained.

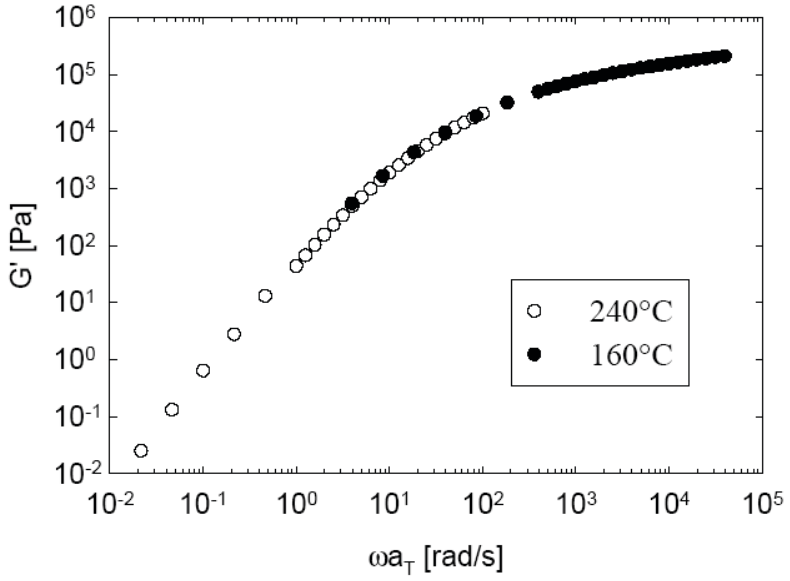

Figure II.3 – The TTS principle

It is important to underline that the shift factor allows knowing the rheological parameters in dependence on temperature, but it even allows enlarging the

frequency domain of the rheological measurements. In fact, in the previous Figure II.2 both the measurements were made between 10^{-2} and 100 rad/s while with the shift factor one curve has obtained from 10^{-2} to 10^{5} rad/s. The curve obtained in the Figure II.3 is called *master curve* at the reference temperature (in this case 240°C).

This means that knowing the shift factor at a certain reference temperature it is possible to know the rheological characteristics at any needed temperature and it is always possible to obtain the master curve at the reference temperature.

The most known model used to evaluate the shift factor for one certain reference temperature is the WLF equation [2], [17]:

$$\log a_T = -\frac{C_0^1 \cdot (T - T_0)}{C_0^2 + (T - T_0)} \qquad (24)$$

where:

T_0 is the reference temperature;
C_0^1 and C_0^2 are two empirical coefficients;

In their paper the authors explain that the values of -8.86 and 101.6 work well for many polymeric materials for C_0^1 and C_0^2. Especially for the modern synthetic rubbers, the two coefficients should be identified through measurements at different temperatures and different frequencies. Anyway, in the proposed model, when the identified parameters were not available, the twos suggested by authors have been used.

II.2 – The heat generation modes in the tire

II.2.1 – The Friction Power

When it interacts with the road, for example in lateral direction, the tire must experience *lateral slip* in order to generate lateral force.

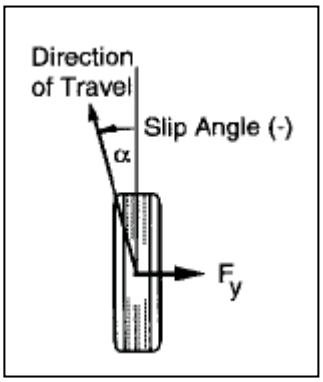

This requires that the direction of the travel is not parallel to the direction of the heading.
The angle between these two directions is called *slip angle* and the following relationship subsists:

$$\tan \alpha = -\frac{V_y}{V_x} \qquad (25)$$

Figure II. 4– The tire slip angle

The higher the slip angle the higher the lateral force generated by the tire.

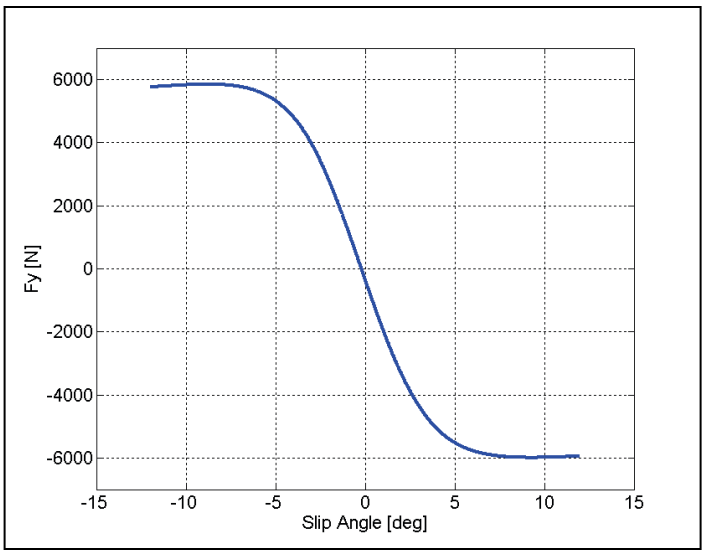

Figure II.5 – The lateral characteristic of a tire

As showed in the Figure II.5, the lateral force increases linearly with the slip angle until 1 deg circa; then the force increases less than proportionally until a peak located at 7-8 deg for this tire; beyond this value, the force saturates even lightly decreasing.

This behavior can be explained considering the contact patch conditions in dependence on slip angle.

Considering a tire fitted on a vehicle, the lateral force is generated because the contact patch is deformed under the centrifugal force acting on the rim hub and the tire reacts with a force opposing this deformation; it is evident that the force cannot increase indefinitely: increasing the slip angle beyond 1 degree part of the contact patch starts sliding against the ground because in these parts the limit of adhesion is reached (this until 6-7 degrees). Because part of the contact patch is in adhesion and part is in sliding, the tire is considered in so called *pseudo-sliding* conditions. Increasing the slip angle again, the entire contact patch goes in sliding and the lateral force cannot increase further (from 7-8 degrees ahead).

Because the tire in cornering is usually in pseudo-sliding conditions – that means part of the contact patch slides against the road surface – a certain

quantity of heat is always generated at the interface between tire tread and roadway.
The power dissipated can be written as:

$$P = F_y \cdot V_y \qquad (26)$$

It is evident that part of this thermal power is dissipated through the convection with air around the tire and through the conduction with ground and part of this tends to flow into the bulk of the tire – if the bulk is colder than the outer surface of course.

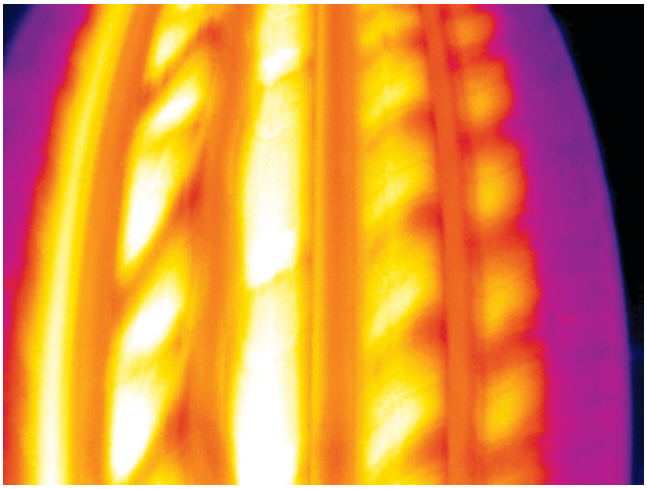

Figure II.6 – The tire surface temperature measured by thermo camera

The same considerations done in lateral conditions can be done in longitudinal conditions.
When a torque is applied to the rim hub – in braking or in traction – the contact patch is deformed and the tire reacts with a longitudinal force so that:

$$M_y = F_x \cdot R_L \qquad (27)$$

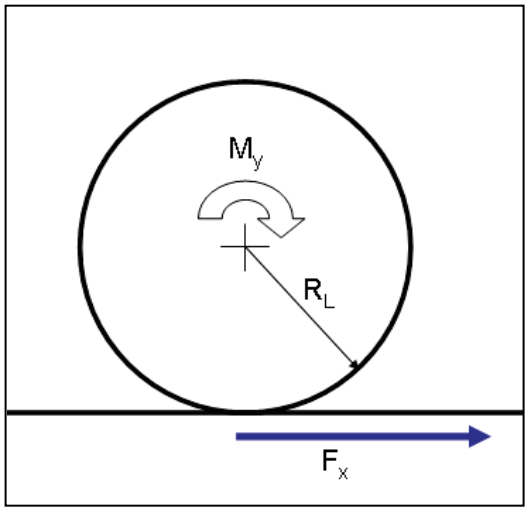

Figure II.7 – Relationship between My and Fx

As described in lateral interactions, as in longitudinal interactions part of the contact patch starts sliding if the torque is increased. The percentage between the sliding speed and the roadway speed is called *slip ratio*:

$$SR = \frac{V_x - R_R \cdot \Omega}{V_x} \qquad (28)$$

The longitudinal force can increase until the entire contact patch goes in sliding so the force reaches a peak and then saturates.

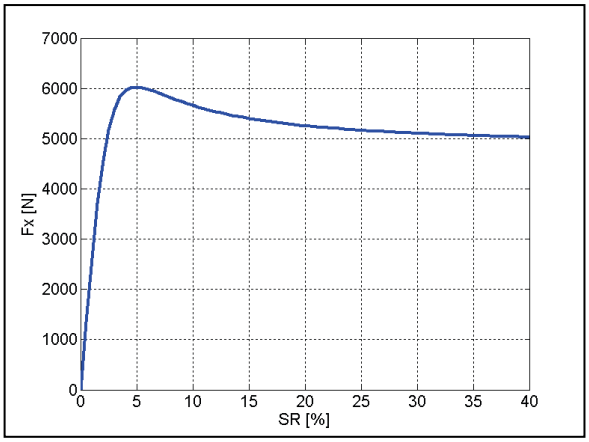

Figure II.8 – Longitudinal characteristic of a tire

II.2.2 – The Strain Energy Loss

As well known, the tire is deflected under the vertical load that means it is always deformed during its exercise.

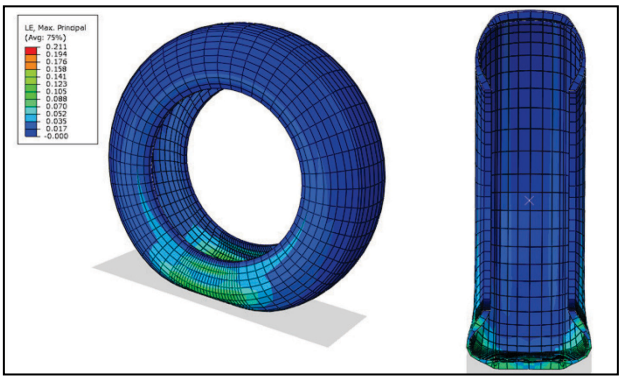

Figure II.9 – FEM simulation of tire deflection

The entity of the deflection depends on multiple parameters: the vertical load, the inflation pressure, the carcass stiffness, etc.

Anyway, being the rubber a viscoelastic material, each part of the tire that deflects every revolution is subjected to a hysteresis cycle. This means that not all the energy is returned when the material relaxes; part of this energy in fact is dissipated in heat.

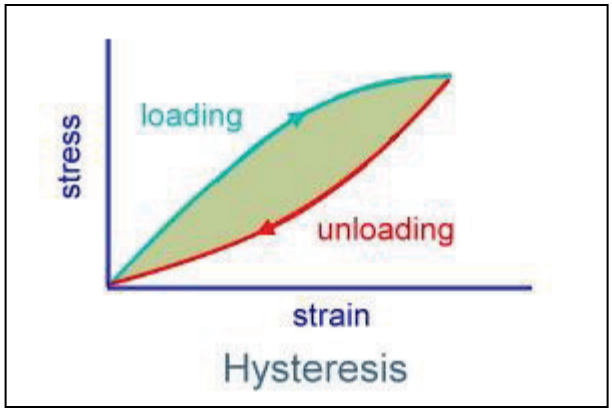

Figure II.10 – Hysteresis cycle

Because in a hysteretic cycle the unloading phase is not equal to the loading phase the contact pressure distribution along the contact patch is not uniform so the resultant force is not aligned with the contact patch center, but it is always ahead (Figure II.11).

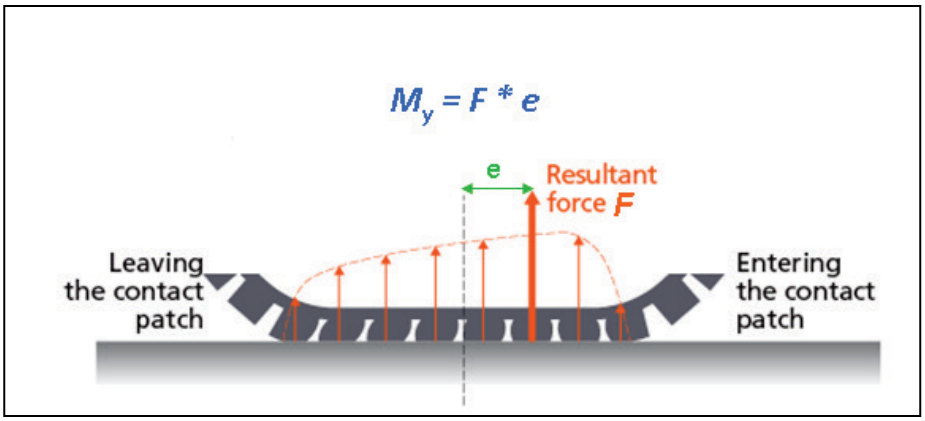

Figure II.11 – The concept of tire rolling resistance

All these considerations involve in a resistant moment that contrasts the motion and that establishes the *rolling resistance* of the tire.

Evidently, the power dissipated in hysteresis can be computed as:

$$\dot{E}_{diss} = M_y \cdot \omega \qquad [W] \qquad (29)$$

when the tire is in free-rolling conditions of course.

As will be showed in the indoor and outdoor experimental activity chapters, the Strain Energy Loss is the main heat generation mechanism for the bulk[2] warm-up.

The tire rubbery components follow the WLF law for what concern the *tand* dependence on temperature and frequency; this is in line with the common know-how [23], [26], [16]: the rolling resistance depends on the compound viscoelastic properties.

[2] With *bulk* term everything is between tread surface and inner liner of the tire will be mean.

When the tire is in traction – or braking – or when the tire is in cornering, the deformations are more complex than the simple tire deflection exposed above (Figure II.12).

These deformations concur to the strain energy loss generation of course; anyway, in the actual version of the proposed model they are not considered.

Figure II.12 – Tire deformation in corner

II.3 – How the temperature influences the handling performance

II.3.1 – Influence of the temperature on tire grip

The influence of the temperature on rubber friction is well-known for at least 60 years when Schallamach [37] experimentally observed the decreasing of the *"pulling force"* with the temperature increasing.

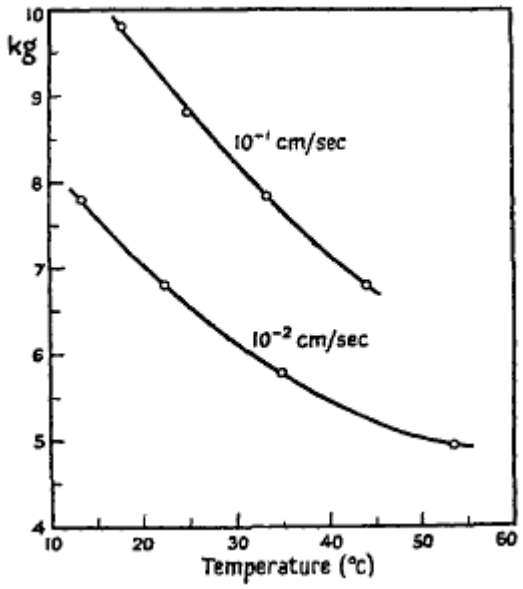

Figure II.13 – Temperature influence on Schallamach studies

To understand the relationship between temperature and friction it could be useful to touch on the mechanism of rubber friction following the theories proposed by Kummer [38] and by Persson later [39].

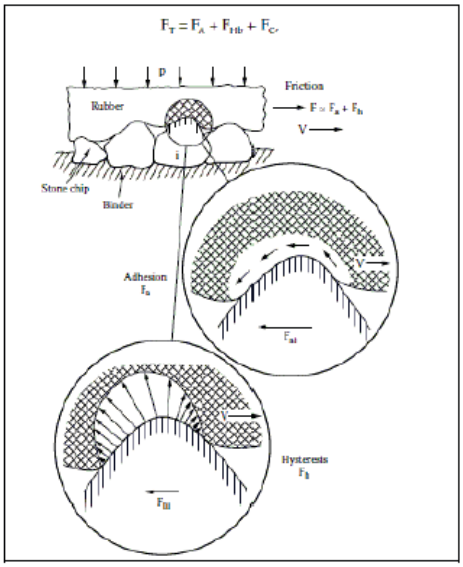

Figure II.14 – The friction mechanism by Persson

Referring to the Figure II.14, the rubber friction should be due to different contributions: an adhesive component, a hysteretic component and a contribution due to the wear (Persson considers only the first two components believing negligible the last one).
So, in dry conditions the friction force can be written as:

$$F_T = F_A + F_{Hb} + F_C \qquad (30)$$

where: F_T is the total frictional resistance, F_A is the adhesive contribution due the Van der Waals' forces between the two surfaces, F_{Hb} is the contribution due to the bulk deformation hysteresis in the rubber and F_c is the contribution due to the removal of the rubber material by the road asperities (that seems to weigh no more than 2%). For what concern the first two contributions Kummer considered them not independent because adhesion increases the extension of the contact area and consequently the zone affected by hysteretic deformations.

Persson hypothesized that the different components are predominant on different scales: the hysteretic contribution is associated with the long-wavelength surface roughness while the adhesion deforms the rubber at short-wavelength roughness.

Because the friction is caused by hysteretic deformations in the rubber it follows that the friction is directly related to the viscoelastic properties of the rubber itself. This means that the friction shows similar trend of the loss Modulus *E''* – i.e. *tand* – of the compound. Thus, increasing the temperature involves in a decreasing of the friction.
Reader is invited to focus his attention on the Modulus curve too in Figure II.15: when the temperature decreases, even if the *tand* increases (until 0°C in this case), the *E'* (or *G'*) increases too involving in a reduction of the *real contact area*. So, even decreasing the temperature the tire friction reduces. Evidently an optimal combination of *tand* and *E'* that maximizes the tire friction exists.

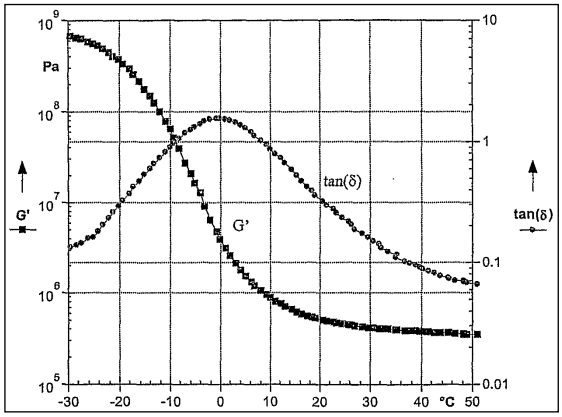

Figure II.15 – G' and tand curves in dependency on temperature

As said the friction follows the viscoelastic behavior of the rubber, so now it is easy to better understand the two curves plotted by Schallamach (Figure II.13 and Figure II.16): increasing the sliding velocity (from 0.01 cm/s to 0.1 cm/s)

means increasing the oscillation frequency of the rubber; the *tand* increases and in consequence the friction increases too.

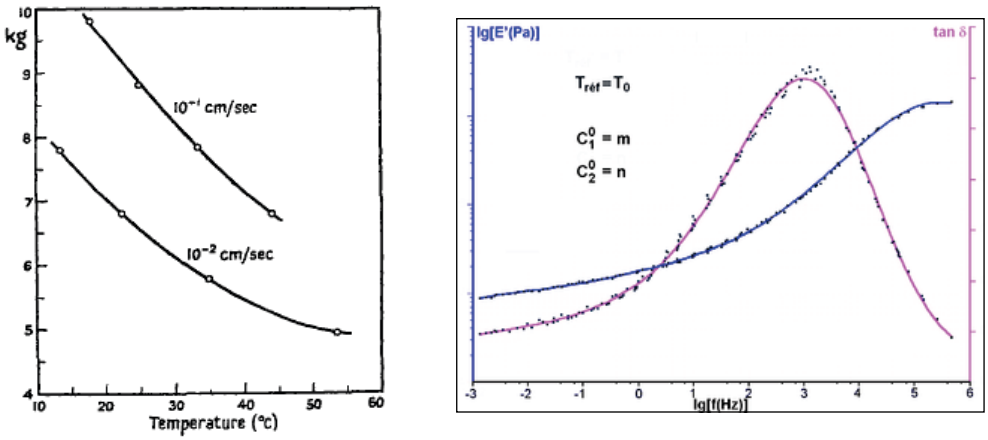

Figure II.16 – Relationship between frequency and temperature for viscoelastic materials

Because the hysteretic deformations dissipate heat, it is clear that the friction between rubber and road is always associated with heat generation at the interface. This concept is clearly explained by Persson [40] who introduces also the concept of *flash temperature*.

Being the friction related to the tread compound characteristics, it is clear that all these considerations are referred to the *surface temperature* – that means the temperature of a very thin layer of the outer surface of the tire (Figure II.17). In the next Chapter III it will be showed how the surface temperature is deeply different from the *bulk temperature* – that means instead the temperature of the core of the tire.

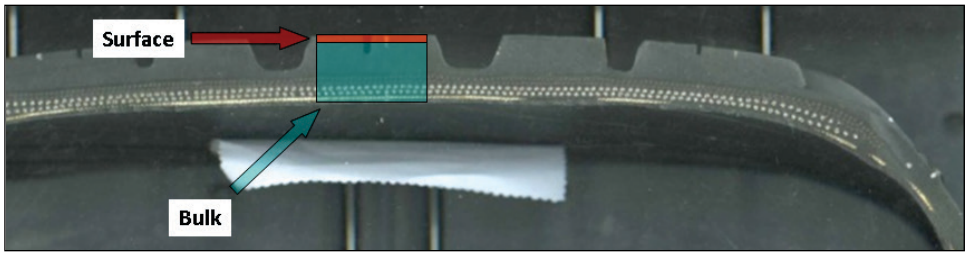

Figure II.17 – The surface and bulk concept

II.3.2 – Influence of the temperature on tire cornering stiffness

The influence of the bulk temperature on tire cornering stiffness will be deeply showed in the next Chapter III. Anyway, herein it could be interesting to make some considerations on this item.

The phenomenon has been investigated during last years. In [16**]** the authors demonstrated that changing the ambient temperature the tire cornering stiffness changes consequently.
As mentioned in the tire models section (ref. Chapter I), the cornering stiffness is directly related to the lateral stiffness of the tire. The lateral stiffness itself consists of the belt stiffness contribution and the tread stiffness contribution; both of them are related to the elastic modulus [15] (Young Modulus in case of steel belt and Storage Modulus in case of rubber) that is well known temperature dependent at least for viscoelastic materials.

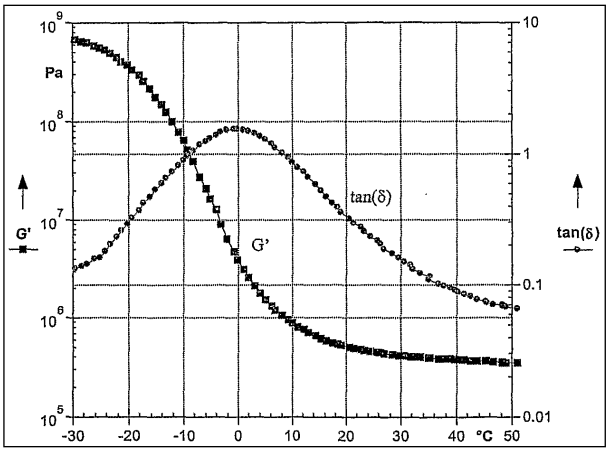

Figure II.18 – G' and tand in dependence on temperature

In the dedicated section, it will be showed that it is not the surface temperature influencing the cornering stiffness but the bulk temperature. This should be not surprising because for a passenger tire the cornering stiffness is influenced by the block stiffness that belongs to what we are calling bulk – as showed in the Figure II.17.

Chapter III – The Indoor Experimental Activity

In this chapter all the indoor experimental activity will be showed.
The first part is about a methodology developed during last years by Department of Industrial Engineering (DIME) of University of Naples Federico II to evaluate the *equivalent* thermal conductivity of the tire; it is useful to show these results for two main reasons:

1. The University of Naples activity demonstrated that the tire is a very isolating material. So, the heat generated by the friction power rather than by the SEL, flows with difficulty through the different layers of the tire itself.
2. In the thermal model proposed in the Chapter V, the thermal conductivity used is based on this evaluations;

The second part is about the test campaign performed in Bridgestone Technical Center Europe indoor laboratories. The influence of the bulk temperature on cornering stiffness has been deeply investigated. To do this, T3M sensors technology, developed by TÜV Automotive, has been used. These are thermo-resistances that can be inserted into the tire to measure the bulk temperature in real-time.
All the tests have been performed in the linear range of the tire characteristic to get the friction power negligible. So, the only heat generation in the tire was the SEL.

III.1 – The Thermal Conductivity evaluation

The Department of Industrial Engineering (DIME) of University of Naples Federico II has conducted an interesting activity on the thermal conductivity evaluation through indirect measurements on tire [28].
The concept is to use a particular in-house thermal model [42] to identify an equivalent thermal conductivity able to simulate the thermodynamically behavior of the entire tire.
As known the tire is a composite material characterized by different layers with different properties: different synthetic rubbers for tread, under-tread etc., plastic fibers (rayon, nylon etc.) for carcass, steel for belt and others.

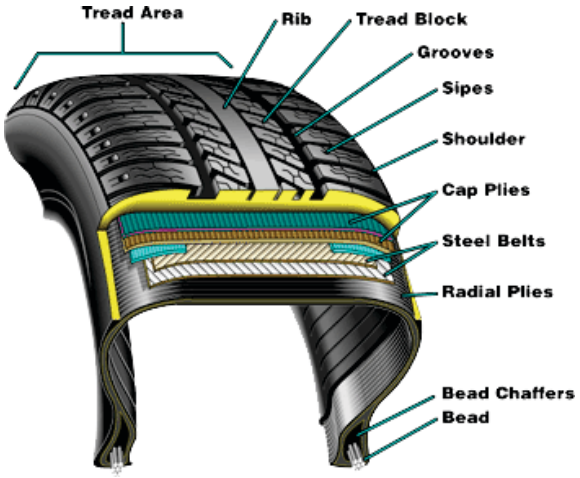

Figure III.1 – The tire structure

Even if each of these materials is characterized by different thermodynamically properties, the experimental activity conducted by DIME showed that the thermodynamic behavior can be well described using two equivalent thermal conductivities. The first one (K_1) is used for the tread surface and the second one (K_2) is used for the bulk and inner-liner (Figure III.2).

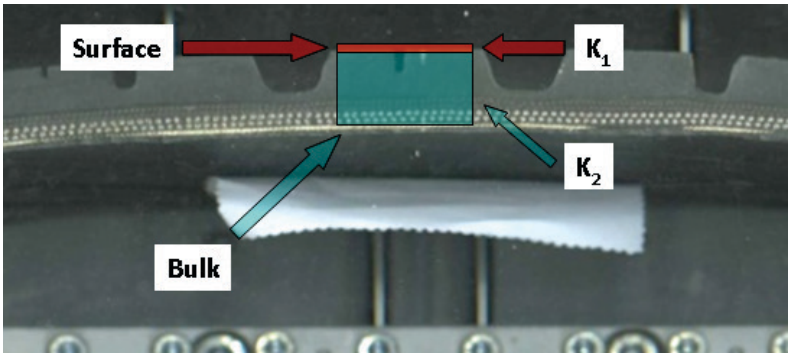

Figure III.2 – The equivalent thermal conductivities

Anyway, the evaluation procedure is characterized by two steps:

- Experimental test on the tire using a laser to warm-up a spot on the tread;

- Reverse engineering to identify the thermal conductivity using a thermal model;

III.1.1 – Experimental Test

The layout of the experimental activity is showed in the scheme below (Figure III.3). A laser is used to warm-up a local spot (1 cm^2) on the tread surface of a tire. The output power of the laser can be changed with continuity from 0 to 3 W. The laser spot diameter is set using a focal lens.

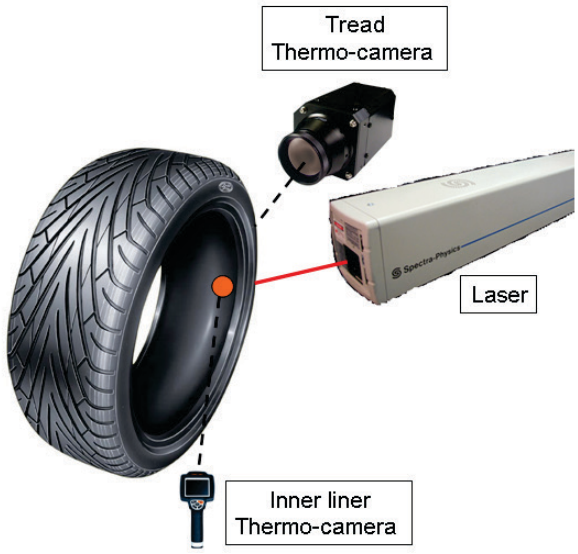

Figure III.3 – The experimental test layout

A thermo-camera is used to acquire the outer surface temperature in correspondence of the laser spot. A second thermo-camera is used to acquire the inner-liner temperature in correspondence of the laser spot.
Sometimes thermocouples are inserted through the inner liner to also acquire the bulk temperature.

The Figure III.4 shows some measurements examples.

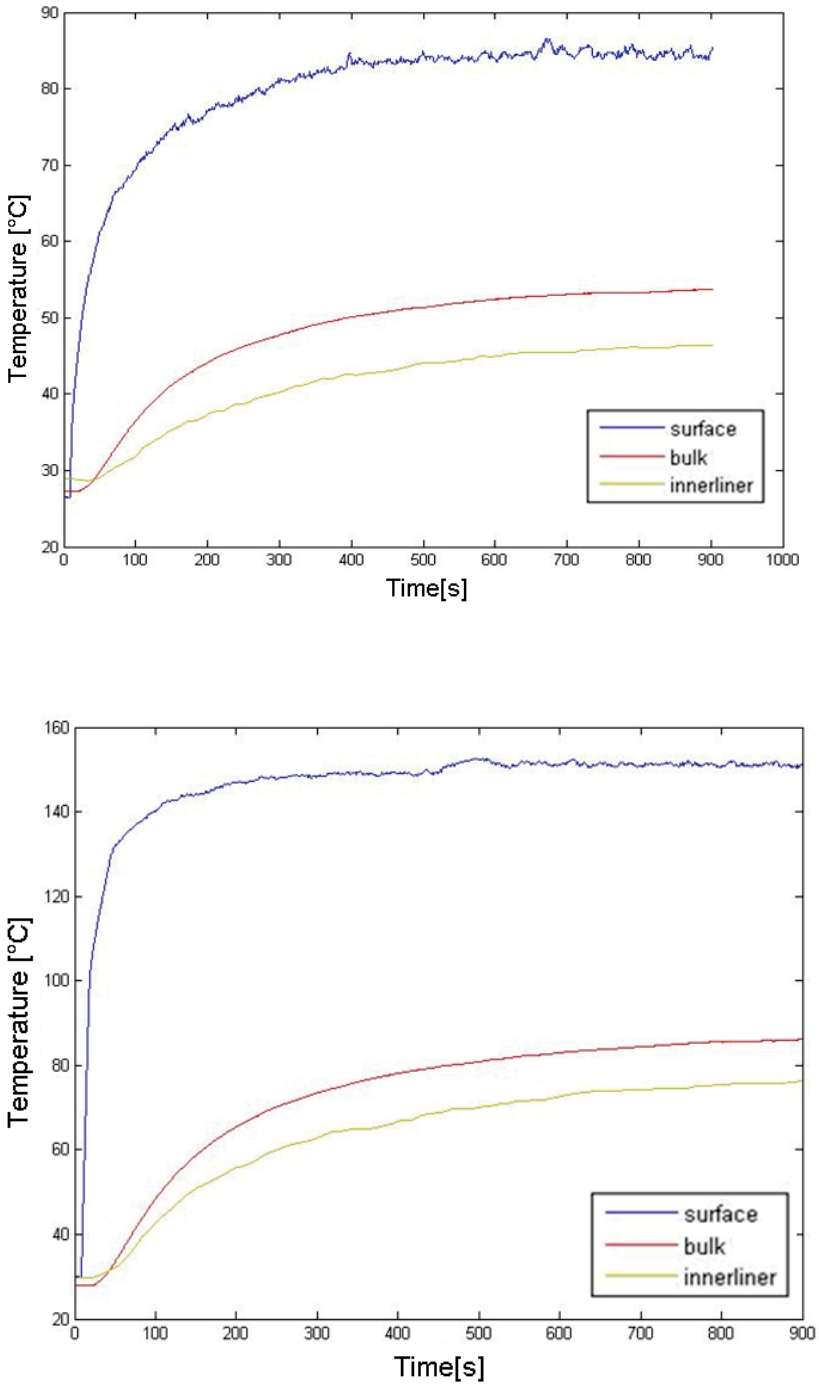

Figure III.4 – Examples of temperature acquisition by DIME

The reader is invited to focus his attention on the difference between surface temperature and inner liner temperature. After a few minutes, the tire reaches

a thermodynamic equilibrium so the temperature does not increase anymore. At the same time, while the outer surface reaches high temperatures (85°C with 1 W and 140°C with 3 W), the bulk and the inner liner remains at very low temperature (40-50°C at 1 W and 60-80°C at 3 W) with a difference of 60% respect to the outer surface. This demonstrates that the tire is an isolating material that means it is characterized by very low thermal conductivity.

III.1.2 – The Thermal Conductivity identification

The procedure uses a thermal model developed by the DIME just for this purpose. For more details on the model, please refer to [42].
In this paragraph an analysis on the equivalent thermal conductivity will be conducted.

The following Figures III.5 and III.6 show the results of the identification.

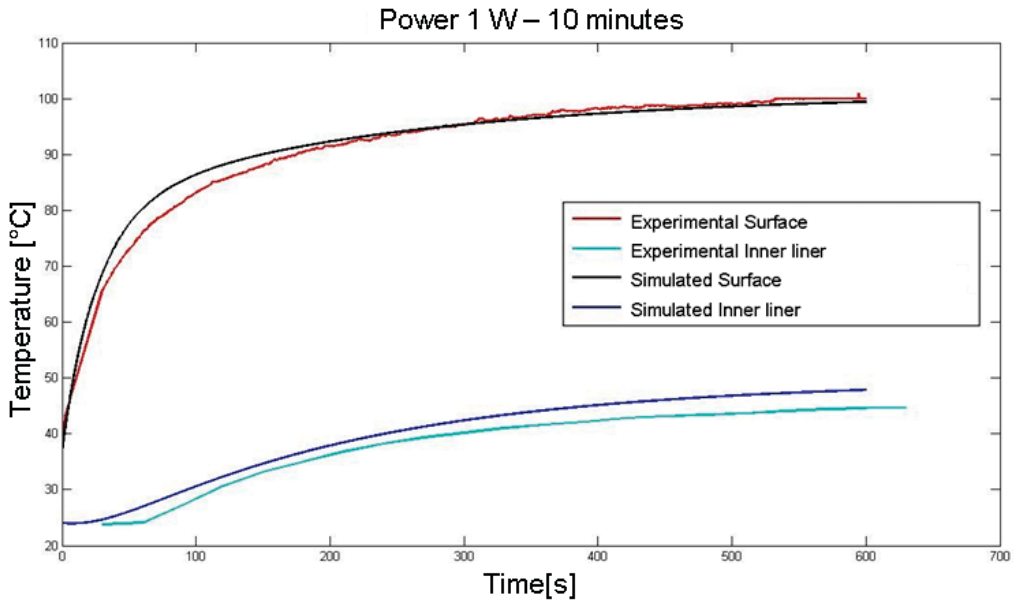

Figure III.5 – DIME simulation at 1 W

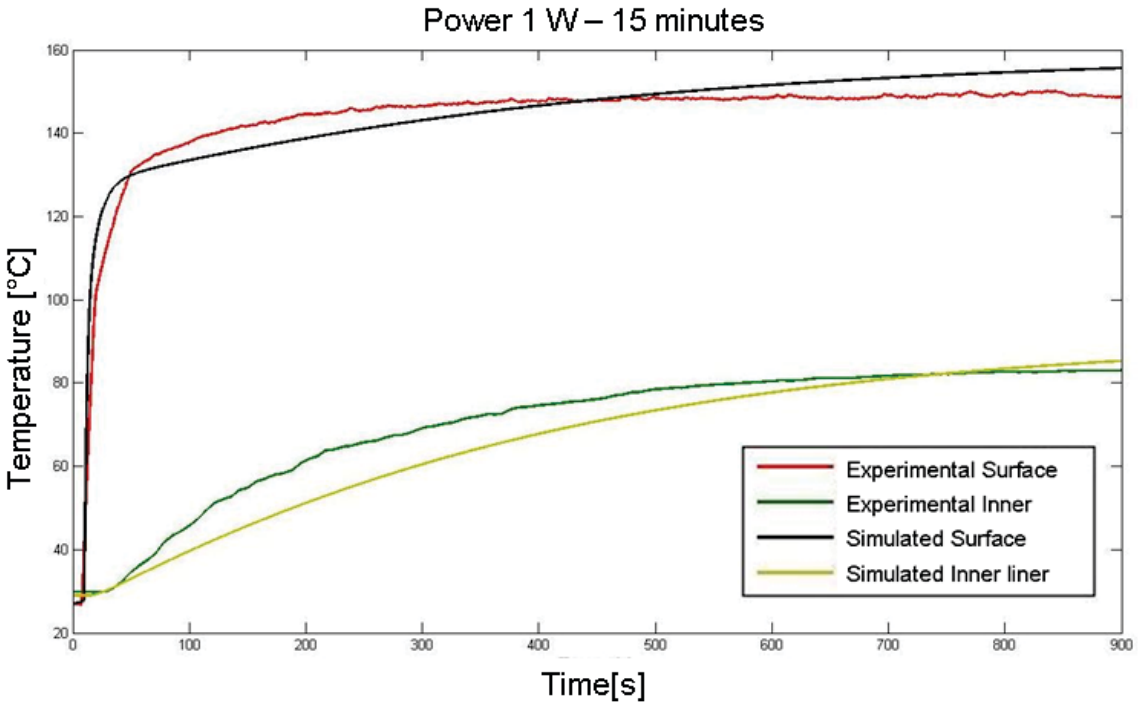

Figure III.6 – DIME simulation at 3 W

Both equivalent thermal conductivities appear dependent on temperature with a 2nd order law as showed in the Figures III.7 and III.8.

The equivalent conductivity is very low as mentioned above: K_1 reaches 0.9-1.00 W/mK at 90°C while K_2 reaches 0.07-0.08 W/mK at the same temperature.

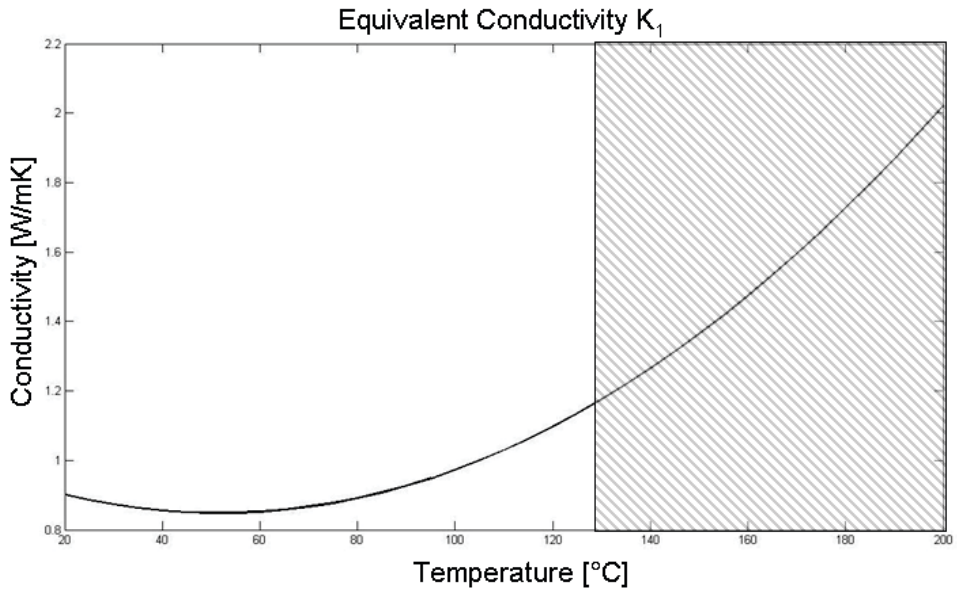

Figure III.7 – Equivalent conductivity of surface layer

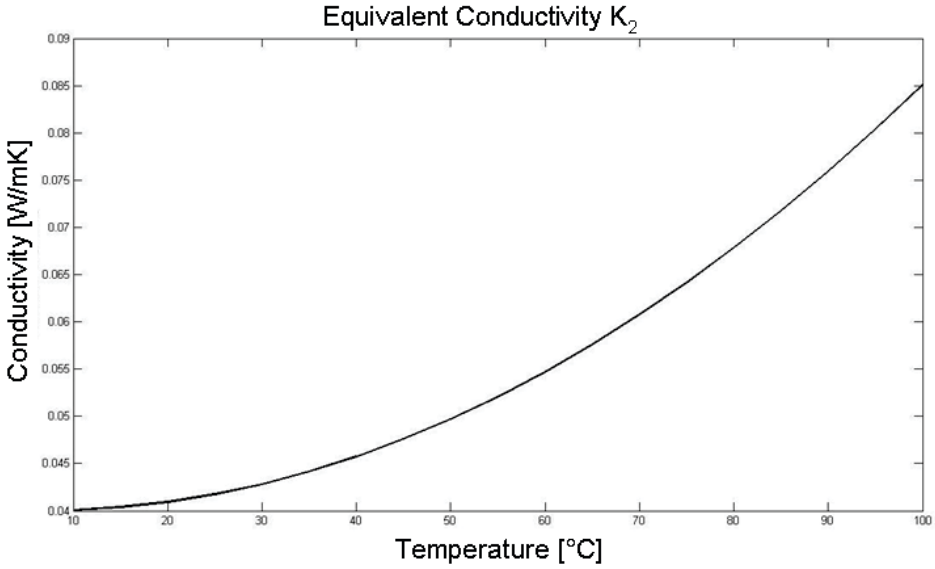

Figure III.8 – Equivalent conductivity of bulk layer

The part in grey has not been investigated, so no info is available for this part.

As will be showed in the next paragraphs, the very low thermal conductivity is a key point: because of this characteristic the tire is not able to dissipate the heat generated during its exercise.
This, in addition to influencing the handling performance as will be showed in the next chapters, can even involve in durability issues.
In fact, durability failure of a tire seems to be related to the bulk temperature: as showed in the Figure III.9 below, a locally peak of temperature happens few moments before the failure, in this case in the bead area. Anyway, the reason of this behavior is not subject matter of this work.

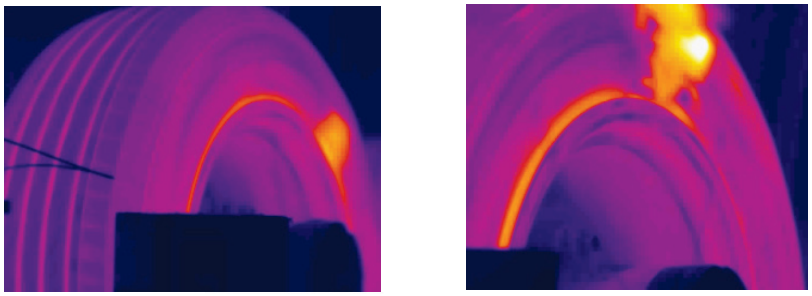

Figure III.9 – Durability failure

III.2 – Indoor Tests in T.C.E.

III.2.1 – Flat Trac Tire Test System

The MTS Flat Trac System (Figure III.10) measures a broad range of tire behavior by controlling roadway speed, vertical load, inflation pressure and all tire motion relative to the road.

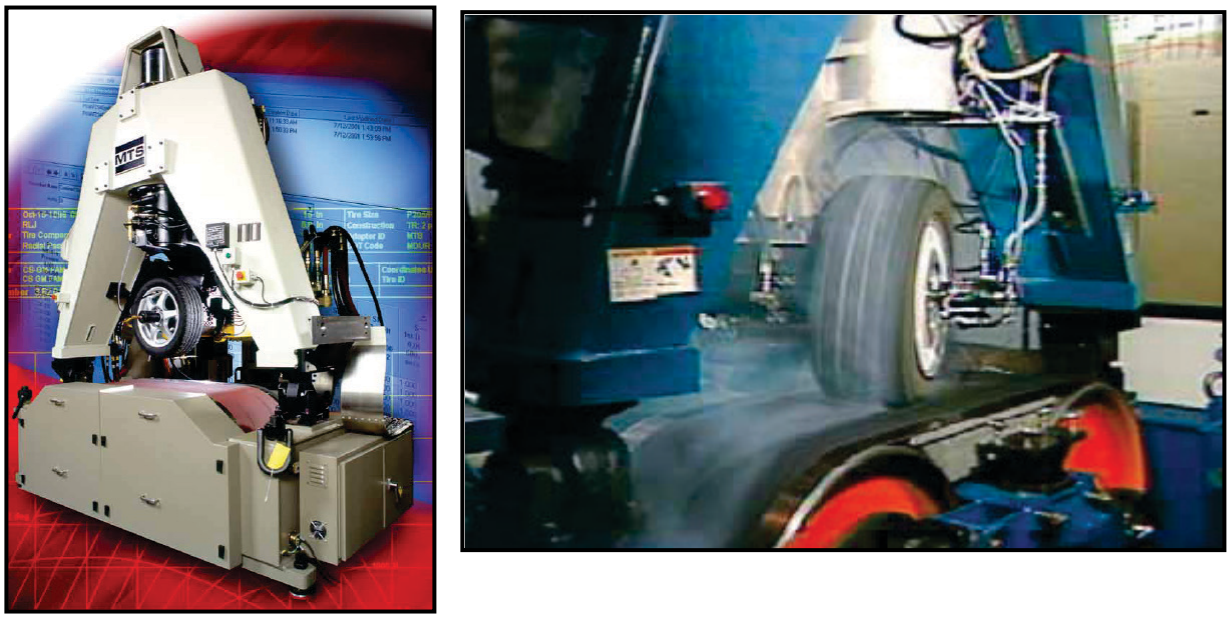

Figure III.10 – The MTS Flat Trac machine

Through the setup is possible to control roadway speed, tire spindle speed, normal force, inflation pressure, slip and inclination angles, giving back wheel forces and moments (Figure III.11) and the loaded radius both in steady state and in dynamic conditions.

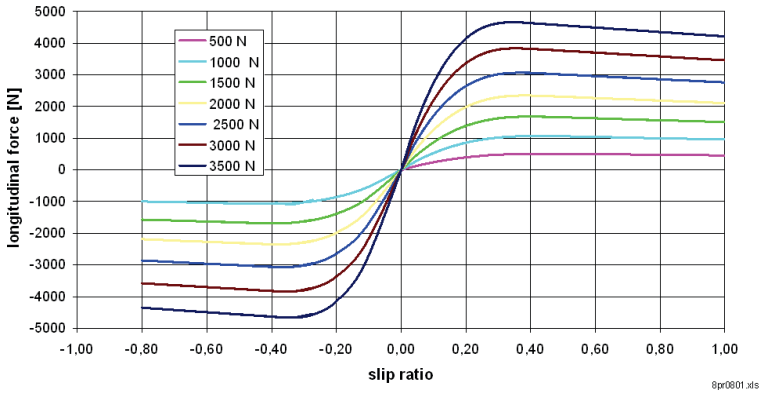

Figure III.11 – lateral characteristic carpet measured by Flat Trac

III.2.2 – The T3M system for tire temperature measurement

The German TÜV Automotive department developed a system to measure in real time the bulk temperature of a tire during its exercise (Figure III.12).

Figure III.12 – The T3M sensors

The system is composed by the sensitive elements constituted by thermo resistances that can be *drown* into the bulk on the shoulders (Figure III.13).

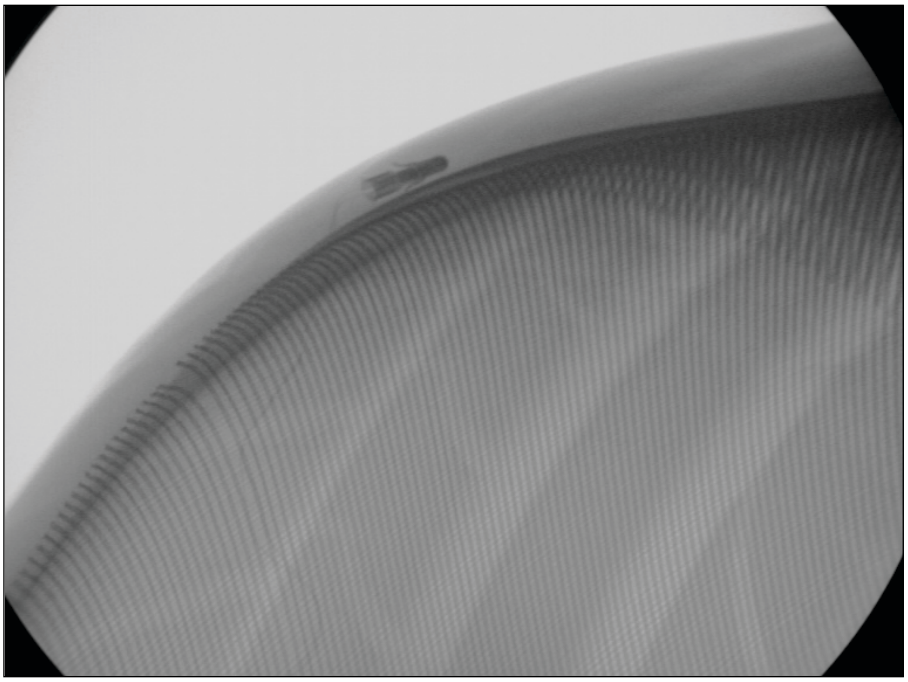

Figure III.13 – An x-ray of a T3M sensor inserted in a tire

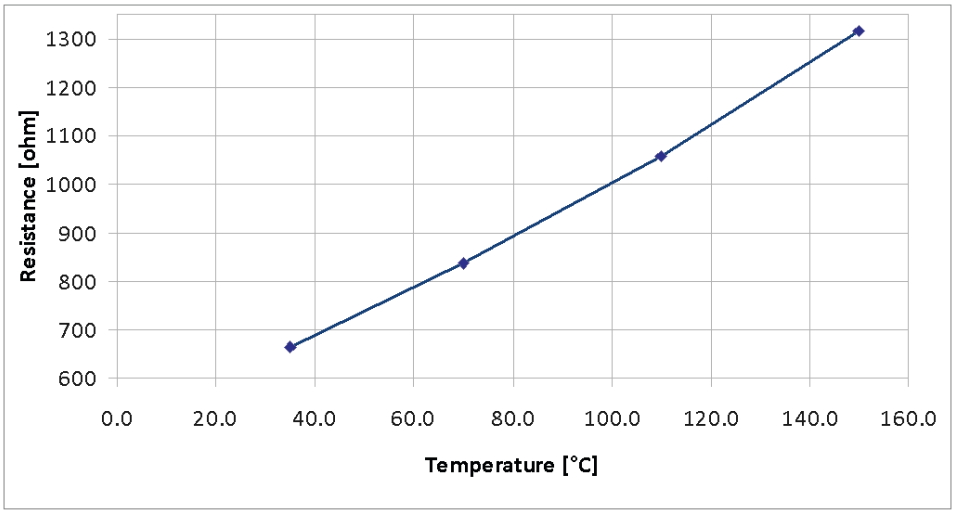

Figure III.14 – The calibration curve of a T3M sensor

The sensitive elements can change linearly their electrical resistance in dependence on temperature (Figure III.14).

The sensors are connected through steel cables to an I/O unit (Figure III.15) able to transmit via *Bluetooth* technology up to 8 signals to a receiver connected via CAN bus to an acquiring system.

Figure III.15 – The I/O unit

As showed in the Figure III.15, the I/O unit is fit on the rim hub through balusters.

III.2.3 – Test Bench Layout

The indoor tests have been performed on Flat Trac with tires equipped with T3M sensors to measure bulk temperature (Figure III.16).

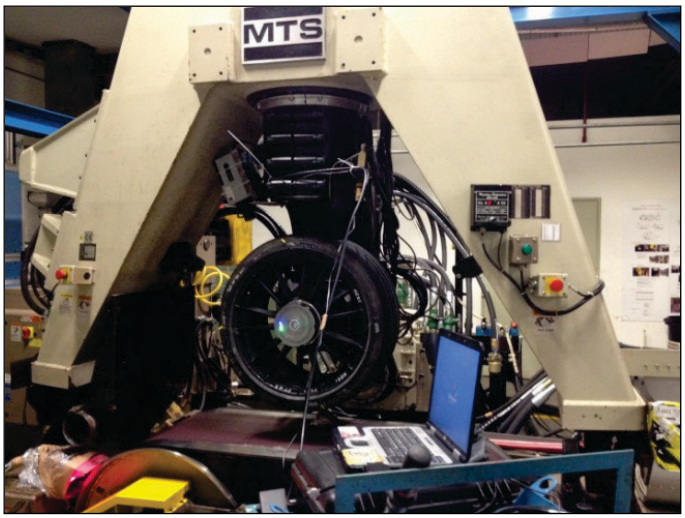

Figure III.16 – Indoor experimental activity layout

The tread surface temperature has been acquired using a thermo camera mounted on the machine (Figure III.17).

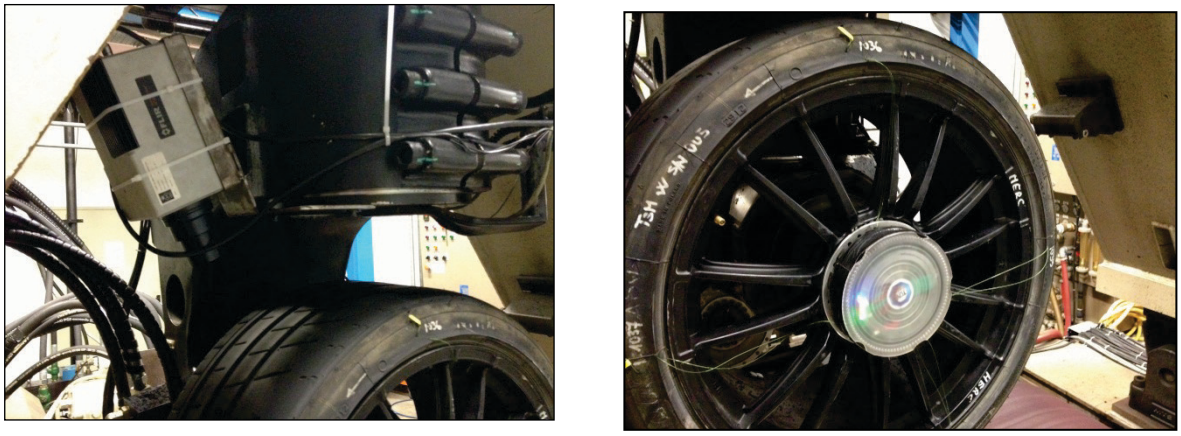

Figure III.17 – The thermo camera to acquire the surface temperature and the I/O unit fitted on the rim

Because the T3M acquiring system needs to be mounted on the hub, a commercial rim has been used during the test; for this reason, the inflation pressure had not been controlled and monitored. This is closer to effective outdoor conditions of course; but at the same time, there was a parameter influencing the results that had not been controlled.

All data have been acquired by a Dewesoft Dewe43 (Figure III.18) connected via USB to a common laptop.

Figure III.18 – The Dewe 43 acquisition unit

III.2.4 – The first Indoor test

As mentioned above, in this activity the target was to investigate the influence of bulk temperature (and in case of the surface temperature) on the cornering stiffness. For this reason, the tire was always working in its linear range. This means that small values of Slip Angle have been used.

Three different procedures have been performed in FT to investigate the influence of bulk temperature.
The first procedure consisted in three different conditions of vertical load (2100 N, 4500 N and 6800 N). For each condition, two cycles at 0.2 Hz of sinusoidal wave of Slip Angle (SA) up to ±1 deg have been applied. The vertical load sequence started from the highest value to the lowest one.

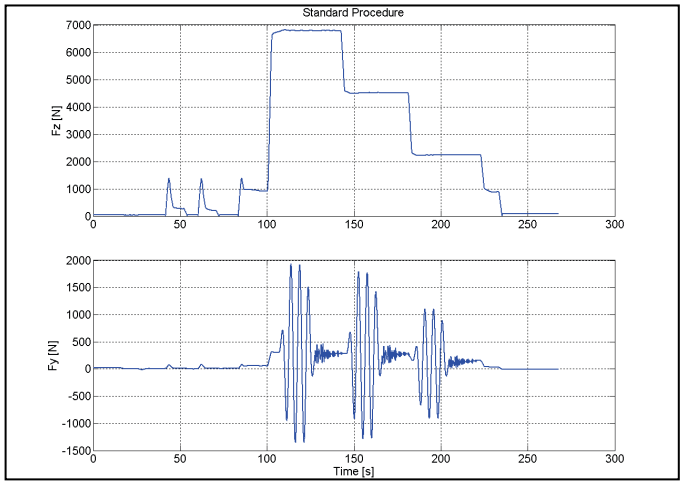

Figure III.19 – The standard procedure adopted in TCE

In the Figure III.19 are plotted the vertical load signal (in the upper plot) and the lateral force signal (in the bottom) due to the SA history. As showed, during the test (from first condition to the third) the tire was constantly rolling and no pauses have been inserted between conditions.

The second procedure consisted in 10 cycles of SA at 0.2Hz and the sequence of the vertical load has been inverted: it started from the lowest value to the highest (Figure III.20).

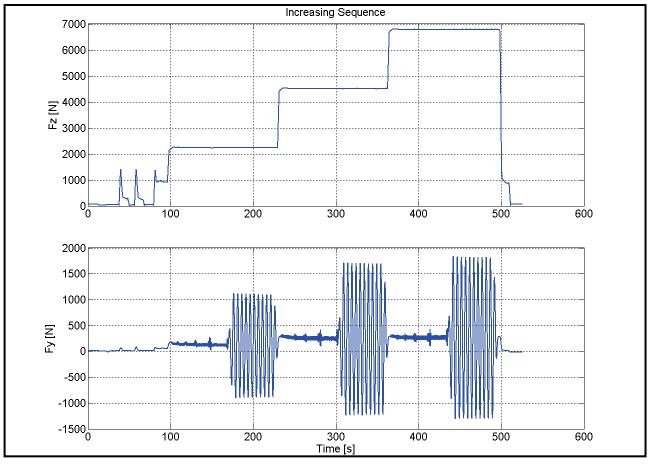

Figure III.20 – The increasing sequence procedure

As showed in the figure, in this case each condition was longer than in the previous one because of the highest number of cycles applied.

The last procedure (Figure III.21) was equal to the second one but the sequence of the vertical load: from the highest to the lowest again. The duration of each condition is the same of the second procedure.

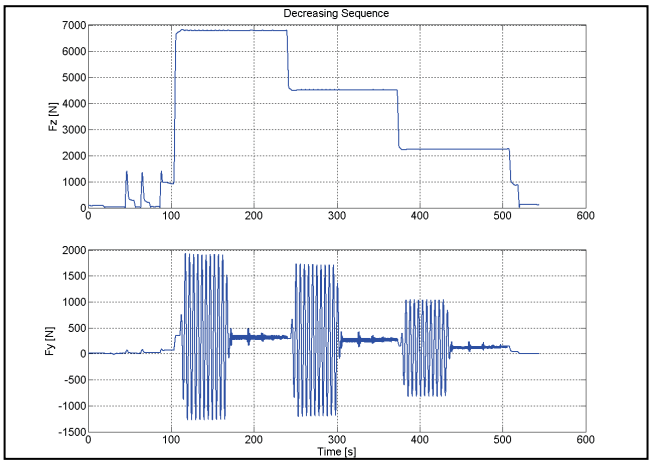

Figure III.21 – The decreasing sequence procedure

The roadway speed was 100 kph for all the tests.

A thermo-camera has been used to acquire the surface temperature of the tire. Four T3M sensors have been used to acquire the bulk temperature; two for each side of the tire to guarantee a redundancy of the measure.
A Dewesoft Dewe43 connected to a laptop has been used to acquire all the data.

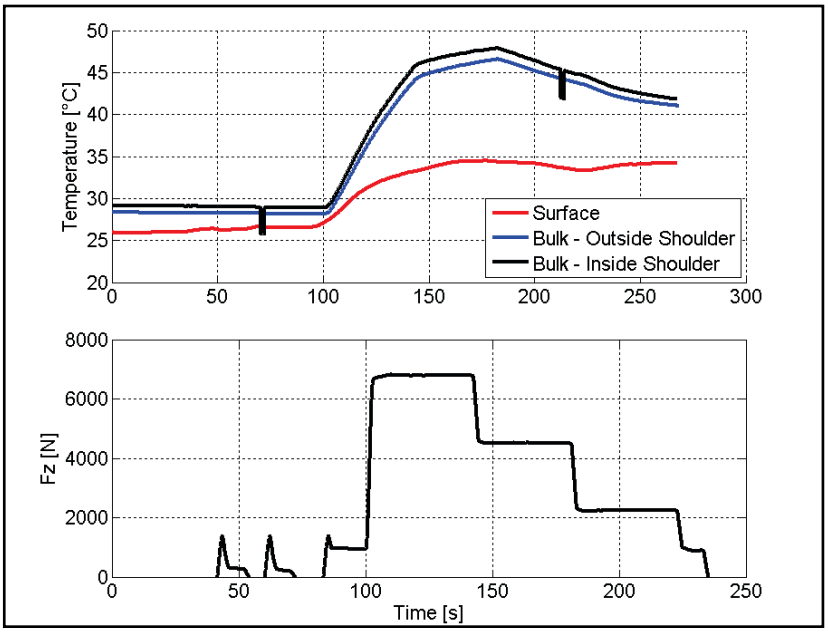

Figure III.22 – The standard procedure temperature time history

In the Figure III.22 the time-history of the tire temperature is showed. In red the surface temperature, in black is the bulk temperature of the inside shoulder of the tire (obtained as the mean between the two sensors of the same side) and in blue the bulk temperature of the outside shoulder.

As showed in the figure, during the first test, the surface temperature passed from 25°C to 35°C. So, the tire increased its surface temperature of 10°C. Furthermore, between the second and the third condition no significant differences in surface temperature appeared.
Instead, the bulk deeply changed its temperature during the test, passing from 27-28 °C to 47-48°C. Furthermore the dependence of the bulk temperature on the vertical load applied to the tire appears clear: passing from the second condition to the third one, the temperature decreased because the SEL decreased.

Comparing the two plots in the figure, it is clear that the bulk temperature is deeply different for each vertical load condition (and in consequence the Slip Angle time history is applied at three different bulk temperatures).

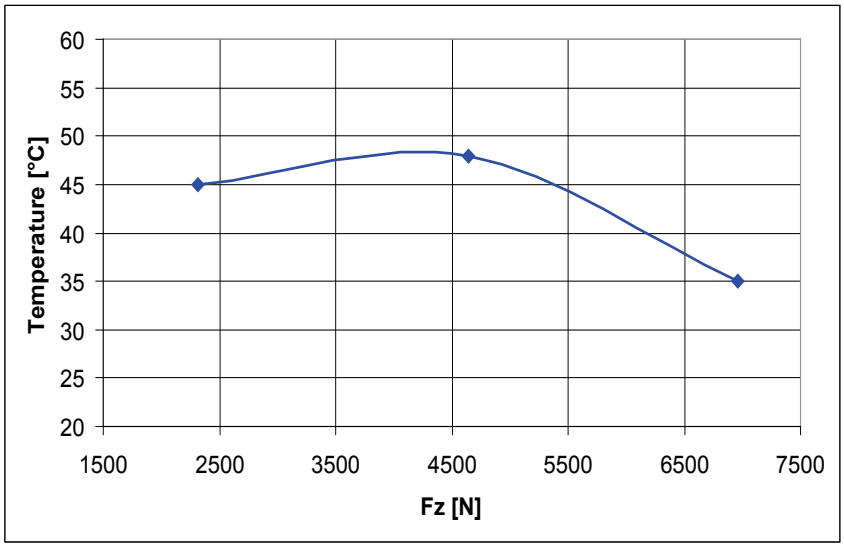

Figure III.23 – The bulk temperature during slip angle application

In the Figure III.23 the average bulk temperature during the Slip Angle application for each vertical load condition has been plotted.

In the second and in the third procedure the same considerations can be made (Figures III.24 and III.25).

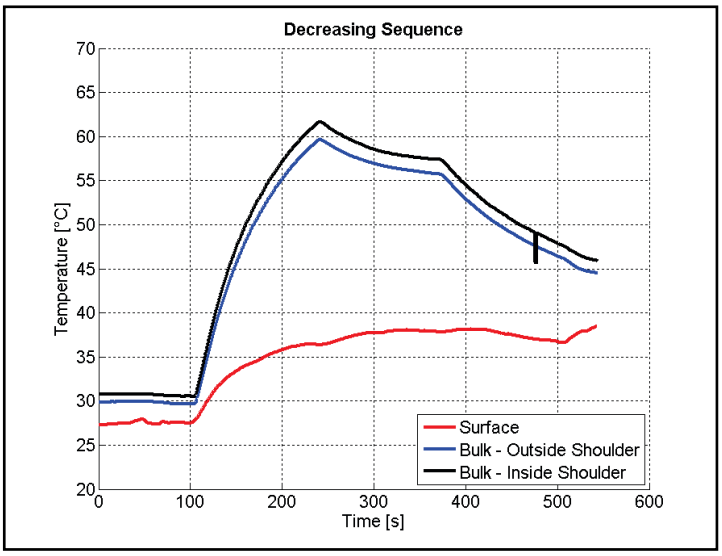

Figure III.24 – Temperature time history in decreasing sequence

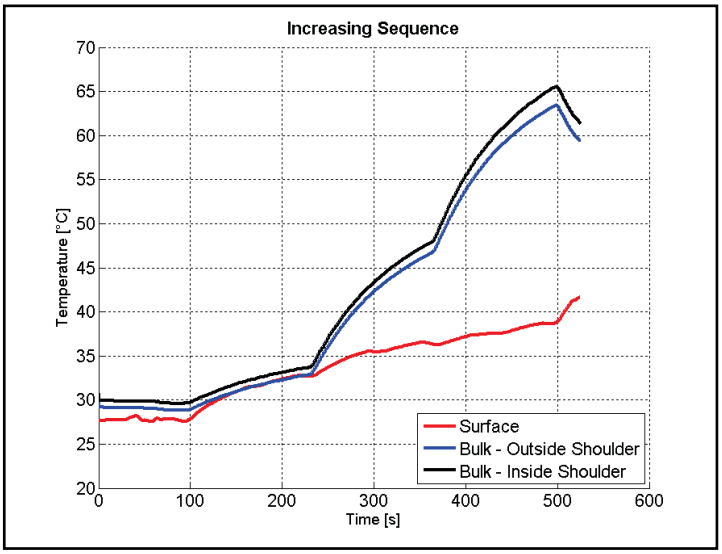

Figure III.25 – Temperature time history in increasing sequence

Due to the higher number of the cycles applied (so the duration of each condition), the bulk reaches more than 60°C, while the surface temperature remains below of 40°C again.

So two considerations can be achieved:

- When the tire works in its linear range (i.e. up to 1° of SA) the surface temperature of the tire does not change significantly.
  Evidently, this was expected because of the low values of the Slip Angle that involves in low values of Friction Power.

- Very different procedures (that involved in very different bulk temperatures) involved in quite constant surface temperature. For this reason, monitoring the surface temperature – for example by infrared sensors – is not sufficient in this kind of test.

The surface temperature is influenced by high values of sliding velocity that means high values of slip angle (>2-3 deg).

On the other hand, the bulk temperature is significantly influenced by the vertical load applied on the tire and by the roadway speed.

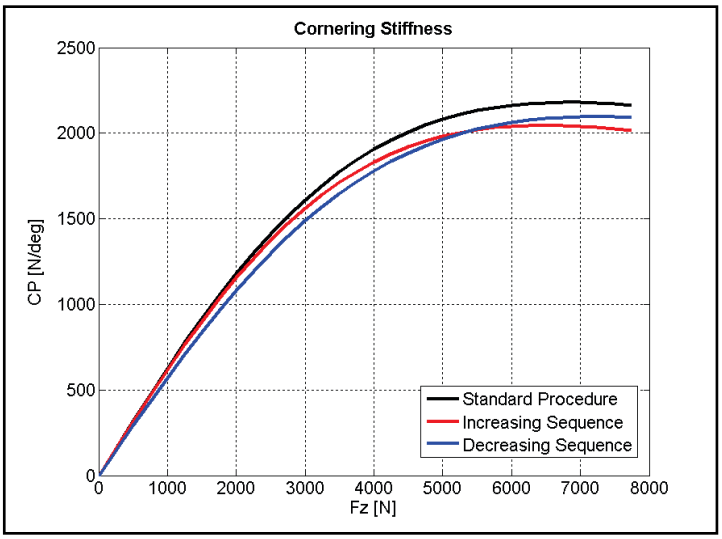

Figure III.26 – Cornering stiffness comparison between the procedures

With the help of the Figure III.26, it is possible to analyze how the three procedures gave back different cornering stiffness characteristics.
The black one is referred to the first procedure. In this case, the bulk of the tire was more cold on average than in the other two and, as expected, this caused the cornering stiffness in the first procedure is significant higher than in the other two cases (because the stiffness of the tread blocks is higher being them colder).

Readers are invited to focus their attention on the red and the blue curves: at low vertical load the red curve is above the blue one and vice-versa happens at the higher vertical loads. The bulk temperature in dependence on vertical load shows the same trend (Figure III.27).

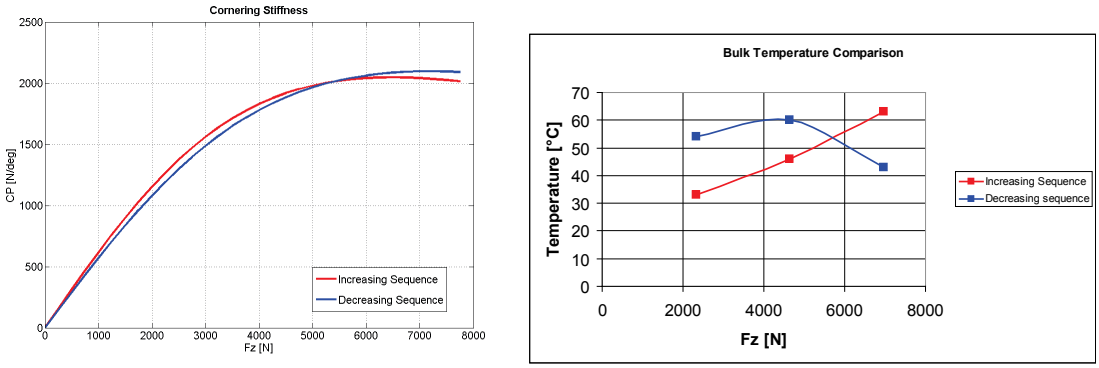

Figure III.27 – Bulk temperature direct influence on cornering stiffness characteristics

This can be considered the umpteenth demonstration that the cornering stiffness is strongly influenced by the bulk temperature of the tire; not by the surface temperature.

Again, a comparison between the black plot (the standard procedure, with 2 cycles per each condition) and the blue plot (10 cycles per each condition) gives back another demonstration about the influence of the bulk temperature.

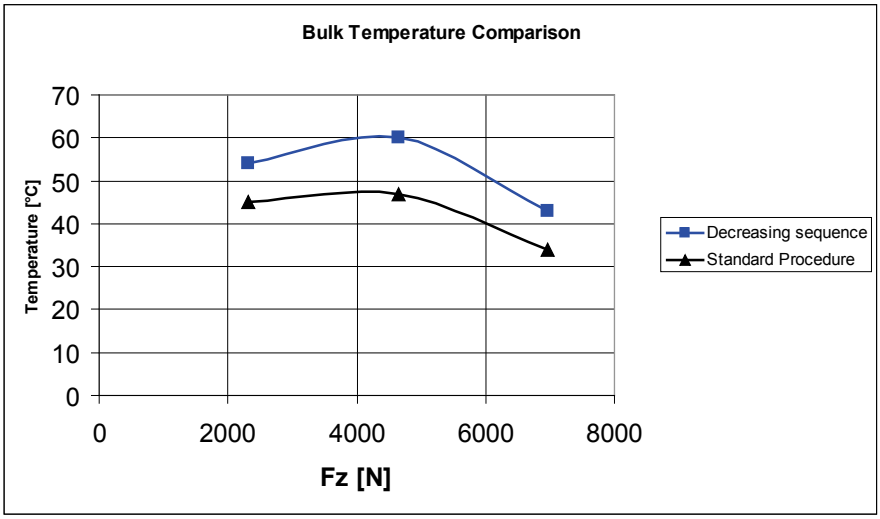

Figure III.28 – Bulk temperature comparison between standard procedure and decreasing sequence

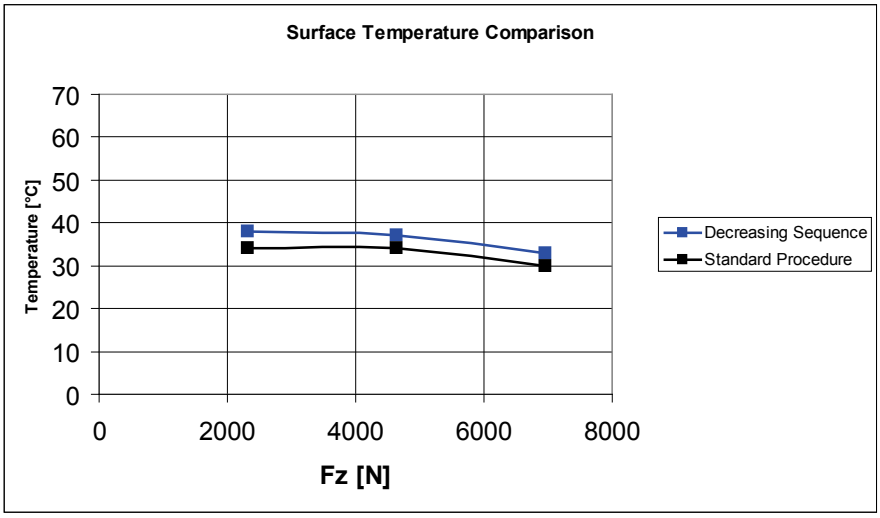

Figure III.29 – Surface temperature comparison between standard procedure and decreasing sequence

The two procedures gave back similar surface temperature (Figure III.29) between each other (30-40°C) while very different bulk temperatures (with differences of 15°C between the two procedures) as showed in Figure III.28.

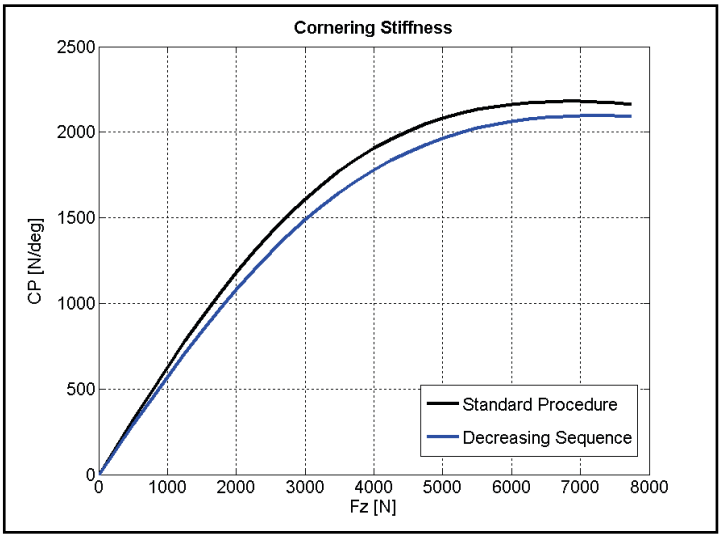

Figure III.30 – Cornering stiffness comparison between standard procedure and decreasing sequence

The cornering stiffness between the two procedures is deeply different (Figure III.30).
The standard procedure, with a colder bulk is characterized by a higher cornering stiffness along the entire exercise.

A question could descend from all these considerations: does the bulk temperature increase indefinitely while a tire rolls?
The answer is no. The bulk temperature saturates to a value that directly depends on the vertical load applied and on its rolling speed.

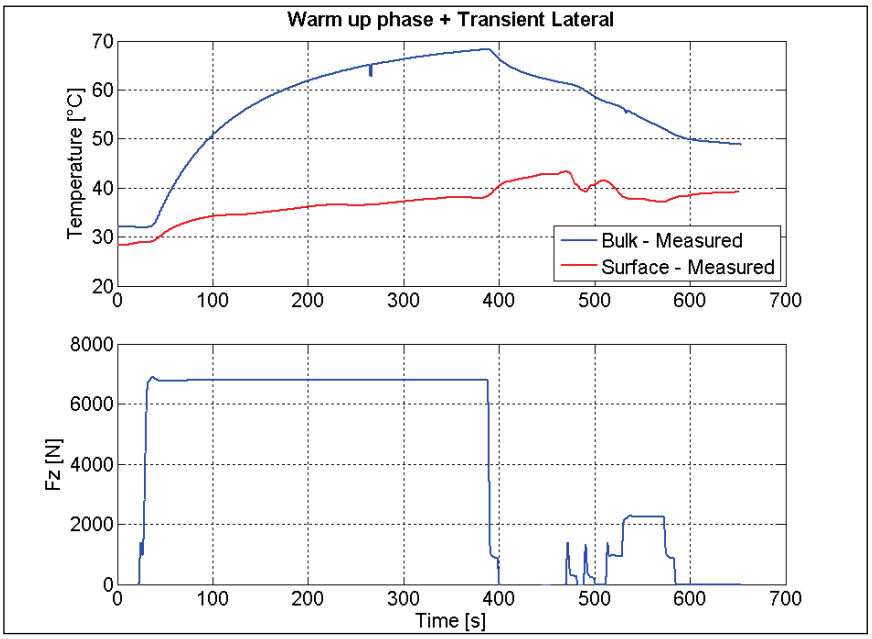

Figure III.31 – The bulk temperature saturation

In the test showed in the Figure III.31 a warm-up phase of about 5 minutes in free rolling condition has been performed before a classical transient test. It is possible to notice that the bulk is going to saturate to 70°C.
This is in coherence to what explained in the paragraph on thermal conductivity evaluation: the tire reaches a thermodynamic equilibrium

between the internal power generated (the SEL in this case) and the power dissipated to the external environment (track and air).

III.2.5 – The second Indoor test

The new tests were conducted in a very different way respect to the previous one. In this case, the target was to evaluate the cornering stiffness at three different – and above all *controlled* – bulk temperatures.
To do this, different warm-up phases (tire in free rolling at constant vertical load and speed) have been introduced to saturate the bulk before applying the slip angle. In this way the cornering stiffness was measured at a constant temperature for each condition. In fact, in the Figure III.32 the bulk temperature time history is showed (in blue) and its saturation can be noticed.

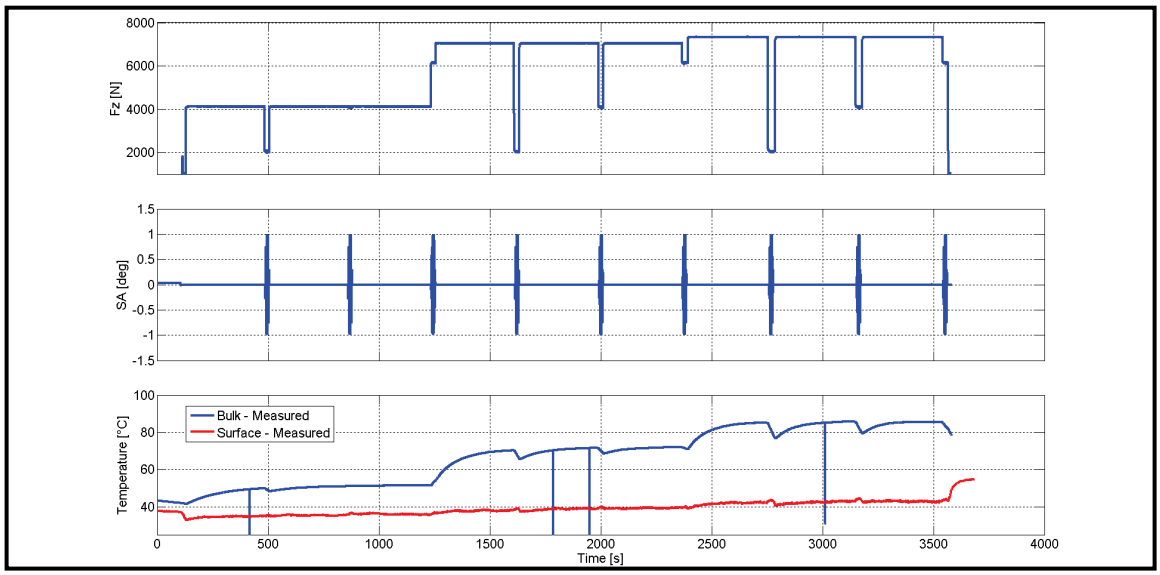

Figure III.32 – The second kind of test bulk temperature time history

The test was characterized by three different phases: in the first phase, between each vertical load condition (and the consequence slip angle

application) a warm-up phase (at 100 kph) has been introduced with the tire loaded at 4000 N until the bulk saturated at about 50°C. In the second phase, the warm-up phase – 7000N always at 100 kph – let the bulk to saturate at 70°C; in the last warm-up phase the speed has been increased until 150 kph with a vertical load of 7500 N and the bulk saturated at 80°C.

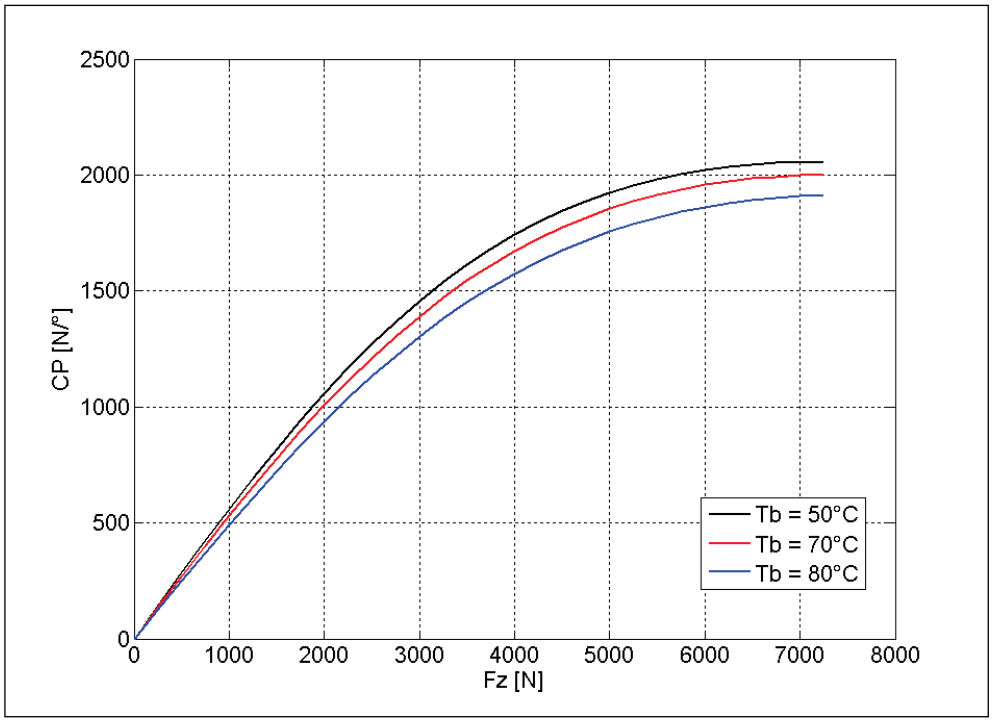

Figure III.33 – Cornering stiffness comparison at different bulk temperature

The results are showed in the Figure III.33. As expected, increasing the bulk temperature, the cornering stiffness decreases. Readers are invited to focus attention on the surface temperature again: as showed in the Figure III.32, the surface temperature remained constant during the entire test; this is the ultimate demonstration that the cornering stiffness is directly influenced just by the bulk temperature of the tire.

Chapter IV – Outdoor Experimental Activity

In this section the results of an outdoor test campaign will be showed.
The reason of this activity was to confirm everything investigated in indoor. So the influence of vertical load and vehicle speed on bulk temperature has been investigated again.
Furthermore, different kinds of ISO objective handling tests were performed to evaluate how they can influence the bulk temperature of the tire – and in consequence the cornering stiffness evaluation in this kind of tests.

IV.1 – First kind of Outdoor Test

The first kind of outdoor tests were performed to investigate the dependence of the bulk temperature on vertical load and speed in outdoor conditions, which means the tires fitted on a vehicle.

The vehicle used for the purpose was a classical European segment C: frontal engine and front wheel drive. It has been equipped with four tires instrumented with T3M sensors to measure the bulk temperature. As made in case of indoor test, each tire was equipped with two sensors on outside shoulder and two sensors on inside shoulder for redundancy reasons. So, in real time the outside shoulder temperature and inside shoulder temperature were available.

All the tests have been performed on the oval track of the Bridgestone European Proving Ground as underlined in the Figure IV.1.

Figure IV.1 – The oval track of EUPG

The presence of the banking corners lets the vehicle to maintain low lateral acceleration (≈ 0.3 g) along the entire test. Furthermore, the speed was constant. For these reasons it is possible to consider all the tires in quasi free rolling condition with the friction power generation negligible.

Three kinds of tests have been conducted to investigate thermal behavior of the tires:

- Test 1: vehicle unladed – constant speed at 140 kph for 20 minutes on the oval;
- Test 2: vehicle full laden – constant speed at 140 kph for 20 minutes on the oval;
- Test 3: vehicle full laden – constant speed at 80 kph for 20 minutes on the oval;

The following weight distribution [kg] has been measured before the test campaign:

Unladed

FL	FR
485	481
RL	RR
354	342

Full laden

FL	FR
494	512
RL	RR
586	581

The unladed condition was characterized by only driver on board.
The full laden condition instead was characterized by the driver, four dummies of 70 kg and 200 kg of baggage.
Unfortunately the sensors on tire FL did not work, for this reason no data are available for it.

IV.1.1 – Unladed condition – 140 kph – Results Analysis

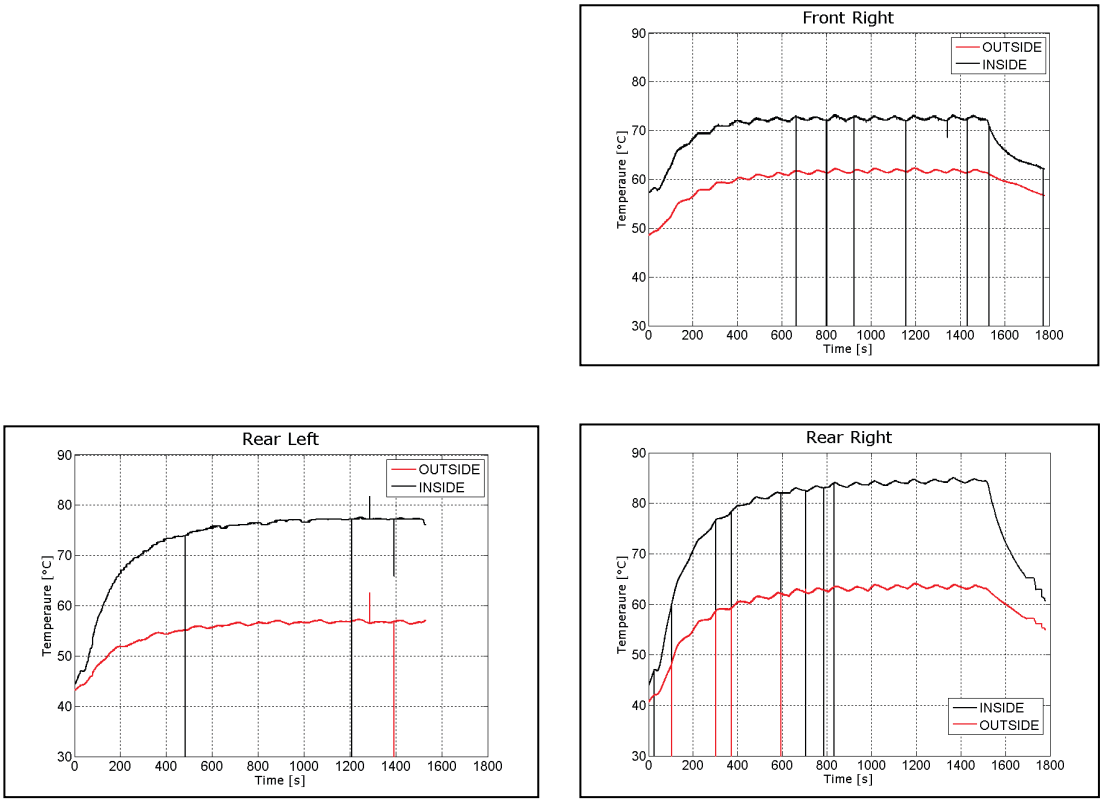

Figure IV.2 – Bulk temperature time histories for all the vehicle corners

In the graphs above, the inside and the outside signals of each tire are showed. First of all, as in the indoor tests, also in outdoor tests the bulk saturated after 10 minutes to a temperature that depends on vertical load and rolling speed of the tire. The tire reaches a thermodynamic equilibrium: the generated power balances the heat exchange with the external environment.

The second consideration is about the zigzag trend of the temperature time-history, especially on the right tires. This shape is due to the banks: on the banks, part of the lateral acceleration becomes vertical acceleration thanks to the inclination of the roadway (≈ 37°) as showed in Figure IV.3.

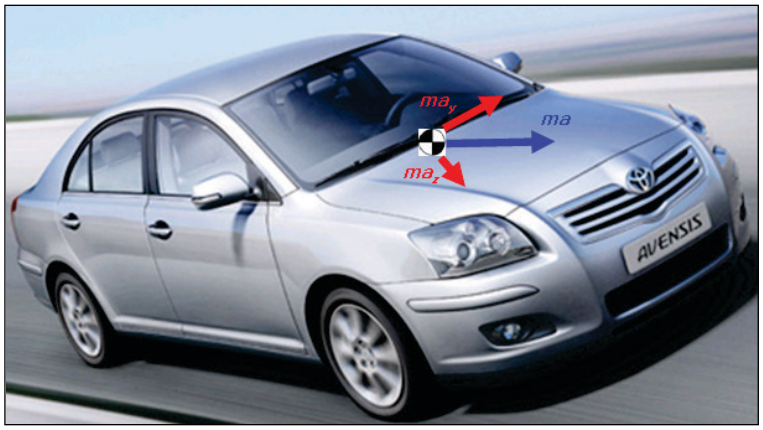

Figure IV.3 – The vehicle on banks

For this reason, along the banks, the vertical load on the tires lightly increases and then the SEL too.
Obviously this phenomenon is highlighted on the right tires that are the outside tires respect to the corners and so the vertical load increases much more because of the lateral load transfer too.
It is not plausible that this trend is due to the friction power – that would mean an increase of the surface temperature heating up the bulk by conduction – because the lateral acceleration is sufficiently low (no more than 0.3g).

Analyzing the temperature time-history, a significant difference between inside shoulder and outside shoulder appears especially for the rear tires. The difference is about 15°C! The inside shoulder is hotter than the outside for both tires. This is coherent with the negative camber angle (Figure IV.4) of the rear axle, that involves in an inside shoulder more loaded than the outside shoulder for both tires.

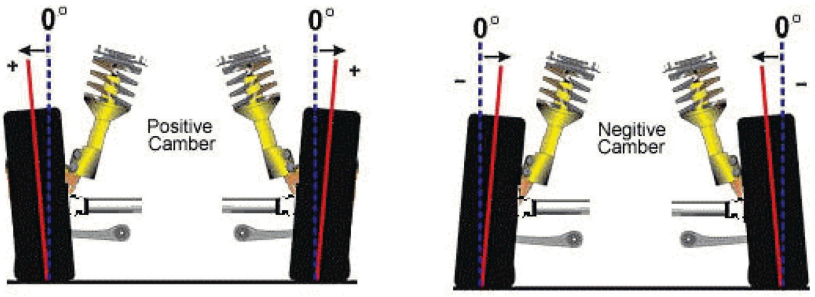

Figure IV.4 – The camber angle sign convention

So, on the inside shoulder the SEL is locally higher because of the higher deformation of the rubber.
The external tire Right Rear is lightly hotter than the internal one (about 4-5°C) and this also is coherent with the vehicle dynamics (on the oval track vehicles run on counter-clockwise direction).

In the Figure IV.5 the average saturated inside and outside shoulder bulk temperatures (°C) for each tire are showed

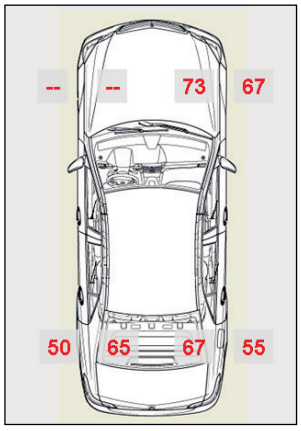

Figure IV.5 – The bulk temperature distribution and the camber influence

It is evident the influence of camber angle, with inside shoulder hotter than the outside one for all the tires.

IV.1.2 – Full laden condition – 140 kph – Results Analysis

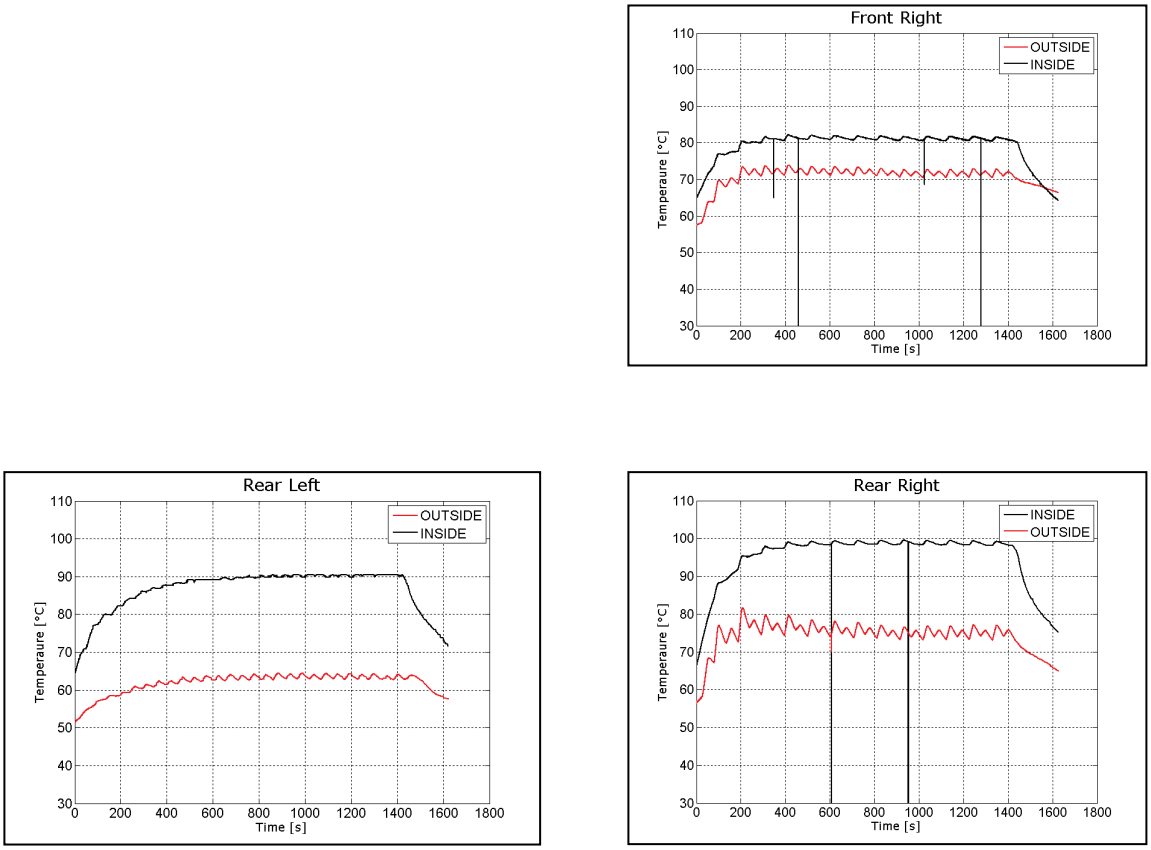

Figure IV.6 – Bulk temperature time histories for all the vehicle corners

In this case, the average bulk temperature increases for all the tires as underlined in the Figure IV.7.

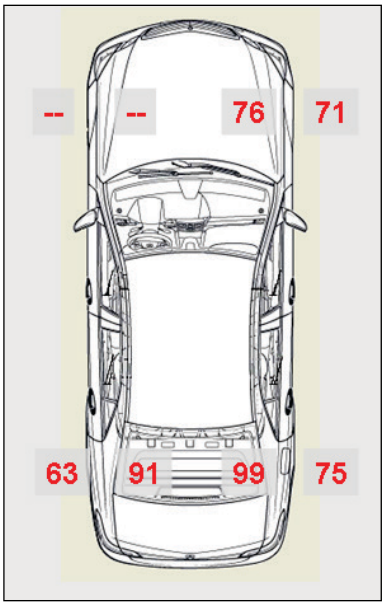

Figure IV.7 – The bulk temperature distribution and the camber influence

Furthermore, the difference between inside and outside shoulders increased. This should be due to the camber angle increase caused by the camber recovery system of the multilink suspension adopted by the vehicle on the rear axle (5 links) and on the front axle (4 links): when a vehicle with these suspensions rolls during a corner, the system allows the camber angle to increase in negative values direction for the outside wheels so to balance the camber angle increase to positive values due to the lateral force and to the vehicle rolling itself.

It is evident that this phenomenon even happens when the vertical load on the wheel increases (Figure IV.8) such as in case of vehicle in full laden conditions.

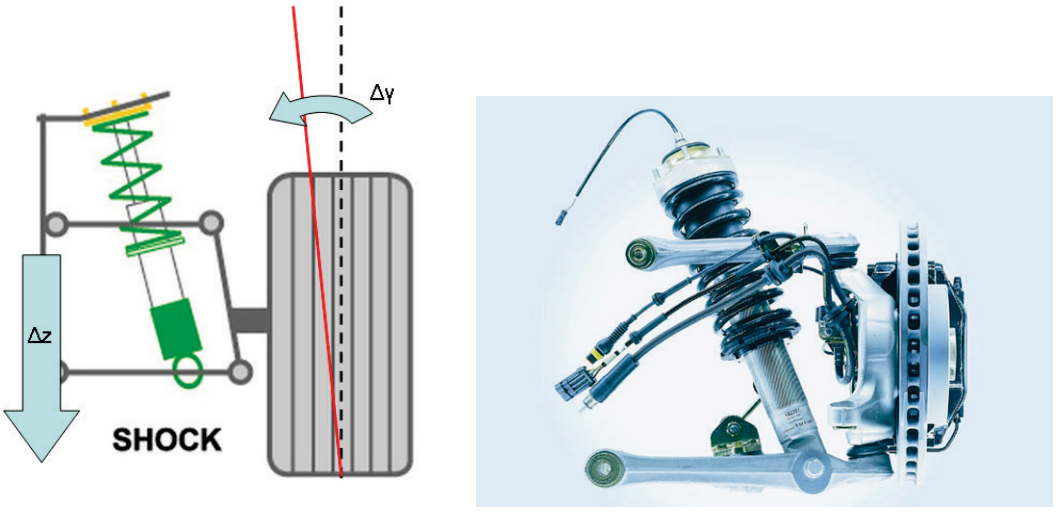

Figure IV.8 – The camber angle recovery concept

IV.1.3 – Full laden condition – 80 kph – Results Analysis

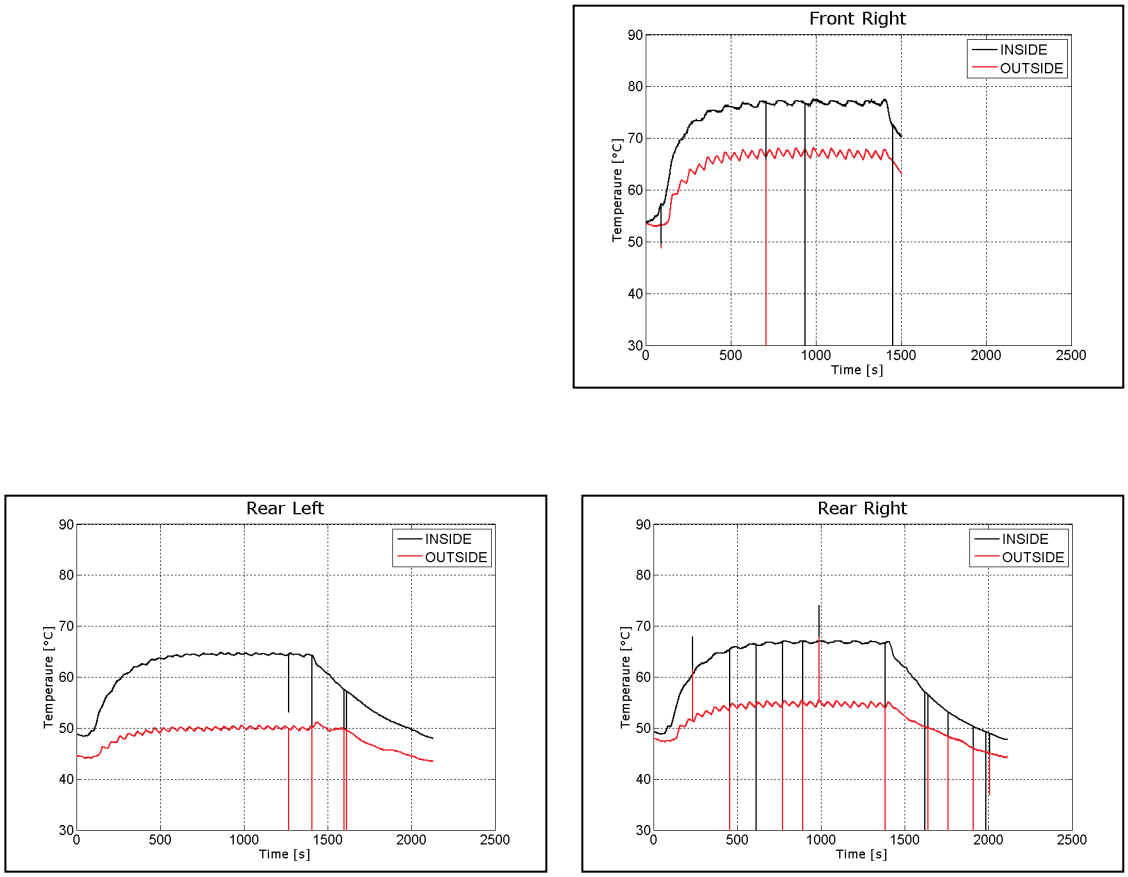

Figure IV.9 – Bulk temperature time histories for all the vehicle corners

In the last test, the bulk temperature decreased because the SEL decreased. Even if the vehicle was in full laden conditions, the difference between the inside and outside shoulders decreased anyway. Evidently, this is due to the decrease of SEL because of the lower speed of the test.

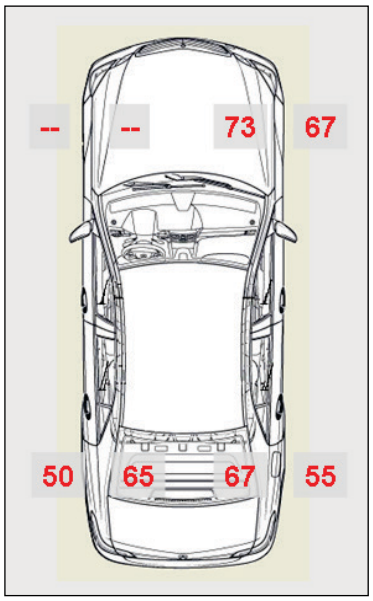

Figure IV.10 – The bulk temperature distribution and the camber influence

IV.2 – Second kind of Outdoor Test

The second kind of outdoor tests performed were typical Objective Handling tests as per ISO standard.
This analysis was to investigate how much the bulk temperature is influenced by the typical Objective Handling maneuvers.

The first tests were the pseudo-random sine sweep.

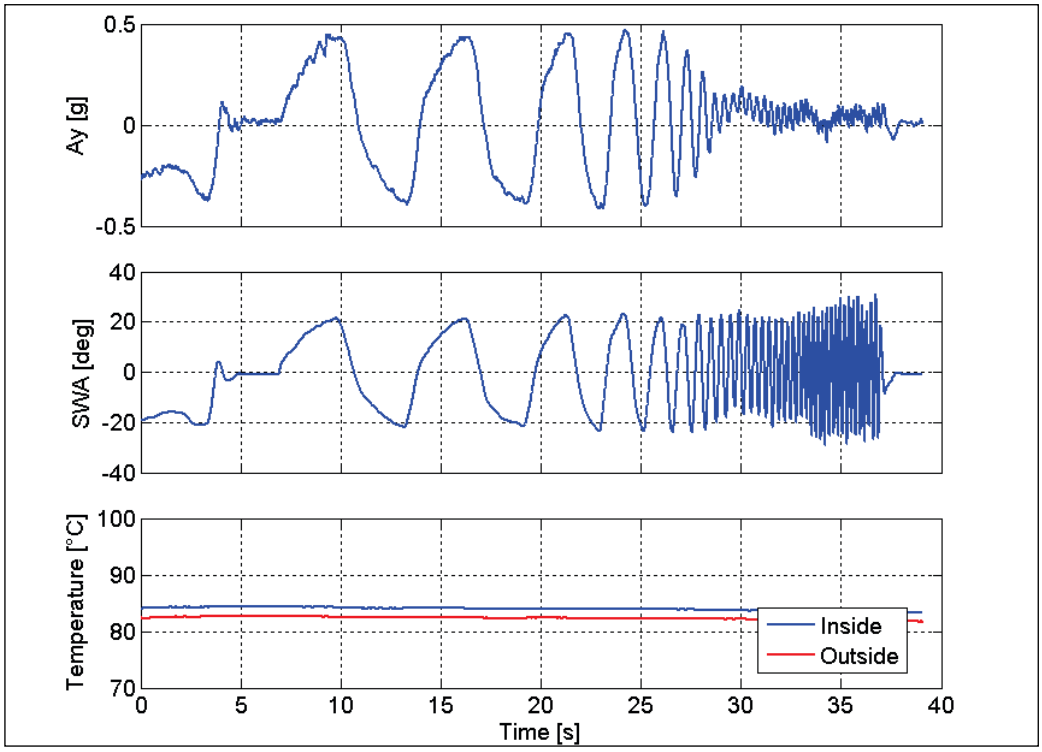

Figure IV.11 – The bulk temperature time history during sine-sweep maneuver

As showed in the Figure IV.11 the lateral acceleration reached was 0.4 g, so the tires remained next to their linear range. The bulk temperature remained constant during the entire test. The temperature reached by the tires depends

on the vertical load acting on the tire and on the speed of the vehicle as demonstrated in the previous paragraph.
Evidently, in this kind of test, the Friction Power is negligible and the only heat generation in the tires is due to the SEL.

This analysis demonstrates the importance of the run-in phase for the tires: to correctly perform the OH tests, the driver should run for 3-4 km at the speed he will perform the test (in this case 100 kph). In this way, the bulk saturates to its exercise temperature and the tires explicate the effective cornering stiffness.

The second kind of test performed is the Steering Pad at constant speed (Figure IV.12).

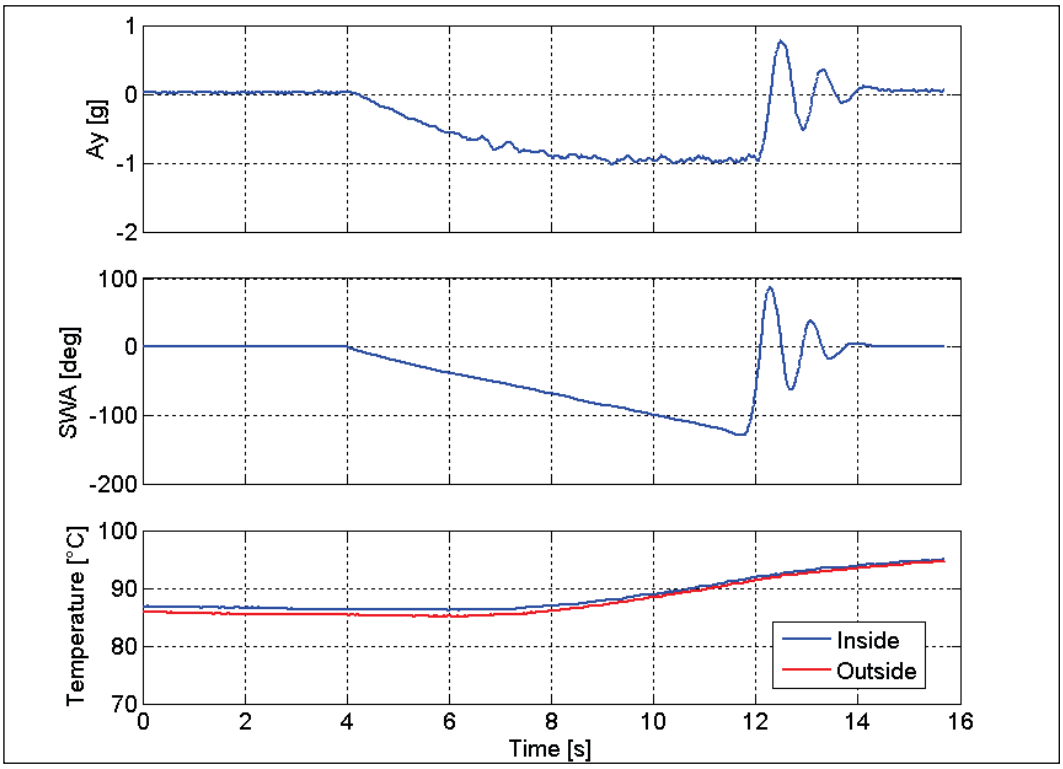

Figure IV.12 – The bulk temperature time history during ramp steer maneuver

The Steering wheel angle reaches more than 100 deg – that means ≈6 deg on road – and the tires on front axle reach their limit. Evidently in this case the Friction Power is the most important heat generator in the tires involving in a significant surface temperature increase. For this reason the bulk temperature increases with a DT of about 15°C.

The third kind of test is the Panic stop from 100 kph (Figure IV.13).

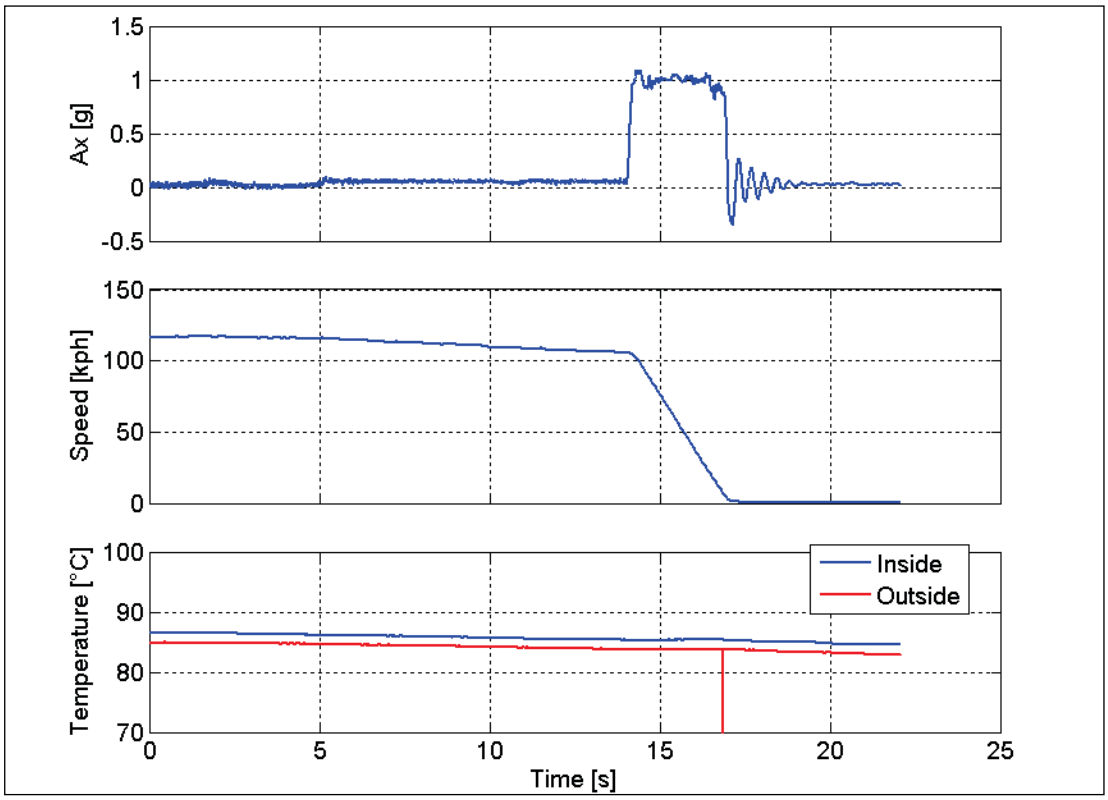

Figure IV.13 – The bulk temperature time history during panic stop maneuver

After a warm up phase, the bulk temperature stabilized at 85°C. As showed in the figure, the panic stop does not influence the bulk temperature. Even if the friction power is high – the tires reach their limit – the maneuver is too short to influence the bulk (3 seconds).

Chapter V – The Proposed Model

In this chapter a tire model able to evaluate the influence of bulk temperature on tire cornering stiffness will be presented. The model is composed by three main parts: the first part is the thermal model.
In it the diffusivity equations are used to model the heat generations and heat exchange of two layers named *surface* and *bulk*.
The second part is used to model the strain energy loss (SEL) that is the main heat generation in the bulk in the linear range of tire exercise. Even if this part could appear very simple – the simplifying hypotheses are very strong – as will be showed in the next chapter, the results appear very satisfactory.
The last part is the cornering stiffness modeling. In this part the model interacts with Pacejka standard formulation correcting the cornering stiffness formulation taking into account the bulk temperature influence.

V.1 – The Thermal Model

The model is based on the following equations, the first one for surface and the second one for bulk:

$$m_{srf} \cdot c_v \cdot \frac{\Delta T_{srf}}{\Delta t} = hpc \cdot \left(F_x \cdot v_{sx}\right) + hpc \cdot \left(F_y \cdot v_{sy}\right) + SEL_{srf} + h \cdot \left(T_{air} - T_{srf}\right) \cdot S_{conv} + H_c \cdot \left(T_{tr} - T_{srf}\right) \cdot S_{cont} + \frac{k}{\Delta Z} \cdot \left(T_{blk} - T_{srf}\right) \cdot S_{tot}$$

$$m_{blk} \cdot c_v \cdot \frac{\Delta T_{blk}}{\Delta t} = SEL_{blk} + \frac{k}{\Delta Z} \cdot \left(T_{srf} - T_{blk}\right) \cdot S_{tot} \qquad (31)$$

with:

m_{srf} surface layer mass [kg];

m_{blk} bulk layer mass [kg];

k thermal conductivity [W/mK];

c_v tire specific heat [J/kgK];

ΔZ bulk measure point depth [m];

hpc heat partition coefficient [-][3];

F_x longitudinal force [N];

F_y lateral force [N];

v_{sx} longitudinal sliding velocity [m/s];

v_{sy} lateral sliding velocity [m/s];

SEL Strain Energy Loss (strain dissipated energy) [W];

h convection coefficient [W/m^{2}K];

[3] The heat partition coefficient [13] takes into account the percentage of the generated friction power that effectively warms up the tire. The rest of this power flows into the road.

H_c track-tire exchange coefficient [W/m²K];

T_{air} air temperature [K];

T_{tr} track temperature [K];

S_{conv} air-tire exchange area [m²];

S_{cont} contact patch [m²];

S_{tot} total tire area [m²];

The following hypotheses have been adopted:

- The tire does not roll; all the boundary conditions act at the same time through different areas;
- The tire has no grooves;
- The contact patch (and consequently the air-tire exchange area) is always rectangular;

V.1.1 – The forced convection coefficient

The convection coefficient is evaluated using the classical dimensionless analysis. Basing on the article [11], the following relationship has been used:

$$h = \frac{k_{air}}{L} \cdot \left[0.318 \cdot \left(\frac{V \cdot L}{\upsilon} \right)^{0.571} \right] \qquad (32)$$

with:

k_{air} Thermal conductivity of the air;

L a characteristic length, evaluated as $L = \frac{1}{\frac{1}{D} + \frac{1}{W}}$ where D is the overall diameter and W the tire width;

V the roadway speed [m/s];

υ kinematic viscosity of the air;

Taking into account the results showed in the article [10], a law similar to the Arrhenius one has been added to the relationship to consider the convection coefficient dependence on the tire surface temperature. So, the final expression becomes:

$$h = \frac{k_{air}}{L} \cdot \left[0.318 \cdot \left(\frac{V \cdot L}{\upsilon} \right)^{0.571} \right] + 8.59 \cdot 10^{-11} \cdot \exp\left(0.0879 \cdot T_{surf}\right) \tag{33}$$

The coefficients in the Arrhenius law have been identified so that the convection coefficient would reach the same values explained in the article in the same operative conditions.

The track-tire exchange coefficient (H_c) is constant.

V.1.2 – The rest of the parameters

Both thermal conductivity and specific heat of the tire are considered function of bulk temperature with the following laws:

$$k = a \cdot T_{blk}{}^2 + b \cdot T_{blk} + c$$

$$c_v = d \cdot T_{blk}{}^2 + e \cdot T_{blk} + f \tag{34}$$

The identified temperature dependence law induces in a thermal conductivity equal to 0.29 W/mK at 20°C that is similar to the value explained in the article [5].
Instead the specific heat has been considered constant and equal to 1800 J/KgK.

The contact patch – and consequently the convection area – is supposed variable with vertical load. It is evaluated using a lookup table directly from measurement on the tire:

$$S_{cont} = f(F_z) \qquad (35)$$
$$S_{conv} = S_{tot} - S_{cont}$$

with

S_{tot} total external area, evaluated as $S_{tot} = 2\pi R_0 \cdot W$;
S_{cont} contact patch function of vertical load;
S_{conv} external area of the tire that exchanges heat with air;

The following scaling factors have been introduced in the model for an eventual tuning:

- λ_x – scaling factor on longitudinal friction power;
- λ_y – scaling factor on lateral friction power;
- λ_h – scaling factor on air-tire thermal exchange;
- λ_{Hc} – scaling factor on track-tire thermal exchange;
- λ_{CP} – scaling factor on cornering stiffness;
- λ_{SELsrf} – scaling factor on surface SEL;
- λ_{SELblk} – scaling factor on bulk SEL;

V.2 – The Strain Energy Loss model

To compute the strain energy loss, the model considers a regular control volume (Figure V.1) characterized by a length equal to the contact patch length (so, in dependence on the vertical load), a width equal to the tread nominal width and a height equal to the sidewall height.

On this control volume the following contact pressure acts:

$$\sigma_0 = \frac{F_z}{A_0} \qquad [N/m^2] \qquad (36)$$

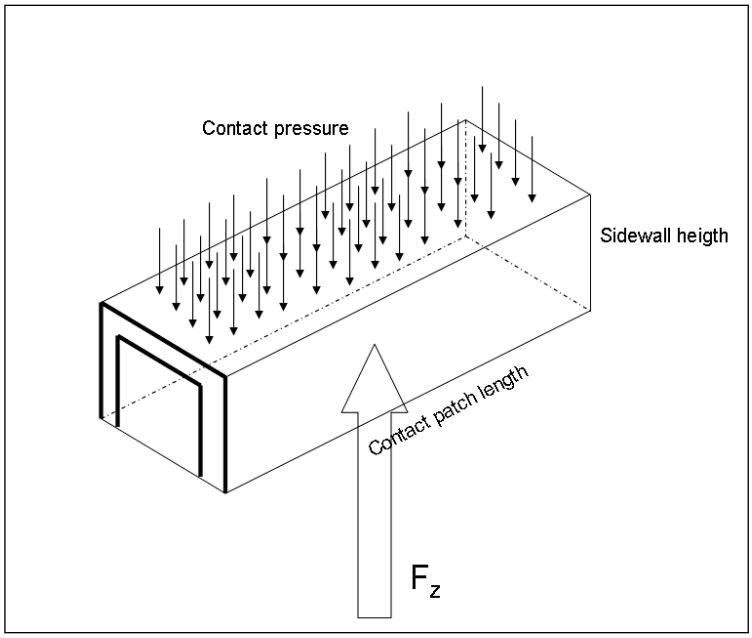

Figure V.1 – The scheme used to model the Strain Energy Loss

that induces the following deformation (supposed uniform on the contact patch) due to the deflection of the tire respect to the initial sidewall height:

$$\varepsilon = \frac{R_0 - R_L(F_z)}{H} \qquad (37)$$

with:

R_0 unloaded radius;

$R_L(F_z)$ loaded radius (in dependence on vertical load), evaluated by a look up table from measurements on tire ;

H sidewall height;

Due to this deformation and contact pressure, it is possible to compute the relative elastic energy stored by the tire:

$$E = \sigma_0 \cdot \varepsilon \qquad [\text{N/m2}] \qquad (38)$$

Evidently, the most part of this energy will be stored by the inflation gas (that participates to the tire deflection). The percentage of the energy effectively stored by the tire can be evaluated taking into account the ratio between the tire cross-section area and the control volume area, as showed in the Figure V.2.

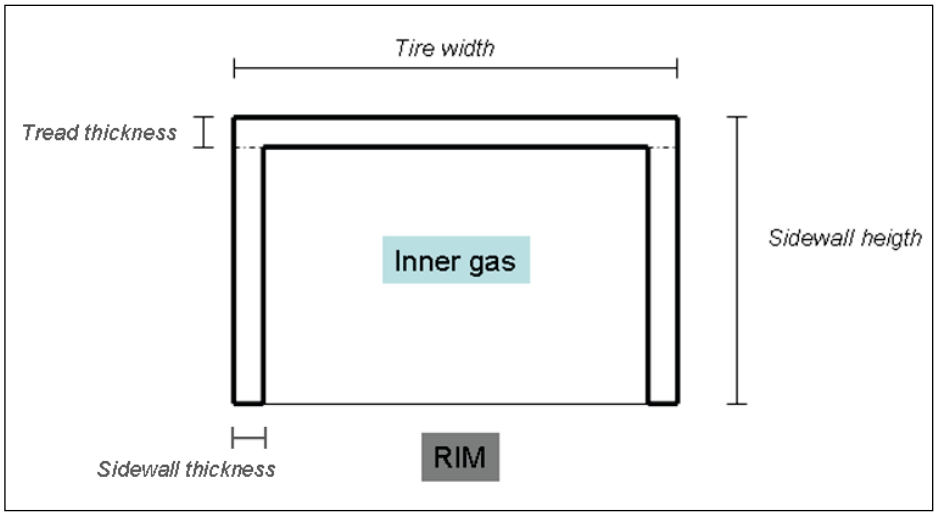

Figure V.2 – The transverse section scheme used in the model

$$Ratio = \frac{A_{CS}}{A_{VC}} \qquad (39)$$

For this reason, the energy stored by only the tire will be:

$$E = \sigma_0 \cdot \varepsilon \cdot Ratio \qquad [\mathrm{N/m^2}] \qquad (40)$$

Evidently, the dissipated energy could be evaluated multiplying the stored energy by the *tand* of the compound [6], [7]:

$$E_d = \sigma_0 \cdot \varepsilon \cdot Ratio \cdot \tan(\delta) \qquad [\mathrm{N/m^2}] \qquad (41)$$

This energy must be multiplied by the control volume to obtain the effective energy dissipated by the tire.

$$E_d = \sigma_0 \cdot \varepsilon \cdot Ratio \cdot \tan(\delta) \cdot A_0 \cdot H \qquad [\mathrm{Nm}] \qquad (42)$$

with:

A_0 contact patch area;

H sidewall height;

Operating the substitutions the dissipated energy becomes:

$$E_d = F_z \cdot \varepsilon \cdot Ratio \cdot H \cdot \tan(\delta) \qquad \text{[Nm]} \qquad (43)$$

This is the energy dissipated by the tire during a single step in the contact patch. To obtain the total dissipated energy per one revolution, this energy must be multiplied by the number of control volumes that can be considered along the tire circumference:

$$N_c = \frac{L}{l} = \frac{2\pi R_0}{l} \qquad (44)$$

with:

R_0 unloaded radius;

l contact patch length (in dependence on vertical load);

So, the energy dissipated by the tire per each revolution will be:

$$E_{diss} = E_d \cdot N_c \qquad (45)$$

This energy, multiplied by the number of revolutions per second $n = \frac{\omega}{2\pi}$ will give the tire dissipation power:

$$\dot{E}_{diss} = E_{diss} \cdot n \qquad \text{[W]} \qquad (46)$$

The angular velocity of the tire is computed taking into account the effective rolling radius by a look up table from measurements on tire:

$$\omega = \frac{V}{R_R} \qquad (47)$$

with:

V roadway speed [m/s];
R_R rolling radius [m];

The *tand* has been considered variable with bulk temperature and rotational speed[4] of the tire using the WLF law [17].

So, starting from the effective bulk temperature, the following equivalent temperature is computed in real-time:

$$T_{eq} = T_b + \frac{C_2 \cdot \log\left(\frac{f}{f_0}\right)}{C_1 - \log\left(\frac{f}{f_0}\right)} \qquad (48)$$

with:

T_b tire bulk temperature;

[4] In reality the oscillation frequency is a little bit less than the rotational speed; anyway they can be considered equal for the purpose.

f oscillation frequency of the compound, evaluated as $f = \frac{\omega}{2\pi}$

f_0 reference compound frequency;

So, the *tand* is evaluated with the following Gaussian law:

$$\tan(\delta) = a \cdot \exp\left[-\left(\frac{T_{eq} - b}{c} \right)^2 \right] \qquad (49)$$

with:

a , *b* and *c* to be identified by experimental data.

Evidently, the Thermal Model will be able to predict the tire rolling resistance in terms of drag force F_x.

In fact, it is possible to write:

$$M_y = \frac{\dot{E}_{diss}}{\omega} = \frac{\dot{E}_{diss}}{\left(V \big/ R_R \right)} = \frac{\dot{E}_{diss} \cdot R_R}{V} \quad \text{[Nm]} \qquad (50)$$

that involves in:

$$F_R = \frac{M_y}{R_L} = \frac{\dot{E}_{diss} \cdot R_R}{V \cdot R_L} \text{ [N]} \qquad (51)$$

with:

V roadway speed [m/s];

R_R effective rolling radius [m];

R_L loaded radius [m];

F_R tire drag force;

The SEL sub-model can take into account the compound characteristics (through the *tand*) and the mass of the tire (through the Area Ratio) that means it could be predictable for a RFT too. Anyway, it cannot take into account the different type of construction; so tires with different constructive characteristics but with same compound and masses will present the same SEL and Rolling Resistance.
Anyway, as will be showed in the chapter VI, even if very simple, this model gave back very satisfactory results on SEL prediction.

V.3 – The Cornering Stiffness model

A simple sub-model to compute tire cornering stiffness in dependence on Vertical Load and bulk temperature has been implemented.

The following equation has been used for the purpose [1]:

$$CP = \frac{1}{2} \cdot E_{eq} \cdot l^2 ; \qquad (52)$$

with:

CP the tire cornering stiffness [N/rad];
E_{eq} the equivalent circumferential Young Modulus of the tire [N/m^2];
l the contact patch length [m];

The equivalent circumferential Modulus has been computed taking into account the mechanical properties of the belt using the following equations [4]:

$$V_c = \frac{\frac{\pi \cdot D^2}{4} \cdot n_c}{t \cdot l} \qquad [-] \qquad (53)$$

where:

D is the diameter of the single cord in the belt [m];
n_c is the number of the cord in the belt [-];
t is the thickness of the belt [m];
l is the width of the belt [m];

$$E_1 = E_c \cdot V_c + E_r \cdot (1 - V_c) \qquad [N/m2] \qquad (54)$$

where:

E_c is the Young Modulus of the cord [N/m2];
E_r is the Storage Modulus of the rubber matrix [N/m2];

$$E_2 = E_r \cdot \frac{1 + 2V_c}{1 - V_c}$$

$$v_{12} = v_c \cdot V_c + v_r \cdot (1 - V_c) \qquad (55)$$

$$v_{21} = v_{12} \cdot \frac{E_2}{E_1}$$

where

v_c is the Poisson modulus of the cord [-];

v_r is the Poisson modulus of the rubber matrix [-];

$$G_r = \frac{E_r}{2 \cdot (1 + v_{12})}$$

$$G_c = \frac{E_c}{2 \cdot (1 + v_{12})}$$

$$G_{12} = G_r \cdot \frac{G_c + G_r + (G_c - G_r) \cdot V_c}{G_c + G_r - (G_c - G_r) \cdot V_c} \tag{56}$$

$$E_x = \frac{1}{\frac{\cos^4(\psi)}{E_1} + \left(\frac{1}{G_{12}} - \frac{2 \cdot v_{12}}{E_1} \right) \cdot \sin^2(\psi) \cdot \cos^2(\psi) + \frac{\sin^4(\psi)}{E_2}}$$

$$G_{xy} = \frac{1}{\frac{\cos^2(\psi)}{G_{12}} + \left(\frac{1 + v_{12}}{E_1} + \frac{1 + v_{21}}{E_2} \right) \cdot \sin^2(\psi)}$$

The Equivalent Modulus E_x has been considered function of contact patch length and temperature, as showed in the following Figure V.3.

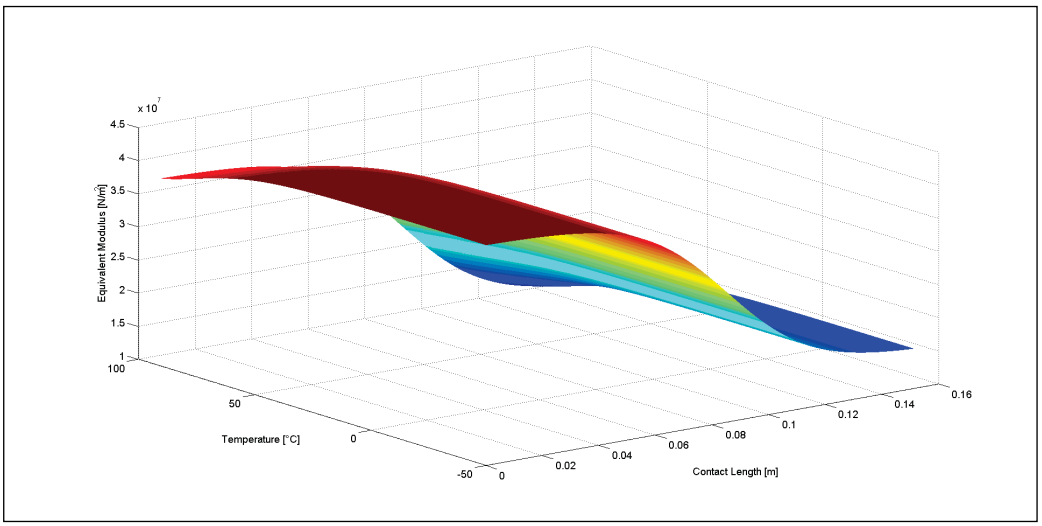

Figure V.3 – The equivalent modulus in dependence on bulk temperature and contact patch length

The contact patch length has been considered function of vertical load. Starting from footprint measurements on the tire at different vertical loads, an equivalent contact patch length is considered in dependence on vertical load, as showed in the Figure V.4.

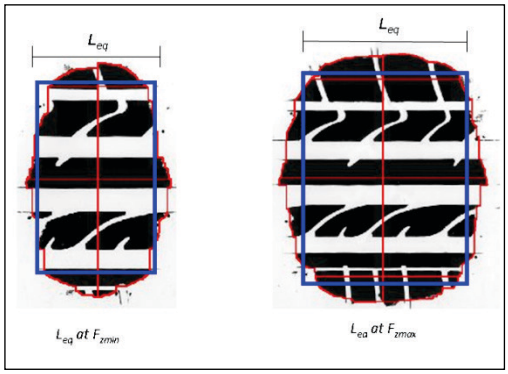

Figure V.4 – The contact patch modeling

Even if a lot of models are available in literature to evaluate the contact length [15], an exponential law to simply fit the experimental measurements has been used for the dependence on vertical load:

$$l = -l_{\max} + \left(\frac{2 \cdot l_{\max}}{1 + \exp^{(k \cdot Fz)}} \right) \qquad (57)$$

With:

$l_{\max}$ the maximum value assumed by the contact patch length;

k a shape factor that determines the slope of the curve;

In the Figure V.5 a comparison between the measured data and the fitting obtained with the described law is showed.

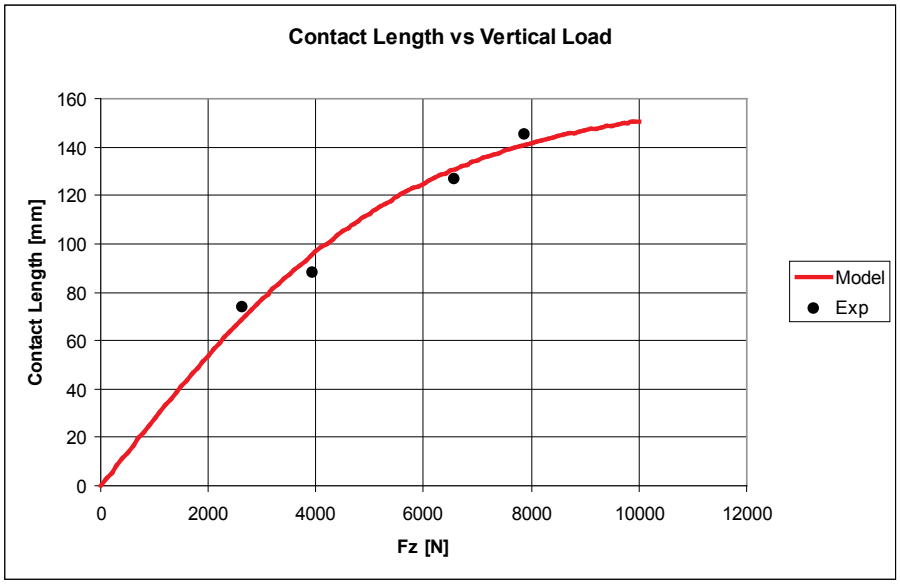

Figure V.5 – The contact patch length variation

V.3.1 – How the Model interacts with Pacejka MF

the proposed model interacts with the cornering stiffness computation of the Pacejka MF5.2:

$$K_{ya}(F_z) = p_{K1} \cdot \left[F_{Z0} \cdot \sin\left(2 \cdot \arctan\left(\frac{F_z}{p_{K2} \cdot F_{Z0}} \right) \right) \cdot (1 - p_{K3} \cdot \gamma) \right] \quad (58)$$

The formula above takes into account only the vertical load acting on the tire and the camber angle.
Pacejka already considers his own scaling factors to correct/adjust all the terms in the formulation.
The purpose is to use one of these scaling factors, getting it dependent on bulk temperature;

So, the model starts from the original formulation correcting it through a scaling factor in dependence on bulk temperature of the tire:

$$K_{ya}(F_z, T_b) = \lambda_{Tb}(T_b) \cdot p_{K1} \cdot \left[F_{Z0} \cdot \sin\left(2 \cdot \arctan\left(\frac{F_z}{p_{K2} \cdot F_{Z0}} \right) \right) \cdot (1 - p_{K3} \cdot \gamma) \right] \quad (59)$$

The scaling factor is computed in real time during the simulation basing on the following equation:

$$\lambda_{Tb}(T_b) = \frac{CP(F_z, T_b)}{K_{ya\_ref}(Fz, \gamma)} \quad (60)$$

Where:

$CP(F_z, T_b)$ is the cornering stiffness computed by the thermal model;

$K_{ya\_ref}(Fz, \gamma)$ is the reference cornering stiffness of the tire proposed by the classical Pacejka formulation;

Evidently this scaling factor varies continually around the unit.
This formulation produces satisfactory results taking into account the vertical load influence and the bulk temperature influence as showed by the Figure V.6.

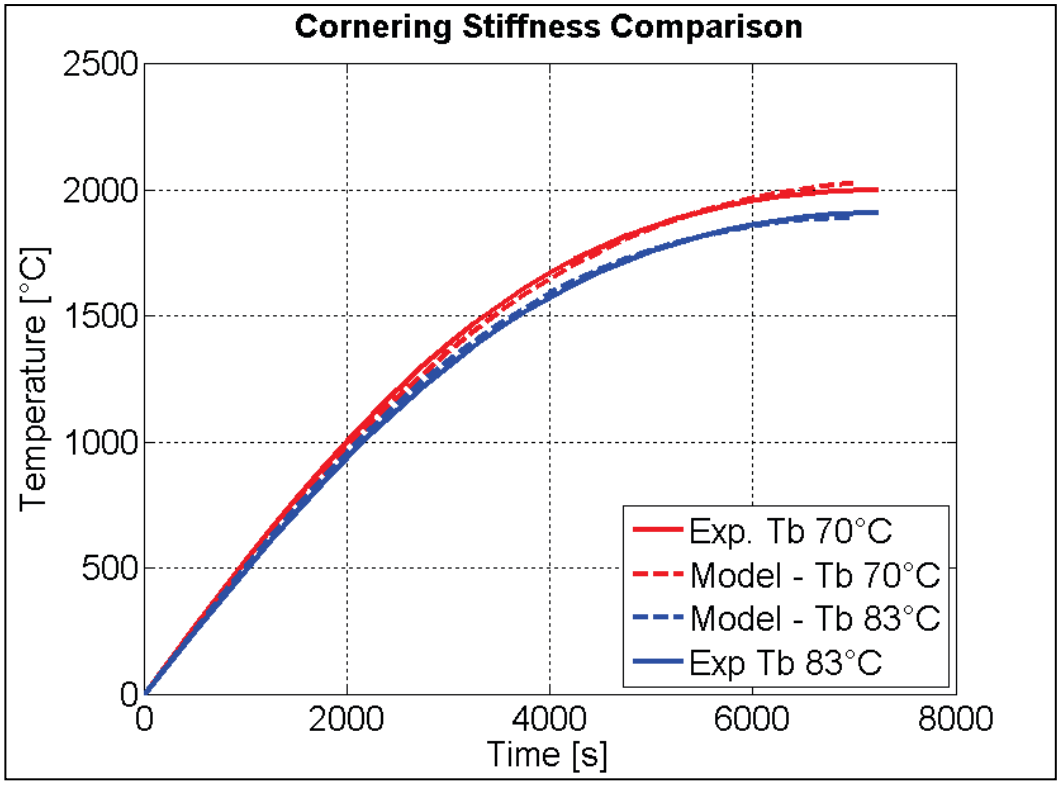

Figure V.6 – Cornering Stiffness comparison between model and measurements

V.4 – The user interface

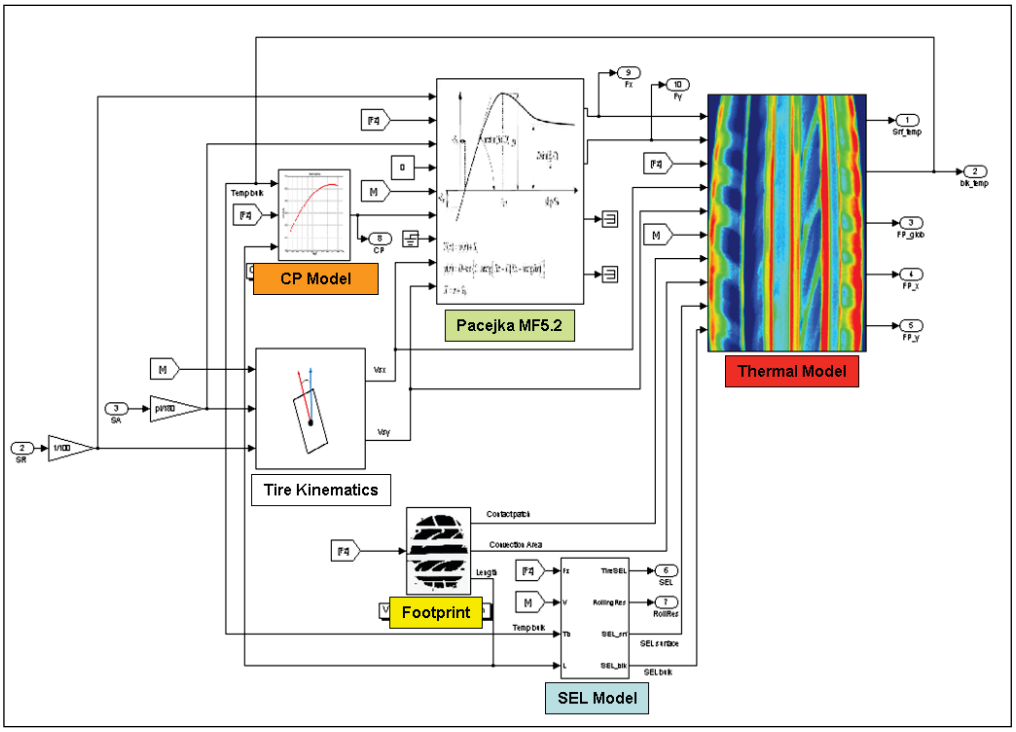

Figure V.7 – The model in Simulink environment

Even if the model has been developed in Matlab/Simulink environment and it could appear very complex (Figure V.7), it has been created to be as much user-friendly as possible; in fact the average user can interact just with an *xls* file where all the parameters are stored.

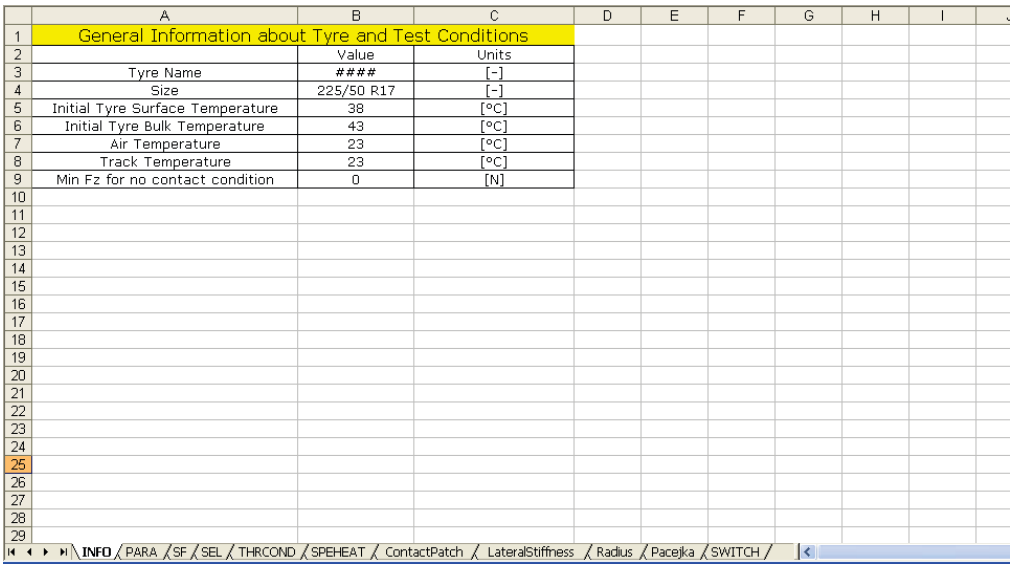

	A	B	C
1	General Information about Tyre and Test Conditions		
2		Value	Units
3	Tyre Name	####	[-]
4	Size	225/50 R17	[-]
5	Initial Tyre Surface Temperature	38	[°C]
6	Initial Tyre Bulk Temperature	43	[°C]
7	Air Temperature	23	[°C]
8	Track Temperature	23	[°C]
9	Min Fz for no contact condition	0	[N]

INFO | PARA | SF | SEL | THRCOND | SPEHEAT | ContactPatch | LateralStiffness | Radius | Pacejka | SWITCH

Figure V.8 – The xls file to set the parameters

The xls file (Figure V.8) contains 10 datasheets that will be described in the next paragraphs.

V.4.1 – Datasheet INFO

It contains

- the tire name (it will be used just to name the output plot figures);
- The tire size. This part is important because these info will be used to define the tire geometry;
- Initial surface and bulk temperature;
- Air and Track temperature;
- The minimum value of Fz below that the model should not consider the tire in contact with the road; this value usually must set on zero, but it has been introduced in case of an input file with noise; in this case the

user could set this value to 10N, 100N, etc. For example, if it is set to 100 N, when Fz is under 100 N, the model forced it to 0 N.

V.4.2 – Datasheet PARA

It contains

- The Unloaded radius of the tire;
- The tire cross-section thickness;
- The percentage of the surface mass on the total tire mass (used to set the mass distribution between surface block and bulk block);
- The depth in the cross-section at which the virtual bulk temperature sensor will be positioned;
- The natural convection coefficient; the model uses this value if the roadway speed becomes zero and/or in every condition in which the forced convection coefficient becomes less than this value;
- The track-tire heat exchange coefficient;
- Tire rubber density;
- Air thermal conductivity;
- Air kinematic viscosity;
- The heat partition coefficient; the friction power generated at the interface is divided by this coefficient between the rubber and the road;

V.4.3 – Datasheet SF

It contains all the scaling factors used in the thermal model

V.4.4 – Datasheet SEL

It contains all the parameters necessary to characterize the *tand* WLF law. In particular, it contains:

- Compound reference frequency;
- *tand* peak temperature;
- Glassy-rubbery state transition temperature range;
- *tand* maximum;
- The coefficients C1 and C2 used in WLF law

V.4.5 – Datasheet THRCOND

It contains the parameters of the parabolic function of the tire thermal conductivity in dependence on bulk temperature. A plot of this function also is showed.

V.4.6 – Datasheet SPEHEAT

It contains the parameters of the parabolic function of the tire specific heat in dependence on bulk temperature. Also in this case a plot with this function is showed.

V.4.7 – Datasheet ContactPatch

In the first part, it contains the parameters to define the contact patch length vs. vertical load law. In particular, the user can define:

- The maximum length of the contact patch;
- The slope of the curve *L=f(Fz)*;

In the second part the user must define the two coefficients A and B to define the contact patch vs. vertical load linear law.

In a third part, the user can insert the experimental data in terms of equivalent contact patch length and contact patch area for different vertical loads. In this way, the user can compare the model results with the experimental data using the dedicated comparison plots.

V.4.8 – Datasheet LateralStiffness

First of all the user can disable the CP computation selecting OFF on the first row of the datasheet.

Anyway, it contains the parameters to determine the variation of the lateral stiffness in dependence on vertical load and bulk temperature.

In fact, the cornering stiffness is computed taking into account the contact patch length and the equivalent modulus of the tire.

The equivalent modulus of the tire is supposed function of the contact patch length and of the bulk temperature. The user can choose:

- The maximum value of the modulus;
- The delta of the modulus itself due to the contact patch length variation;
- The slope of the curve $E_{eq}=f(Fz)$;
- The delta of the modulus due to the bulk temperature variation;
- The slope of the curve $E_{eq}=f(Tb)$;
- The horizontal shift of the curve $E_{eq}=f(Tb)$ respect to 0°C

V.4.9 – Datasheet Radius

The layout is very similar to the *ContactPatch* one.
In the first part the user must insert the coefficient A and B to define the linear law loaded radius vs. vertical load.
In the second part the user must insert the coefficients A and B to define the power law rolling radius vs. vertical load.
In the third part, the user can insert experimental data to compare the model results with them.

V.4.10 – Datasheet SWITCH

Through this datasheet the user can switch off one or more part of the model.
In particular is possible:

- To exclude the friction power in the model; just the SEL generates heat in the tire.
- To exclude just the longitudinal friction power
- To exclude just the lateral friction power
- To exclude the heat exchange with air; the tire exchanges heat just with track
- To exclude the heat exchange with track; the tire exchanges heat just with air.
- To exclude SEL generation; just the friction power generates heat.
- To exclude heat exchange between surface and bulk.

V.5 – How to Build-up a tire model

In the next paragraphs how to identify all the parameters the model needs will be explained.

V.5.1 – Geometrical Parameter Definition

Geometrical and Thermo dynamical Parameters		
	Value	Units
Unloaded Radius	0.3308	[m]
Tread Thickness	12	[mm]
Sidewall Thickness	9	[mm]
Tire Surface Mass percentage	15	[%]
Bulk Measure Point Depth	10	[mm]
Natural convection coeff.	30	[W/m^{2}K]
Hc	500	[W/m^{2}K]
Tire Rubber Density	1100	[kg/m^3]
Air Thermal Conductivity	0.025	[W/mK]
Air kinematic viscosity	1.50E-05	[m^2/s]
Heat Partition coefficient	0.6	[-]

The first step to build-up a model is to set the geometrical parameters of the tire; of course the user must set the size – used in the model to build the control volume; for this purpose the unloaded radius is an important parameter too; the model in fact uses this parameter to compute the exchange areas of the tire.

Again the thickness of the cross section is important; the user can set the *Tread Thickness* and the *Sidewall Thickness* separately (Figure V.9).

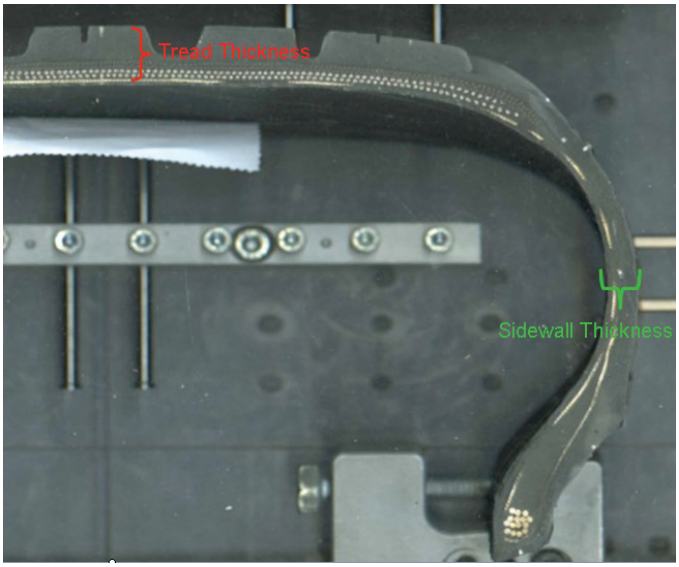

Figure V.9 – The tread thickness and the sidewall thickness in the model

This could be very useful in case of RFT in which the sidewall appears very thick or in case of Light Truck tires where the tread is thicker than the sidewall. The parameter *Tire Surface Mass percentage* can be set basing on experience (10-15% gives back good results); the model uses this parameter to separate the surface mass – a thin layer on the outer surface warmed up above all by the friction power – to the bulk mass that is heated up by the SEL mainly (Figure V.10).

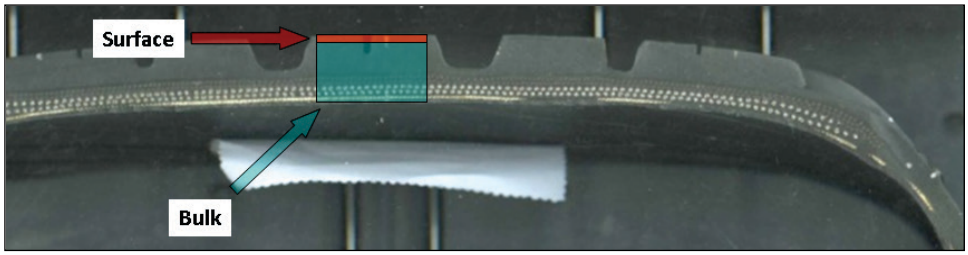

Figure V.10 – The surface layer and the bulk layer in the model

Through the parameter *Bulk Measure Point Depth* the user sets the depth of the virtual bulk temperature sensor point. Evidently, in the case of the tire equipped with T3M sensors, this parameter has been set as much equal as the real position of the sensors.

The *Natural convection coefficient* acts when the roadway speed becomes zero. In this case the tire is subjected to natural convection cooling (30 W/m^2K is a typical value for this kind of geometry).

Hc is the Track-Surface Heat Exchange coefficient. This is based on Newton formula for heat exchange and its typical value (500 W/m^2K) has been found out through experimental activities [42].

The rest of the parameters are available in literature evidently but the *Heat Partition coefficient*. For simplicity this parameter has been set to 0.6; this value has been found out in past activities [42], [29].

V.5.2 – The SEL Model Parameters

To define the SEL model, it is necessary to set the tread compound parameters; in particular it is necessary to set the *tand* variation law.

Strain Energy Loss functionality Parameters		
Parameter	Value	Units
WLF Parameters		
Reference Frequency	52	[Hz]
Tand peak Temperature	-8	[°C]
C1	-8.86	[-]
C2	101.60	[-]

So, the user must set the reference frequency for the WLF law, the glassy transition temperature and the two coefficients C1 and C2.

Model Parameters		
Tand Parameter a1	2.14E+15	[-]
Tand Parameter b1	-4989	[-]
Tand Parameter c1	882	[-]

Then the user must set the three coefficients of the *tand* law in dependence on temperature:

$$\tan(\delta) = a \cdot \exp\left[-\left(\frac{T_{eq} - b}{c}\right)^2\right] \qquad (61)$$

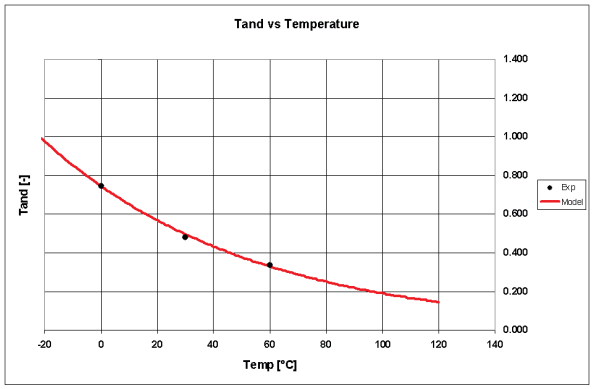

Figure V.11 – The tand variation with temperature

Through standard Flat Trac test it is possible to evaluate the Rolling Radius and the Loaded Radius dependency on vertical load.

Model Parameters							
		Value	Units			Value	Units
Loaded Radius	Coeff A	-4.20E-06	[m/N]	Rolling Radius	Coeff A	0.3483	[m]
	Coeff B	0.3308	[m]		Coeff B	-0.009	[1/N]

To fit the Rolling Radius a power law has been considered:

$$R_R = a \cdot (F_z)^b \qquad (62)$$

while to fit the Loaded Radius a linear law has been used:

$$R_L = a \cdot F_z + b \qquad (63)$$

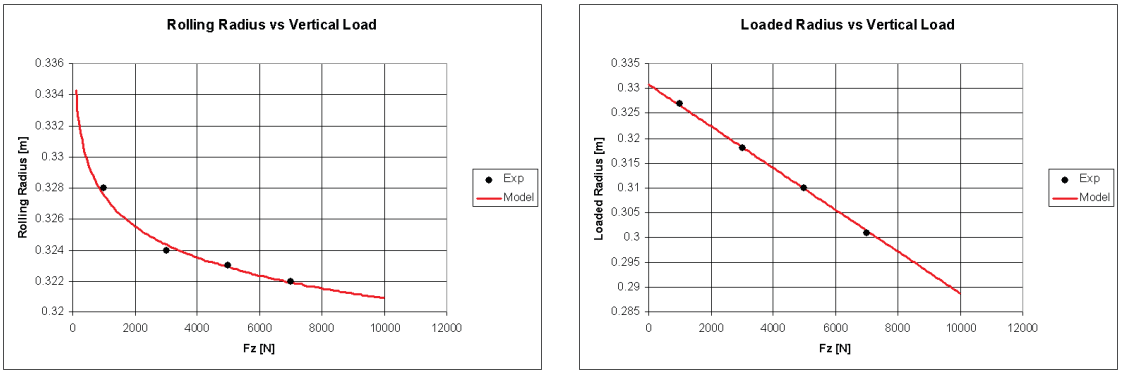

Figure V.12 – The rolling radius and the loaded radius in dependence on vertical load

V.5.3 – Footprint test

Even if to obtain the best results dynamic footprint tests should be used in the model, good results have been obtained with static footprint tests too.
So, at least a static test must be performed to evaluate Contact patch extension and contact patch length law in dependence on vertical load.
Evidently, the test must be performed at three different vertical loads at least.

The contact patch length could be evaluated taking into account the average value between the three values available from the test:

- Contact length at the center;
- Contact length at the outside shoulder;
- Contact length at the inside shoulder;

In this way an equivalent footprint area can be obtained (Figure V.13).

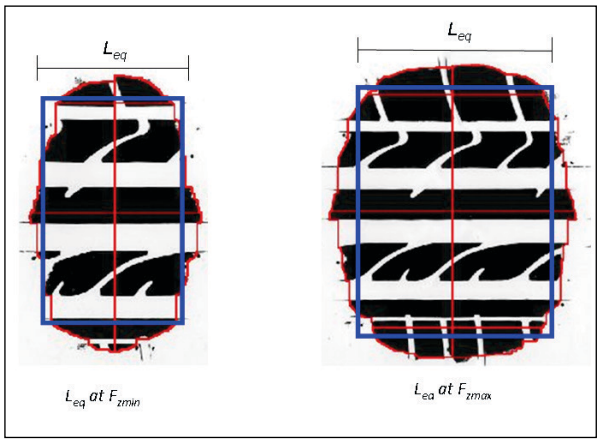

Figure V.13 – The footprint modeling

Model Parameters							
		Value	Units			Value	Units
Contact Length	max length	160	[mm]	Contact Patch	Coeff A	2.333	[mm²/N]
	length curve slope	0.35	[-]		Coeff B	0	[mm²]

As mentioned in the previous paragraphs for the vertical load dependence of the footprint length, the following law has been used:

$$l = -l_{\max} + \left(\frac{2 \cdot l_{\max}}{1 + \exp^{(k \cdot Fz)}} \right) \qquad (64)$$

In the figures below different laws setting different l_{max} and k are shown.

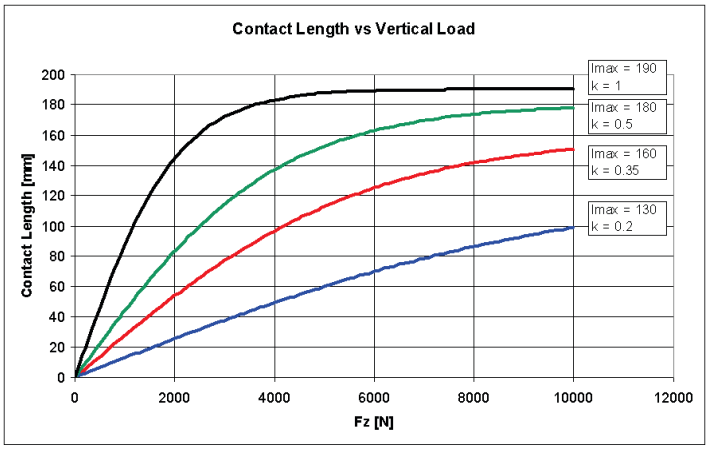

Figure V.14 – Footprint length variation changing the parameters

For the contact patch area instead a linear law has been used (Figure V.15).

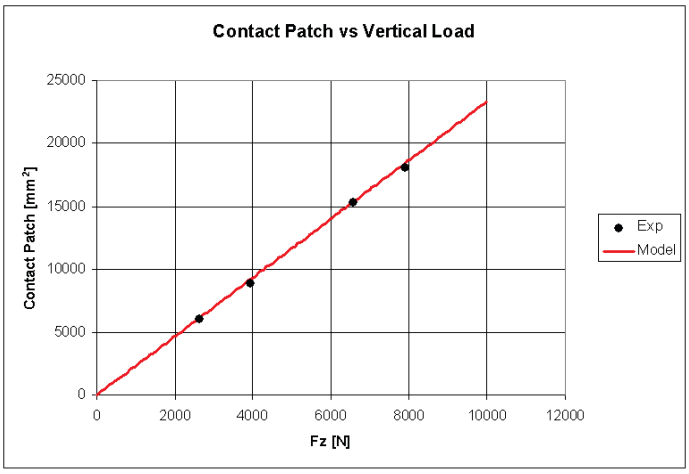

Figure V.15 – Contact patch vs. vertical load linear law

V.5.4 – The Equivalent Modulus

The equivalent Modulus of the model has been divided into two contributions: one is considered dependent on contact patch length (Figure V.16); this to simulate the in-plane belt stiffness that directly influences the cornering-stiffness.

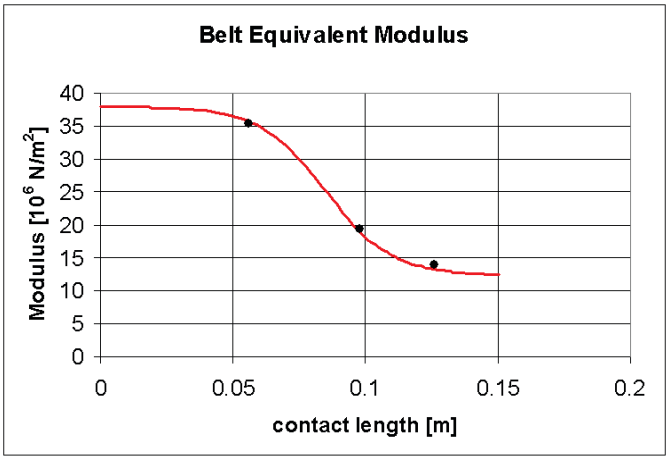

Figure V.16 – Equivalent Modulus in dependence on contact patch length

And the other one is considered dependent on temperature (Figure V.17); this to simulate the tread rubber behavior.

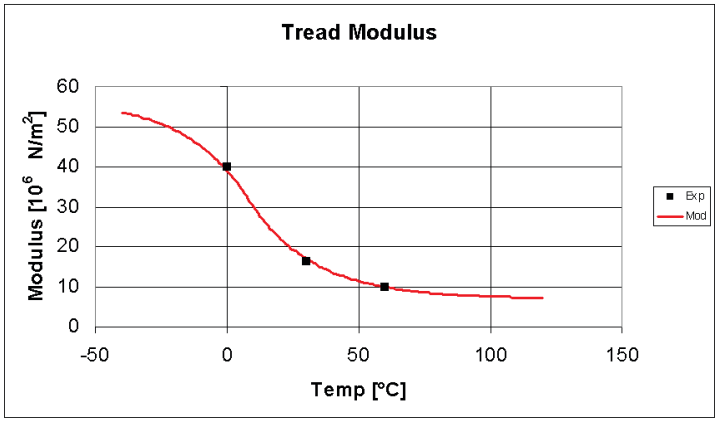

Figure V.17 – The equivalent modulus in dependence on bulk temperature

The two contributions are then combined as two springs in series (Figure V.18).

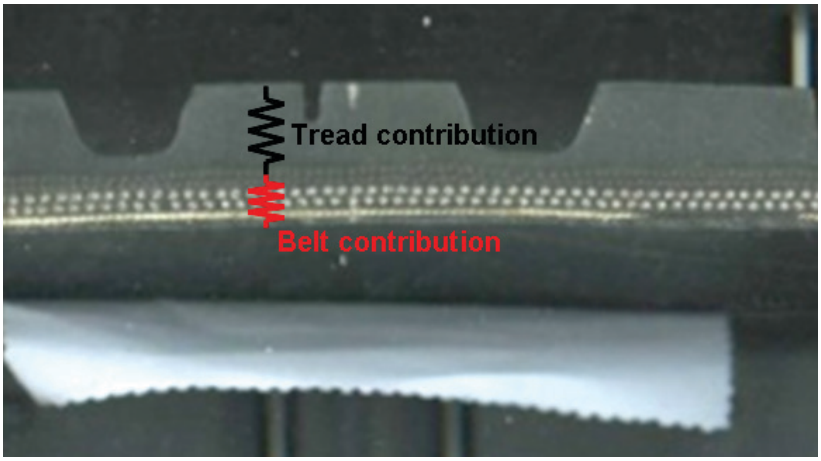

Figure V.18 – The contribution of tread and of belt

At least for now, to evaluate the equivalent modulus – and the relative laws – a sort of *reverse engineering procedure* is needed.

Starting from two different Flat Trac procedures (with increasing order and decreasing order of vertical load application) the Modulus is *tuned* so to let the model evaluate the correct Cornering Stiffness dependence on vertical load in both conditions (increasing and decreasing i.e. at different bulk temperature). Anyway, future upgrade will let the model to use physical modeling also for Dynamic Modulus.

V.6 – How the model interacts with the user file

An automatic routine in Matlab has been created to read all the parameters set by the user in the xls file and to compute the rest of the parameters the model needs.
In the next paragraphs will be explained how the routine computes these parameters.

V.6.1 – Area Ratio in SEL model

The first important step is the computation of the sidewall height. The routine starts from the *size* indication set in the xls parameters file and it computes the sidewall height as:

$$H = \frac{AR}{100} \cdot W \qquad (65)$$

with:

W tire width;

AR tire aspect ratio;

Then, it computes the ratio between the effective cross-section area and the SEL control volume nominal section area.
Evidently is:

$$\begin{aligned} A_{tot} &= W \cdot H \\ A_{trd} &= W \cdot h \\ A_{sdw} &= (W - h) \cdot H \end{aligned} \qquad (66)$$

where:

A_{tot} is the SEL control volume nominal section area;

A_{trd} is the area corresponding just to the tread (without sidewalls);

A_{sdw} is the area of the sidewall;

For simplicity, all these sections are considered perfectly rectangular.

So, the area of the effective cross-section will be:

$$A_{CS} = A_{trd} + (2 \cdot A_{sdw}) \qquad (67)$$

V.6.2 – Mass distribution computation

It starts from the computation of the entire tire mass:

$$m = \rho \cdot 2\pi R_0 \cdot W \cdot h \qquad (68)$$

with:

ρ rubber of the tire;

R_0 unloaded radius;

W tire width;

h tire thickness;

Then it divides this mass between surface and bulk taking into account the mass percentage defined by the user.

V.6.3 – Look up tables' preparation

In the last part, the routine creates all the vectors used by the model in the look up tables for the equivalent modulus. So, it creates:

- The vector of equivalent modulus in dependence on contact patch length;
- The vector of equivalent modulus in dependence on bulk temperature;

The first vector is created following the formula:

$$E_{eq} = E_{eq\,\max} - \left[\frac{\Delta E}{1 + \exp\left(slope \cdot \left(-l + l_{trsh}\right)\right)} \right] \qquad (69)$$

with:

$E_{eq\max}$ maximum value of equivalent modulus (defined by the user);

ΔE the variation of modulus (set by the user)

$slope$ the slope of the equivalent modulus vs. contact patch length curve (defined by the user);

For what concern the dependence on bulk temperature, the following formula has been used:

$$E_{eq} = -sign(T_{comp}) \cdot \left[1 - \exp\left(-a \cdot T_{comp} \cdot sign\left(T_{comp}\right)\right)\right] \qquad (70)$$

where

$$T_{comp} = T - T_{plateau} - \frac{\Delta T}{2}$$

$$T_{plateau} = T_g - \frac{\Delta T}{2} \qquad (71)$$

$$a = \frac{-2 \cdot \log\left(1 - 0.997\right)}{\Delta T}$$

V.7 – The Parameters List

It follows a list of all the parameters needed by the Simulink library model.

Scaling Factor Friction Long – a multiplier on the product $F_x \cdot v_{sx}$

Scaling Factor Friction Lat – a multiplier on the product $F_y \cdot v_{sy}$

Scaling Factor Air-Tire Therm. Exch. – a multiplier on the convection coefficient

Scaling Factor Track-Tire Therm. Exch. – a multiplier on the track-tire exchange coefficient

Scaling Factor Cornering Stiffness – a multiplier on Cornering Stiffness output

Scaling Factor SEL surface – a multiplier on surface block SEL

Scaling Factor SEL bulk – a multiplier on bulk block SEL

Surface Mass – surface block mass

Bulk Mass – bulk block mass

Unloaded Radius – Tire unloaded radius

Tire Width – Tire global width

Sidewall Height – height of the tire sidewall (taken from the tire Aspect Ratio)

Area Ratio – Ratio between the effective cross-section area and the SEL control volume area

Carcass Measure Depth – bulk temperature measure point depth in the carcass

Cross-section height – Tire cross-section height

Lowest value of Fz below that SEL and friction is zero – In this way model takes into account that if there is no contact with ground, no heat generation is.

Thermal Conductivity coeff. A – coefficient A in the thermal conductivity law

Thermal Conductivity coeff. B – coefficient B in the thermal conductivity law

Thermal Conductivity coeff. C – coefficient C in the thermal conductivity law

Specific heat coeff. A – coefficient A in the specific heat law

Specific heat coeff. B – coefficient B in the specific heat law

Specific heat coeff. C – coefficient C in the specific heat law

Heat partition coefficient – Heat partition coefficient between tire and road

Reference compound frequency – the excitation reference frequency used in the compound characterization

Glassy transition temperature – corresponding to the *tand* peak temperature

Glassy-Rubbery transition range – the temperature range through which the transition happens

Tand Maximum – the highest value of tand

WLF C1 Coefficient – The coefficient C1 in the WLF law

WLF C2 Coefficient – The coefficient C2 in the WLF law

Air thermal conductivity – thermal conductivity of the air

Air kinematic viscosity – kinematic viscosity of the air

Characteristic Length – Tire characteristic length for the convection coefficient

External Total Area – the tire total area (Width by Length)

Track-Tire Exchange coefficient – Exchange coefficient in Newton equation

Natural convection coefficient – Convection coefficient in natural conditions

Air Temperature – This value must be constant in this version

Track Temperature – This value must be constant in this version

Surface Initial Temperature – surface block initial temperature

Bulk Initial Temperature – bulk block initial temperature

Vertical Load vector for contact length – The Fz vector necessary to create look-up table for contact patch length vs. vertical load dependence

Contact Length vector – The vector of contact length values on dependence of Fz

Vertical Load vector for contact patch – The Fz vector necessary to create look-up table for contact-patch vs. vertical load dependence

Contact Patch vector – The vector of contact patch values on dependence of Fz

Vertical Load vector for Loaded Radius – The Fz vector necessary to create look-up table for Loaded Radius vs. vertical load dependence

Loaded Radius Vector – The vector of loaded radius values on dependence of Fz

Vertical Load vector for Rolling Radius – The Fz vector necessary to create look-up table for rolling radius vs. vertical load dependence

Rolling Radius Vector – The vector of rolling radius values on dependence of Fz

Vertical Load vector for Lateral Stiffness – The Fz vector necessary to create look-up table for lateral stiffness vs. vertical load dependence

Temperature Vector for lateral stiffness – The temperature vector necessary to create look-up table in cornering stiffness sub-model

Tire Lateral stiffness – Lateral stiffness values on dependence of Fz and tire temperature.

Switch on/off Global Friction Power – a switch to exclude the friction power in the model; just the SEL generates heat in the tire.

Switch on/off Longitudinal Friction Power - a switch to exclude just the longitudinal friction power

Switch on/off lateral Friction Power - a switch to exclude just the lateral friction power

Switch on/off Air-Tire Exchange – a switch to exclude the heat exchange with air; the tire exchanges heat just with track

Switch on/off Track-Tire Exchange – a switch to exclude the heat exchange with track; the tire exchanges heat just with air.

Switch on/off Strain Energy generation – a switch to exclude SEL generation; just the friction power generates heat.

Switch on/off Surface-Bulk conduction – a switch to exclude heat exchange between surface and bulk.

Chapter VI – The Model Validation

In this last chapter, all the simulations results will be showed to validate the entire model.

The first showed results will be on strain energy loss modeling. A test campaign has been performed on ZF machine with different tires (in terms of sizes, construction and compounds). The results are very satisfactory.

The second kinds of results will be of the thermal model. In this case different indoor tests have been simulated. Also in this case good results appear, especially taking into account that no scaling factors have been used to tune the model.

The last part is on cornering stiffness evaluation results and how the Pacejka formulation in the linear range gives back better results taking into account the bulk temperature influence.

VI.1 – Strain Energy Loss Model Results

The Strain Energy Loss model is one of the most important sub-part of the entire thermal model; it simulates one of the two heat generation mechanism in the tire. In particular, at least in the linear range (slip angles no greater than 1 degree), this is the main heat generation mechanism.
To validate the model, an indoor test campaign has been conducted on 6 different tires. They have been tested on Rolling Resistance ZF machine.

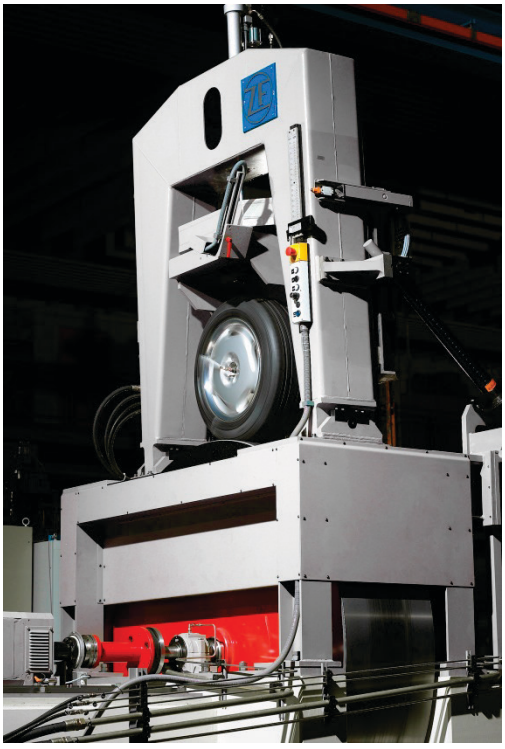

Figure VI.1 – The ZF machine to measure tire rolling resistance

The tires used for the campaign were:

- Passenger tire 225/50 R17 (Spec 1)
- Passenger tire 205/55 R16 RFT (Run-Flat Tire)
- Passenger tire 225/50 R17 (Spec 2)
- Passenger tire 245/40 R18
- Passenger tire 235/45 R17
- Light truck tire 265/65 R16C

All the tires were characterized by different specifications such as tread compound, body ply construction, crown stiffness, etc.

For all the tires but the light truck and the RFT the following testing conditions have been used:

Time [min]	SPEED [kph]	Fz [N]
30	40	3500
30	40	5000
30	40	6000
30	80	3500
30	80	5000
30	80	6000
30	120	3500
30	120	5000
30	120	6000
30	150	3500
30	150	5000
30	150	6000

In case of the light truck tire, the vertical load has been increased; so the testing conditions were:

TIME [min]	SPEED [kph]	Fz [N]
30	40	3500
30	40	6000
30	40	9000
30	40	12000
30	80	3500
30	80	6000
30	80	9000
30	80	12000
30	120	3500
30	120	6000
30	120	9000
30	120	12000
30	150	3500
30	150	6000
30	150	9000
30	150	12000

In case of the RFT, available previous tests have been used for this purpose and the testing conditions were:

TIME [min]	SPEED [kph]	FZ [N]
30	40	3500
30	40	4000
30	40	4500
30	80	3500
30	80	4000
30	80	4500
30	120	3500
30	120	4000
30	120	4500

The tires were tested with zero camber angle, zero slip angle and zero slip ratios; so they were in free rolling conditions during the entire test.
The following channels were acquired:

- Drum speed (roadway speed) V;
- Drag Force F_x;
- Rolling Resistance Moment M_y;
- Tire Angular Speed ω;
- Loaded Radius R_L

The Strain Energy Loss (in terms of dissipated power) of the tire was computed as:

$$\dot{E}_{diss} = M_y \cdot \omega \qquad [W] \qquad (72)$$

where evidently is also:

$$M_y = F_x \cdot R_L \qquad [\text{mN}] \qquad (73)$$

The simulations were performed in the same conditions: tire in free rolling at different roadway speed and different vertical load for 30 minutes for each condition.

It is important to highlight that no particular tuning has been used but a single scaling factor (besides very close to the unit) on the entire dissipated power for each tire.

As known the model gives back the dissipated power in real time during a simulation.

The results for the different tires are in the figures below.

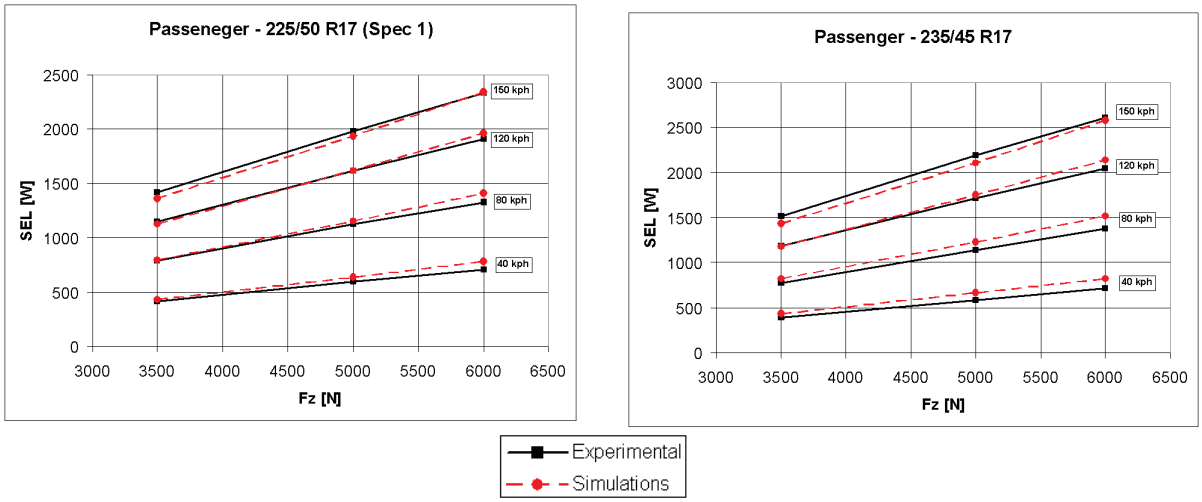

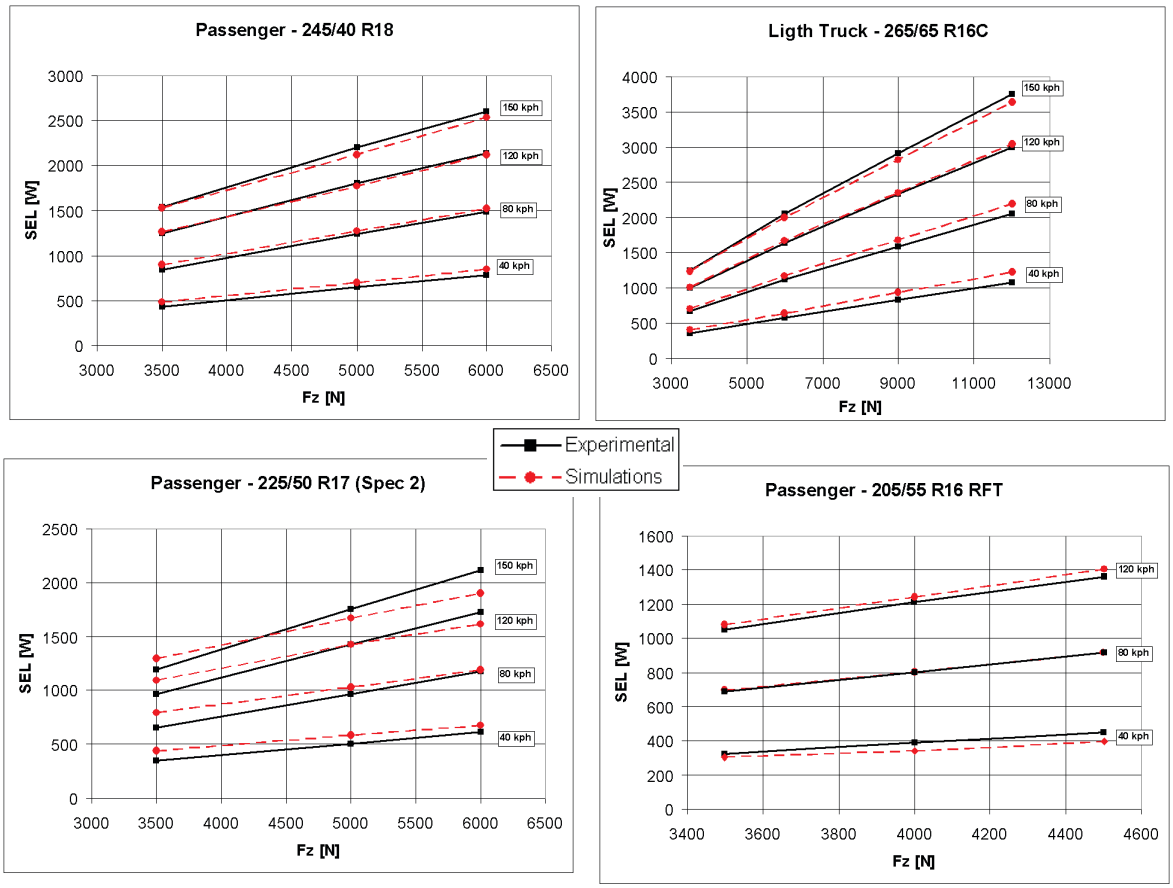

Figure VI.2 – The validation of SEL model

Even if the model appears very simple and it adopts strong simplifying hypotheses, it gives back satisfactory results, well simulating as the dependence on vertical load as the dependence on roadway speed for all the tires but the passenger 225/50 R17 Spec 2 that is shown again in the figure below.

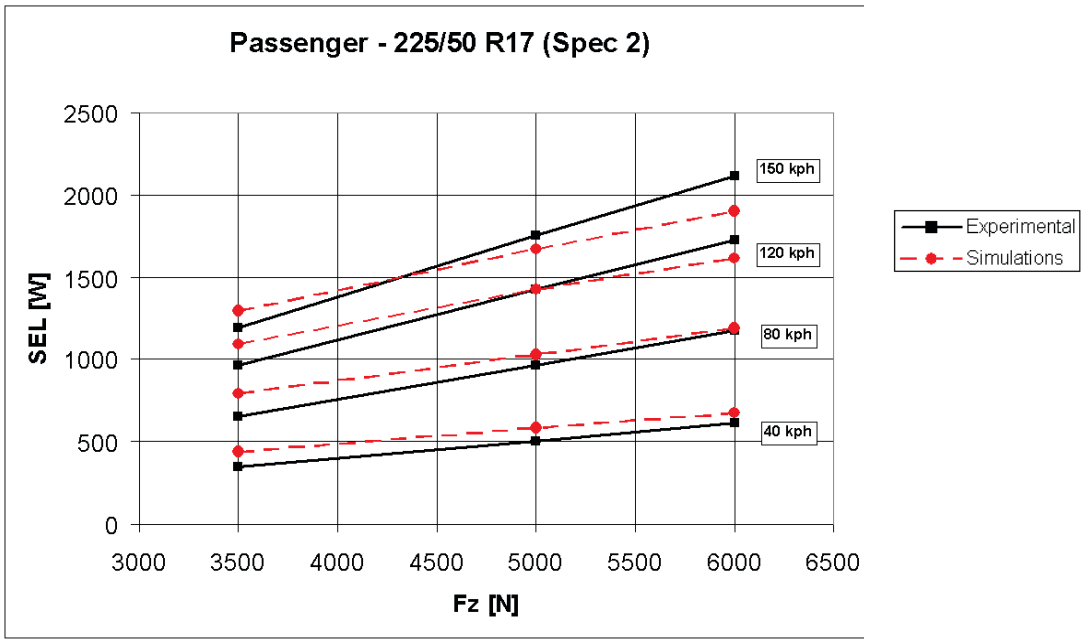

Figure VI.3 – Simulation results on Spec 2 tire; not satisfactory results

In this case the dependence on vertical load seems to be overestimated at the low vertical load and underestimated at the highest vertical load.

The reasons must be investigated.

VI.2 – Thermal Model Results

To validate the thermal model, the different tests performed in Flat Trac with the tire equipped with T3M sensors to investigate the bulk temperature influence have been used. In particular, in a first phase of the activity, the dependence of the bulk temperature on vertical load and the roadway speed has been investigated testing the tire in free rolling conditions.
Then, all this tests have been simulated.

It is very important to highlight – especially in this phase – that no tuning has been used in the model: all the scaling factors were set to 1. All the parameters necessary to the model have been measured on the real tire.

In the first test the dependence of bulk temperature on the roadway speed was investigated. The following testing conditions were performed:

TIME [s]	SPEED [kph]	Fz [N]
25	50	5000
1200	50	200
25	80	5000
1200	50	200
25	120	5000

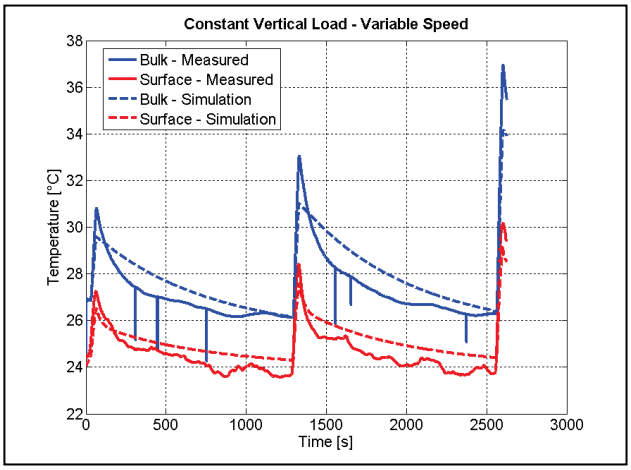

Figure VI.4 – Thermal model results

The second test was conducted at constant roadway speed and different vertical loads.

TIME [s]	SPEED [kph]	Fz [N]
25	80	1000
1200	50	200
25	80	3000
1200	50	200
25	80	5000
1200	50	200
25	80	7000

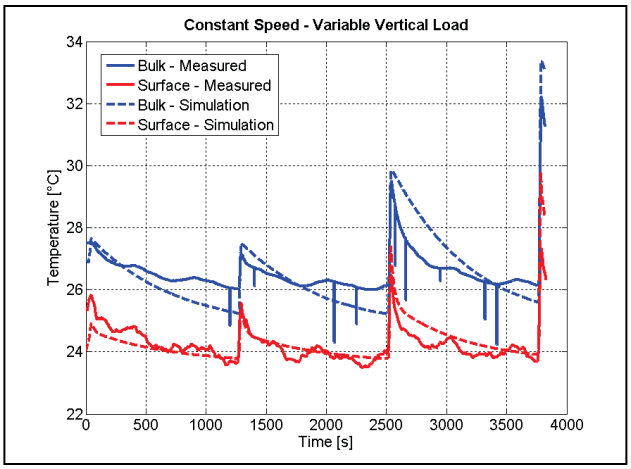

Figure VI.5 – Thermal model results

In the third kind of test, both the roadway speed and the vertical loads varied.

TIME [s]	SPEED [kph]	Fz [N]
25	50	1000
300	50	200
25	120	5000
700	50	200
25	150	7000

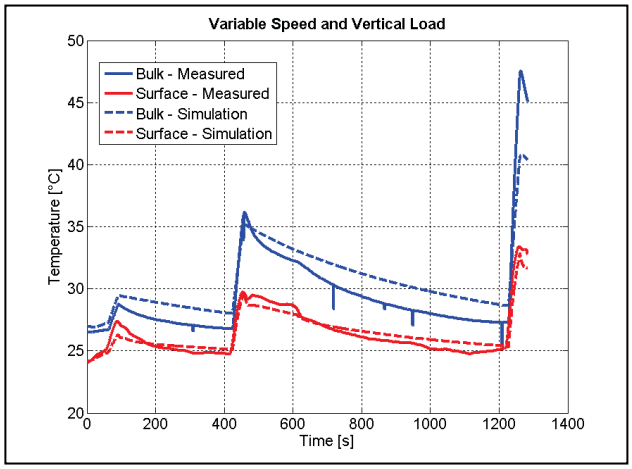

Figure VI.6 – Thermal model results

In the Figure VI.7, the increasing sequence and the decreasing sequence of the lateral tests discussed in Chapter III have been simulated.

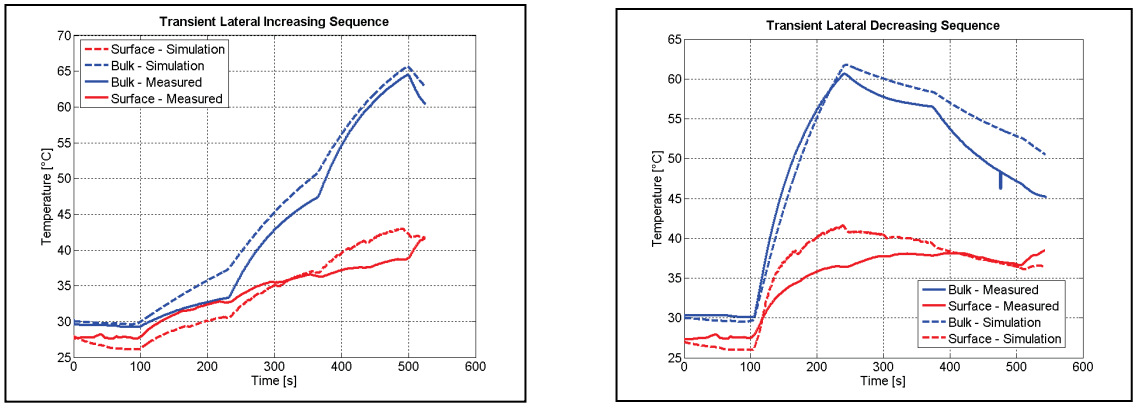

Figure VI.7 – Thermal model results in two different indoor test simulations

In the Figure VI.8, a warm-up phase followed by the transient lateral test has been simulated.

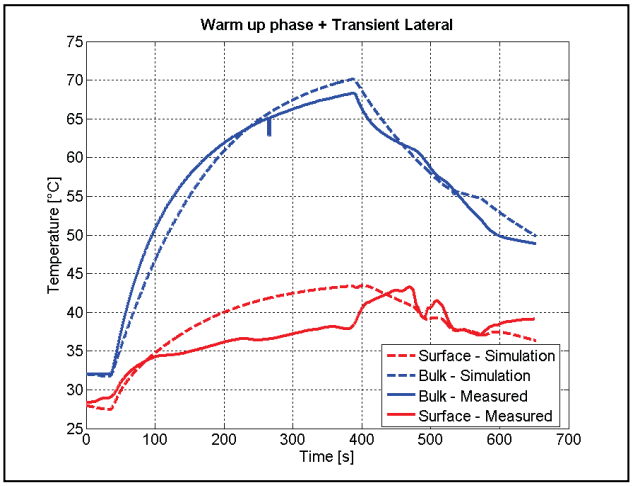

Figure VI.8 – Thermal model results

Reader is invited to focus attention on the main target of the model: starting from simple measurements on a tire – such as footprint dependence on vertical load, loaded radius vs. vertical load, etc. it is possible to estimate the bulk temperature with satisfactory approximation, without any tuning on the thermal model! From this point of view, it seems that the model gives back good results even if some discrepancies with real measurements appear.

VI.3 – Cornering Stiffness Estimation

To evaluate the Cornering Stiffness estimation and how this influences on Lateral characteristic in the linear range, the second kind of indoor test (ref. Chapter III) has been simulated.

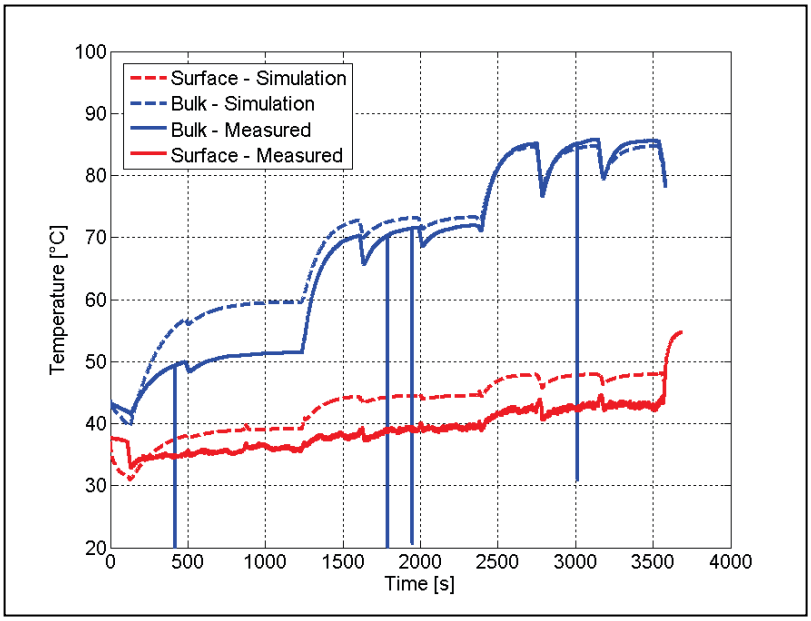

Figure VI.9 – Thermal model results

As showed in the plot, the second part and the third part can be considered satisfactory; during the first part, instead, the model seems to overestimate the bulk temperature.

Anyway, due to this discrepancy the first part has not been considered in the cornering stiffness evaluation.

In the Figure VI.10, the cornering stiffness at 70°C and the cornering stiffness at 83°C will be compared together with the experimental results.

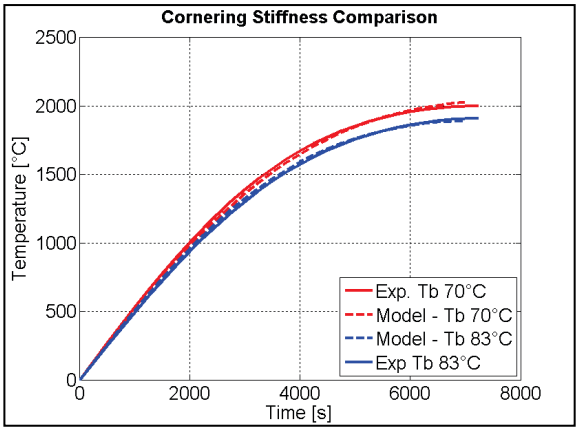

The model produces satisfactory results taking into account the vertical load influence and the bulk temperature influence in the cornering stiffness evaluation.

Figure VI.10 – Cornering stiffness comparison between model and measurements

In the next Figure VI.11, the standard Pacejka formulation and the proposed Pacejka with thermal model will be compared with experimental data in terms of tire lateral force in the linear range; this with a bulk temperature of 70°C and 83°C.

It is evident that – especially at 70°C – the thermal model helps Pacejka model to better fit the lateral force at all the vertical load. Of course nothing changes between 70°C and 83°C in the standard Pacejka.

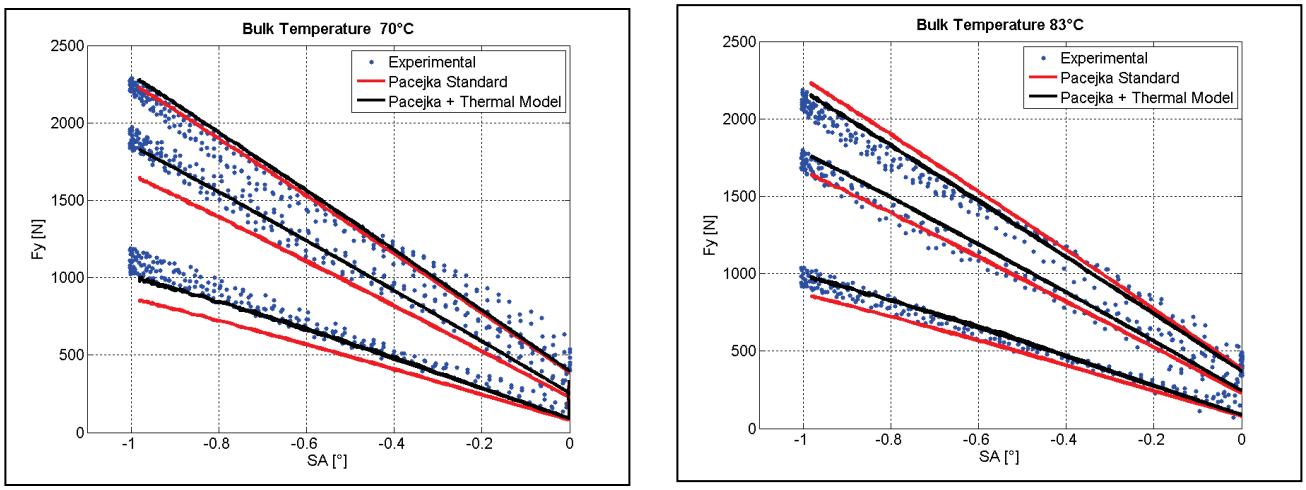

Figure VI.11 – Comparison between Pacejka standard model and the proposed model

Conclusions and future upgrades

The influence of the bulk temperature on tire handling performance has been deeply investigated. Indoor and outdoor tests have been conducted for the purpose. In particular the activity was focused on the linear range of the tire lateral characteristic (slip angle limited to +- 1°). The indoor test campaign has been performed on the Flat Trac machine using a tire equipped with particular sensors developed by the TUV Automotive and named T3M sensors. These sensors consist of thermo resistances temperature sensitive that can be introduced in the bulk of a tire.

Different procedures to evaluate the cornering stiffness have been performed. The results have been surprising in terms of the bulk temperature reached during the test. The procedures gave back difference on bulk temperature of even 15°C involving in variation in cornering stiffness of 10% (this can give back sensible variance in vehicle balance).

The outdoor tests have been conducted on the oval track of EUPG so to remain again in the linear range of the characteristic. Also in this case the results have been surprising for some aspects: the bulk temperature reached very high values (100°C at 140 kph) saturating at a temperature that depends on vertical load (that means the loads on the corners) and on angular velocity (that means the roadway speed). Furthermore the test showed a deep difference between inside and outside shoulder of the tire. This is in line with the negative camber angle influence that loads the inside shoulder more than the outside (negative camber angle).

A thermal model has been developed to evaluate the bulk temperature of a tire during its exercise and correcting the cornering stiffness – through Pacejka formulation – taking into account the influence of the bulk temperature itself.

The model is physical, the thickness of the tire is divided into two layers: the outer one – thinner – simulates the tread, while the inner one simulates the carcass (together with the belt). For the two layers the equations of thermal diffusivity have been written in Matlab/Simulink environment.
A physical model has been implemented even to evaluate the Strain Energy Loss (the energy dissipated by hysteresis). The SEL model is based on different simplifying assumptions that did not influence the results anyway.
All the parameters are easily measurable and the model demonstrated it needed no tuning. In fact even if a certain numbers of scaling factors have been introduced, all of them have been set to 1; few corrections have been needed in the SEL model; anyway always close to unit (0.95-1.1 the maximum variations).
The thermal model interacts with Pacejka MF (Magic Formula) through a dedicated scaling factor in the cornering stiffness equation; this factor varies around the unit in dependence on the bulk temperature. In this way, the Pacejka MF can take into account the influence of the temperature on the cornering stiffness, which means on the lateral characteristic in the linear range.
The model has been validated comparing the simulations with the indoor measures and it appeared very satisfactory. The SEL model in particular gives back great results, taking into account in the right way as the influence of the vertical load as the influence of the roadway speed; this has been confirmed for very different tire specifications (different sizes, different compounds and different constructions).
In the next future new upgrades are under evaluation; first of all the opportunity to model the mechanic properties of the tire in relation to geometric characteristics [25].
Furthermore, the model is going to be used in high speed durability simulations. Is well known that the high speed durability is temperature related; for this

reason the thermal model could be a useful tool to estimate the maximum bulk temperature in high speed tests.

Bibliography

[1] Pacejka, H. B., "*Tyre and Vehicle Dynamics*" – Butterworth Heinemann, 2002.

[2] Ferry, J. D., *"Viscoelastic properties of polymers"* – John Wiley & Sons editions

[3] Johnson, K. L., *"Contact Mechanics"* – Cambridge University Press,1985.

[4] Clark, S. K., "Mechanics of Pneumatic Tire" – U.S. Department of Transportation, NHTSA

[5] Edeskar, T., *"Technical and Environmental properties of tyre shreds focusing on ground engineering applications"* – Technical Report of Lulea University of Technology

[6] Ghosh, S., Sengupta, R. A., and Heinrich, G., "*Investigations on Rolling Resistance of Nanocomposite Based Passenger Car Radial Tyre Tread Compounds Using Simulation Technique*" – Tire Science and Technology, TSTCA, Vol. 39, No. 3, July–September 2011, pp. 210–222.

[7] Rhyne, T. B., Cron, S. M., *"A Study on Minimum Rolling Resistance"* – Tire Science and Technology, TSTCA, Vol. 40, N° 4, pp. 220-233. (2012)

[8] Ebbott, T.G., Hohman, R. L., Jeusette, J. P., Kerchman, V., *"Tire Temperature and Rolling Resistance Prediction with Finite Element Analysis"* – Tire Science and Technology, TSTCA, Vol. 27, No. 1, January–March 1999, pp. 2-21.

[9] Janssen, M. L., Hall, G. L., *"Effect of Ambient Temperature on Radial Tire Rolling Resistance"* – SAE Tehcnical Paper series. Presented at SAE Congress and Exposition, Detroit, 25-29 February 1980.

[10] Assaad, M. C., Kimble, B., Huang, Y.-M., Burgan, R., Fralick, G. C., Wrbanek, J. D., and Gonzalez, J. M., *"Thin-Film Heat Flux Sensor for Measuring the Film Coefficient of Rubber Components of a Rolling Tire"* – Tire Science and Technology, TSTCA, Vol. 36, No. 4, October – December 2008, pp. 275-289.

[11] Ozerdem, B., *"Measurement of convective heat transfer coefficient for a horizontal cylinder rotating in quiescent air"* – Int. Comm. Heat Mass transfer, Vol. 27, No. 3, pp. 389-395, 2000

[12] Browne, A. L. and Wickliffe, L. E., *"Parametric Study of Convective Heat Transfer Coefficients at the Tire Surface"* – Tire Science and Technology, Vol. 8, Nos.3-4, July - Dec. 1980, pp. 37-67.

[13] Hisham A. Abdel-Aal, *"On Heat Partition among Dry Sliding Anisotropic Solids"* – The Annals of University "Dunarea de Jos" of Galati; Fascicle VIII, 2004, ISSN 1221-4590.

[14] Knauss, W. G., *"Rupture phenomena in viscoelastic materials"* – PhD Thesis at California Institute of Technology

[15] Hewson, P., *"Method for estimating tyre cornering stiffness from basic tyre information"* – Proceedings of the Institution of Mechanical Engineers Part D; Journal of Automobile Engineering, 219 (12). pp. 1407-1412. ISSN 0954-4070 (2005)

[16] Dorrie, H., Schroder, C., Wies, B., *"Winter Tires: Operating Conditions, Tire Characteristics and Vehicle Driving Behavior"* – Tire Science and Technology, TSTCA, Vol. 38, N° 2, April - June 2010, pp. 119-136.

[17] Williams, M. L., Landel, R. F., Ferry, J. D., *"The Temperature Dependence of Relaxation Mechanisms in Amorhpus Polymers and Others Glass-forming Liquids"* – Journal of American Chemical Society, Vol. 77, pp. 3701-3707 (1955).

[18] J. Lacombe, *"Tire Model for simulations of vehicle motion on high and low friction road surfaces"*, Proceedings of the 2000 Winter Simulation Conference

[19] B. A. J. de Jong, *"Development and validation of the MC-Swift concept tire model"* – PhD thesis at Eindhoven University of Technology.

[20] V. Ivanov, "*Analysis of Tire Contact Parameters Using Visual Processing"* - Advances in Tribology, Vol. 2010, Article ID 491723, 11 pages

[21] D. M. Xu, R. N. Yong, A. M. O. Mohamed, *"Modeling of Tyre-Clay Soil Interaction via Quasi-Static Moving Boundary Displacement Method"* – Journal of forest engineering.

[22] D. S. Stutts, W. Soedel, *"A Simplified Dynamic Model of the Effect of Internal Damping on the Rolling Resistance in Pneumatic Tyres"* - Journal of Sound and Vibrations, Vol. 155 pp. 153-164 (1992).

[23] G. Heinrich, M. Kluppel, *"Rubber friction, tread deformation and tire traction"* – Wear, Vol. 265, pp.1052–1060 (2008).

[24] Johnson and C. J. Quigley, "*A Viscohyperelastic Maxwell Model for Rubber Viscoelasticity*". Rubber Chemistry and Technology: March 1992, Vol. 65, No. 1, pp. 137-153.

[25] K. Kabe, N. Miyashita, *"A Study of the cornering power by use of the analytical tyre model"* – Vehicle System Dynamics, Vol. 43 Supplement, pp. 113-122. (2005)

[26] G. Heinrich, T. A. Vilgis, *"Why Silica Technology Needs S-SBR in High Performance Tires?"* – KGK. Kautschuk, Gummi, Kunststoffe, Vol. 61, pp. 370-376, (2008).

[27] S. Chalignè, *"Tire thermal analysis and modeling"*, Master's thesis, Chalmers University of Technology.

[28] Allouis, C.; Amoresano, A.; Giordano, D.; Russo, M.; Timpone, F., *"Measurement of the Thermal Diffusivity of a Tire Compound by Mean of Infrared Optical Technique"* – International Review of Mechanical Engineering, Vol. 6 Issue 6, p1104-1108 (2012).

[29] Flavio F., Timpone F., Giordano D., Russo M., *"TRT: thermo racing tyre a physical model to predict the tyre temperature distribution"* – Meccanica Ottobre 2013

[30] P. W. A. Zegelaar, *"The Dynamic Response of Tyres to Brake Torque Variations and Road Unevenness's"* – PhD Thesis, Delft University of Technology, (1998).

[31] J. P. Maurice, *"Short Wavelength and Dynamic Tyre Behaviour under Lateral and Combined Slip Conditions"* – PhD Thesis, Delft University of Technology, (2000).

[32] M. Gisper, *"FTire: a physically based application-oriented tyre model for use with detailed MBS and finite-element suspension models"* – Vehicle System Dynamics, Vol. 43, Supplement 1, pp. 76-91, (2005).

[33] M. Gisper, *"FTire, a new fast tire model for ride comfort simulations"* – International ADAMS User's Conference Berlin; (1999).

[34] M. Gisper, *"ADAMS/FTire-A Tire Model for Ride & Durability Simulations"* - ADAMS User's Conference Tokyo; (2000).

[35] C. Oertel, A. Fandre, *"Ride Comfort Simulations and Steps Towards Life Time Calculation: Rmod-K and ADAMS"* – International ADAMS Users' Conference, 1999.

[36] C. Oertel, A. Fandre, *"Rmod-K 7.09c Flexible Belt Model RFNFB User's Manual"*

[37] A. Schallamach, *"The velocity and Temperature Dependence of Rubber Friction"* – Proceedings of the Physical Society. Section B, Vol. 66 N° 5, pp. 386-392. (1955).

[38] H. W. Kummer, *"Unified Theory of Rubber and Tire Friction"* – Engineering Research Bulletin B-94, The Pennsylvania State University College. (1966).

[39] B. N. J. Persson, *"On the theory of rubber friction"* – Surface Science, Vol. 401, Issue 3, pp. 445-454. (1998).

[40] B. N. J. Persson, *"Rubber Friction: role of the flash temperature"* – Journal of Physics: Condensed Matter, Vol. 18, N° 32, pp. (2006).

[41] F. Farroni, M. Russo, R. Russo, F. Timpone, *"A Physical Analytical Model for local Grip Estimation of Tyre Rubber in Sliding Contact with Road Asperities"* – Tribology International. (Article under consideration for publication).

[42] A. Corollaro – "*Un modello termodinamico di pneumatici da competizione per simulazioni real time in impianti HIL"* – Master's thesis, Università degli Studi di Napoli Federico II (Italian).